Summer 8-12-2010

Measures of the Dynamics of G Protein Interaction With the Ribosome With Applications to Antibiotic Screening

Haiou Qin
University of Pennsylvania, haiouqin@sas.upenn.edu

Measures of the Dynamics of G Protein Interaction With the Ribosome With Applications to Antibiotic Screening

Abstract
Ribosomes catalyze protein synthesis via the translation cycle, in which the translation initiation is recognized as a key step to regulate the process. The functional complexes of the bacterial ribosome undergo large conformational changes during the initiation of protein synthesis. Dramatic progress in the elucidation of ribosome structure by both X-ray crystallography and cryoelectron microscopy (cryo-EM) has provided some of the best evidence for such changes. At the same time, detailed rate studies of initiation, even though for the most part incomplete, have shown this process to be complex, multistep reactions, raising the question of the extent to which specific structural changes can be assigned to specific steps described in the proposed kinetic mechanism. By using fluorescence stopped-flow, quenched flow and FRET approaches to elucidate the kinetic mechanism of initiation, particularly the formation of a 70S initiation, we have found that following GTP hydrolysis by IF2 bound within a 70S complex, the G-domain moves toward L11-NTD, leading to increased FRET efficiency, and that Pi is released following such movement. Our results also showed that two G-proteins, IF2 and EF-Tu, can bind to the ribosome simultaneously during the transition from initiation to elongation. In vitro fluorescence assays were also developed to identify biologically active thiopeptide precursor compounds as potential new antibiotics. It is shown that some of these precursors represent novel compounds with respect to their ability to bind to ribosomes. These findings provide not only insight into the mechanism of action of thiopeptide compounds, but also demonstrate the potential of such assays for identifying novel lead compounds that might be missed using conventional inhibitory screening protocols.

Degree Type
Dissertation

Degree Name
Doctor of Philosophy (PhD)

Graduate Group
Chemistry

First Advisor
Barry Cooperman

Keywords
protein synthesis, initiation factor 2, FRET, antibiotics

Subject Categories
Biochemistry

MEASURES OF THE DYNAMICS OF G PROTEIN INTERACTION WITH THE RIBOSOME WITH APPLICATIONS TO ANTIBIOTIC SCREENING

Haiou Qin

A Dissertation

In

Chemistry

Presented to the Faculties of the University of Pennsylvania

in

Partial Fulfillment of the Requirements for the

Degree of Doctor of Philosophy

2010

Supervisor of Dissertation

_____

Barry S. Cooperman, Professor of Chemistry

Graduate Group Chairperson

_____

Gary A. Molander, Professor of Chemistry

Dissertation Committee

Ronen Marmorstein, Wistar Institute Professor

Ivan Dmochowski, Associate Professor of Chemistry

Yale Goldman, Professor of Physiology

ACKNOWLEDGEMENTS

The writing of this doctoral dissertation has been the most significant academic challenge I have ever faced. It would not have been completed without the guidance, support, and help of many people, to whom I owe the deepest gratitude.

I would like to thank my dissertation supervisor, Dr. Barry Cooperman, for giving me the great opportunity to explore these exciting research areas, as well as his insight, inspiration, and motivation. I am grateful to my committee – Dr. Ronen Marmorstein, Dr. Ivan Dmochowski, and Dr. Yale Goldman – for their time, expertise, and advice. I would also like to express my appreciation to Dr. Christina Grigoriadou, Dr. Dongli Pan, Hanqing Liu, and lots of others of Cooperman lab, who provided suggestions and assistance during the course of these studies.

Lastly, and most importantly, my heartfelt thanks have to go to my family for their endless love and support. This dissertation is dedicated to my parents, Zhongfu Qin and Xiuling Ye, who have always encouraged, supported, and believed in me, in whatever I have been pursuing. It is also dedicated to my husband Feng Chen, without whom all these efforts would have been worth nothing.

ABSTRACT

MEASURES OF THE DYNAMICS OF G PROTEIN INTERACTION WITH THE RIBOSOME WITH APPLICATIONS TO ANTIBIOTIC SCREENING

Haiou Qin

Barry Cooperman

Ribosomes catalyze protein synthesis via the translation cycle, in which the translation initiation is recognized as a key step to regulate the process. The functional complexes of the bacterial ribosome undergo large conformational changes during the initiation of protein synthesis. Dramatic progress in the elucidation of ribosome structure by both X-ray crystallography and cryoelectron microscopy (cryo-EM) has provided some of the best evidence for such changes. At the same time, detailed rate studies of initiation, even though for the most part incomplete, have shown this process to be complex, multistep reactions, raising the question of the extent to which specific structural changes can be assigned to specific steps described in the proposed kinetic mechanism. By using fluorescence stopped-flow, quenched flow and FRET approaches to elucidate the kinetic mechanism of initiation, particularly the formation of a 70S initiation, we have found that following GTP hydrolysis by IF2 bound within a 70S complex, the G-domain moves toward L11-NTD, leading to increased FRET efficiency, and that Pi is released following such movement. Our results also showed that two G-proteins, IF2 and EF-Tu, can bind to the ribosome simultaneously during the transition from initiation to elongation. In vitro fluorescence

assays were also developed to identify biologically active thiopeptide precursor compounds as potential new antibiotics. It is shown that some of these precursors represent novel compounds with respect to their ability to bind to ribosomes. These findings provide not only insight into the mechanism of action of thiopeptide compounds, but also demonstrate the potential of such assays for identifying novel lead compounds that might be missed using conventional inhibitory screening protocols.

TABLE OF CONTENTS

LIST OF TABLES

LIST OF ILLUSTRATIONS

CHAPTER 1

INTRODUCTION

1.1 BACTERIAL PROTEIN SYNTHESIS

Protein synthesis occurs on large macromolecular ribonucleoprotein complexes named ribosomes in a process called translation. The *E.* coli ribosome is composed of a large 50S subunit and a small 30S subunit. The large ribosomal subunit is composed of 34 proteins and two RNAs, sedimenting at 5S and 23S, containing about 120 and 2,900 nucleotides, respectively. The small ribosomal subunit is composed of 21 proteins and a RNA of approximately 1,500 nucleotides sedimenting at 16S. It has three tRNA binding sites designated as the aminoacyl (A), peptidyl (P), and exit (E) sites.

Translation consists of four phases: initiation, elongation, termination, and ribosome recycling. In prokaryotic cells, the initiation of translation begins with the formation of a "pre-initiation complex" that contains the 30S ribosomal subunit, mRNA, initiator tRNA (fMet-tRNA^{fMet}) and the initiation factors IF1, IF2, IF3. These factors and at least one GTP molecule are necessary for the efficiency and fidelity of translation initiation. In the "pre-initiation complex" both mRNA and fMet-tRNA^{fMet}, are randomly bound to the 30S subunits, but do not interact with one another. Only after a conformational change of the 30S ribosomal subunit which brings about a specific interaction of the anticodon tRNA and the initiation triplet of mRNA is the functional "30S initiation complex" formed (Gualerzi et al., 2001).

During the transition from the 30S to the 70S initiation complex, IF1 and IF3 are ejected from the ribosome and IF2 hydrolyzes GTP. Subsequently, the initiation phase is completed with the formation of first peptide bond between the P-site bound initiator

tRNA and the A-site bound aminoacyl tRNA (formation of the initiation dipeptide) and the ribosome enters the elongation phase of translation (Gualerzi and Pon, 1990; Gualerzi et al., 2000; Boelens and Gualerzi, 2002; Gualerzi et al., 2002).

The elongation cycle of protein synthesis consists of three major steps: 1) binding of aminoacyl-tRNA to the A site, 2) peptide bond formation, and 3) translocation of the A- and P- site-bound tRNAs to the P and E sites, respectively, accompanied by the concomitant advancement of the mRNA by one codon.. Two elongation factors, EF-Tu and EF-G, greatly accelerate steps 1 and 3: EF-Tu by delivering aminoacyl-tRNA (aa-tRNA) in the form of the ternary complex (EF-Tu·GTP·aa-tRNA) to the A site of the elongating ribosome, whereas EF-G promotes the translocation step. Both EF-promoted events are accompanied by GTP hydrolysis, the intrinsic GTPase activity of the factors being greatly stimulated by the ribosome (Nishizuka and Lipmann, 1966). Whether the energy librated by GTP hydrolysis is used directly for tRNA binding and translocation or for the release of the factors has been a matter of debate for a long time. However, a recent kinetic study (Rodnina et al., 1997; Savelsbergh et al., 2003) has shown that the EF-G-dependent GTP hydrolysis drives translocation (Wintermeyer et al., 2004).

The termination step begins when a stop codon appears in the decoding site and is recognized by either termination factor RF1 or RF2 (in bacteria), depending on its nature. Ribosomal binding of these factors in response to the appropriate stop codon in the A site triggers the hydrolysis and release of the peptide chain from the tRNA present in the P site, yielding a post-termination complex having a deacylated tRNA bound to the mRNA

in the P site and an empty A site. The turnover of RF1 and RF2 is promoted by factor RF3, another G protein with properties similar to initiation factor IF2 and elongation factors EF-G and EF-Tu. Transfer RNA and messenger RNA need to be released from the post-terminating ribosome to allow a new round of protein synthesis to take place. This recycling process requires another factor, the ribosome recycling factor (RRF), which acts in concert with EF-G and IF3 (Peske et al., 2005; Zavialov et al., 2005).

1.2 INITIATION OF PROTEIN SYNTHESIS

Among the four phases that characterize protein synthesis, initiation is the step displaying the most diversity between prokaryotic and eukaryotic cells and is regarded as the rate-limiting and the most tightly regulated step of translation (Mathews et al., 1996).

1.2.1 Initiation of protein synthesis in prokaryotes

As previously stated, in the 30S "pre-initiation complex" the ribosome bound mRNA and the fMet-tRNA^{fMet} are not interacting with each other. The interaction between the Translation Initiation Region (TIR) of the mRNA and the 30S ribosomal subunit is facilitated by an interaction with ribosomal protein S1 and by base pairing between the anti-Shine-Dalgarno sequence of 16S rRNA and the Shine-Dalgarno sequence, when this is present on the mRNA. The SD interaction was shown to be mechanistically irrelevant for the 30S initiation complex formation and for the selection of the mRNA reading frame but to contribute to the efficiency of translation (Calogero et al., 1988). In the "pre-

initiation complex" the mRNA occupies a ribosomal "stand-by" site corresponding to the region where the SD interaction takes place and is subsequently shifted towards a second site closer to the decoding site (Canonaco et al., 1989; La Teana et al., 1995). These processes are controlled kinetically by the initiation factors IF1, IF2 and IF3 (Spurio, et al., 1993). (Figure 1.1)

1.2.2 Initiation factor 1 (IF1)

IF1 is a small protein (8.1 kDa), encoded by *infA,* an essential gene in *Escherichia coli* (Sands et al., 1987). IF1 binds to both 30S subunit and, at least transiently, to 70S monomers, thus it affects both association and dissociation rates of 70S monomers (Grunberg et al., 1975; van der Hofstad et al., 1978; Dottavio-Martin et al., 1979). IF1 enhances the affinity of the 30S subunit for IF2 and IF3 (Gualerzi and Pon, 1990) and stimulates the activities of these factors (Pon and Gualerzi, 1984). IF1 binds to the A-site of the 30S subunit (Moazed et al., 1995; Carter et al., 2001) and it may prevent premature access of aminoacyl-tRNA, thereby cooperating with IF2 to ensure that only fMet-$tRNA^{fMet}$ binds to the P-site and interacts with the starting codon of the mRNA. During 70S initiation complex formation IF1 is ejected from 30S ribosomal subunit and this may serve the dual purpose of opening the A site for binding aminoacyl tRNA and weakening the interaction of IF2 on the ribosome (Celano et al., 1988; Gualerzi et al., 1989).

1.2.3 Initiation Factor 2 (IF2)

Bacterial IF2 is the largest initiation factor in bacteria (i.e. 741 amino acids in *Bacillus stearothermophilus* and 890 amino acids in *E. coli*) (Brombach et al., 1986; Sacerdot et al., 1984). It is composed of 3 major segments with a total of five structural domains (Figure 1.2) (Gualerzi et al., 1991; Roll-Mecak et al., 2000; Spurio et al., 2000). These segments are: A) a variable N-terminal region, which in *Bst* consists of the first 227 residues and is apparently dispensable for all basic translational functions of the factor (Cenatiempo et al., 1987; Gualerzi et al., 1991); B) a highly conserved 40 kDa segment including the highly conserved GI domain (from residue 228 to 412), which contains all of the structural motifs characteristic of the family of GTP/GDP binding proteins (Cenatiempo et al., 1987; Roll-Mecak et al., 2000) and the GII domain (from residues 413 to 520) which includes a β-barrel module (al-Karadaghi et al., 1996; Roll-Mecak et al., 2000); C) a 25 kDa C-terminal segment consisting of two domains: the C-1 domain, rich in helical structures (Misslwitz et al., 1997; Krafft et al., 2000; Spurio et al., 2000), and the C-2 domain (from Glu632 to Ala741) which consists of the C-terminal 110 amino acids and contains the entire binding site for the 3'-terminus of fMet-tRNA^{fMet} (Guenneugues et al., 2000; Krafft et al., 2000; Spurio et al., 2000).

Part of my thesis work is directed toward understanding the dynamics of the interaction between IF2 and fMet-tRNA^{fMet} as it exists in the binary complex, the 30S initiation complex, and the 70S initiation complex. Pertinent structural work of others is discussed below.

IF2 forms a well-characterized binary complex with the acceptor end of fMet-tRNA^{fMet} via its C2 domain (Meunier et al., 2000). In this binary complex, residues within the GII peptide Asn 611–Arg 645 of *E. coli* IF2 (corresponding to Asn 464–Glu 498 of *B. stear*.) were found to be close to the elbow region of the tRNA (Wakao et al. 1989; Yusupova et al. 1996). Within the 30S initiation complex, the linkage between IF2 and tRNA is maintained by a tight interaction (strong continuous density in the cryo-EM map) between the C2 domain of IF2, the conserved 3' hexa-nucleotide CAACCA end and part of the acceptor stem of the tRNA (Fig. 1.3), while the GII domain of IF2 separates from the elbow region of fMet-tRNA^{fMet}. Within the 70S initiation complex, IF2 losses contact with initiator tRNA and the GII domain of IF2 remains distant from the elbow region of the tRNA (Myaniskov et al., 2005). Our results regarding the interaction between IF2 and fMet-tRNA^{fMet} are presented in Chapter 5.

Additionally, previous data from cross-linking and chemical probing experiments confirmed the existence of at least a partial overlap between the ribosomal-binding sites of IF2, EF-G and EF-Tu (Heimark et al., 1976; Moazed et al., 1988; Porse et al., 1999; Brandi et al., 2004). This localization has been confirmed by a more recent Cryo-EM study which has localized IF2 on the ribosome (Allen et al. 2005). IF2 is a “GTP/GDP binding protein” which stimulates ribosomal subunit association, increases the affinity of the 30S subunit for IF1 and promotes the adjustment of fMet-tRNA^{fMet} in the ribosomal P-site to allow the formation of the first peptide bond (Grunberg-Manago et al., 1975). This activity is accomplished through an acceleration of the codon-anticodon interaction

in the ribosomal P-site (Gualerzi and Pon, 1990; Spurio et al., 2000) and is probably because IF2 recognizes and binds the initiator tRNA. The specific recognition of initiator tRNA by IF2 is primarily due to the recognition of the formyl group, blocking the α-NH2 group. Like all G-proteins, IF2 undergoes a conformational change upon GTP hydrolysis resulting to a proper contact of the fMet-tRNA^{fMet} and the ribosome (Myaniskov, 2005).

1.2.4 Initiation Factor 3 (IF3)

IF3 (20.7 kDa and 180 amino acids in *E. coli*) is encoded by *infC* (Olsson et al., 1996). IF3 displays multiple activities in the formation of the initiation complex. It acts as a dissociation factor of 70S ribosomes by binding tightly to 30S subunits and shifting the equilibrium of the 70S toward free subunits (Kaempfer et al., 1972; Gottlieb and Davis, 1975; Grunberg-Manago et al., 1975). This factor also influences the binding of IF1 and IF2 to 30S subunits and also acts as a "fidelity factor" by destabilizing the non canonical initiation complex formed in the presence of the initiator fMet-tRNA^{fMet} and a non canonical initiation triplet (i.e. AUU), or the pseudo-initiation complex formed in the presence of aminoacyl-tRNAs or tRNAs other than initiator fMet-tRNA^{fMet} (Pon and Gualerzi, 1974; Hartz et al., 1989; Hartz et al., 1990; Haggerty and Lovett, 1993; Sussman et al., 1996). In addition, IF3 destabilizes 30S ternary complexes made with leaderless mRNA by promoting the dissociation of fMet-tRNA^{fMet} (Tedin et al., 1999). This capacity of IF3 to act as a "fidelity factor" in the different cases has been shown to occur when the factor is present in excess amount over the ribosome, while when present

at a stoichiometry equal to the ribosome, it stimulates translation regardless of the initiation triplet present on the mRNA (La Teana et al., 1993; Pediconi et al., 1995). Finally, IF3 stimulates the “shift” of mRNA from the “stand-by” to the P-decoding site of the 30S subunits (La Teana et al., 1995).

Griogoriadou et al. (2007b) demonstrated that the presence or absence of IF3 has, at most, minor effects on the rate of 30SIC formation using either AUG or AUU as the initiation codon, and concludes that the high affinity of IF2 for both 30S subunit and initiator tRNA overrides any perturbation of the codon-anticodon interaction resulting from AUU for AUG substitution. In contrast, replacement of AUG by AUU leads to a dramatic reduction in the rate of 70SIC (70S Initiation Complex) formation from 30SIC upon addition of 50S subunits. Interpreting their results in the framework of a quantitative kinetic scheme (Figure 5.3) leads to the conclusion that, within the overall process of 70SIC formation, the step most affected by substituting AUU for AUG involves the conversion of an initially labile 70 S ribosome into a more stable complex. In the absence of IF3, the difference between AUG and AUU largely disappears, with each initiation codon affording rapid 70SIC formation, leading to the hypothesis that it is the rate of IF3 dissociation from the 70S ribosome during 70SIC formation that is critical to its fidelity function. By FRET methods, Milon et al. (2008) also proved that IF3 was released during 70SIC formation. However, Antoun et al. (2006) reported that prior release of IF3 from the 30S pre-initiation complex was required for 50S association. As

discussed further in Chapter 3, this discrepancy in conclusions might be explained by different messenger RNAs used in these experiments.

IF3 is composed of two independent domains, C- and N- terminal domains connected by a lysine-rich flexible linker (Lammi et al., 1987; Fortier et al., 1994; Kycia et al., 1995). Studies using cryo-electron microscopy (cryoEM) suggest that both the C- and the N- terminal domains of IF3 are located in the interface side of the 30S subunits inside a region that involves many contacts with the 50S subunits in the whole 70S ribosome (McCutcheon et al., 1999; Yusupov et al., 2001). In another study, the crystal structure of a complex of T30S (30S subunits of *T. thermophilus*) with IF3C has shown an alternative location for the C-terminal domain of IF3. This crystal structure shows that IF3C is located within a cavity close to the anti-SD region of the 16S rRNA (Pioletti et al., 2001); the existence of this location is consistent with some data obtained by NMR spectroscopy, mutagenesis, cross-linking, and foot-printing experiments (Petrelli et al., 2003). If the N-terminal domain of IF3 is docked to the 30S subunit near the P-site, there is only limited space left for the binding of cognate tRNA in this site so that the discrimination of the near cognate and non cognate tRNA interactions by IF3N may be explained by space exclusion principles (Pioletti et al., 2001). NMR (deCock et al., 1999) and biochemical studies (Moreau et al., 1997) had shown that the linker region of IF3 is extremely mobile. This flexibility is maintained also when both IF3C and IF3N are bound to the 30S subunits and it has been suggested that the mobile inter-domain linker may act as a strap between the two domains, presumably for transmitting signals between the two

IF3 domains. However, work carried out by Petrelli et al. (2003) had shown that the C-domain is necessary and sufficient for all IF3 functions, at least in vitro.

1.2.5 Initiator tRNA (fMet-tRNA^{fMet})

The kingdom-specific recognition and binding of fMet-tRNA is one of the main properties of bacterial IF2. Formylation of the αNH2 group of Met-tRNA^{fMet} is catalyzed by 10-formyltetrahydrofolate: L-methionyltRNA^{fMet} N-formyltransferase (the product of *fmt*) and is essential for the interaction of initiator tRNA with IF2. Disruption of *fmt* results in an almost tenfold reduction of the growth rate and in a conditional lethal phenotype (Guillon et al. 1992).

1.3 CRYO-EM STRUCTURES OF THE INITIATION COMPLEX

A cryo-EM density map of the 70S-IC from *E. coli* was recently obtained by using GDPNP to stall progression of initiation by inhibiting GTP hydrolysis (Figure 1.4) (Allen *et al*., 2005). Interpretation of this map using X-ray structures of the components helped to delineate their positions and binding modes. IF1, IF2 and fMet-tRNA^{fMet} were clearly identified as filling the intersubunit space between the 50S and 30S subunits, confirming the findings of biochemical studies of the initiation complex (Marzi *et al*., 2003). The N2 domain of IF2, an important 'anchor' to the 30S (Caserta *et al*., 2006) required for optimal growth (Sacerdot *et al*., 1992), was also found in the cryo-EM map.

Translational fidelity is controlled on the subunit by monitoring the base pairing between the codon and anticodon in the process known as decoding. The decoding center located at the upper part of the body and lower part of the head of the subunit is constructed entirely of RNA and contains, among other elements, the upper part of helix 44 and the 3' and 5' ends of the 16S rRNA. The recognition and binding of the translational initiation region (TIR) of the mRNA by the 30S ribosomal subunit depends to various degrees on the structural elements of a canonical TIR, which include the initiation triplet (most frequently AUG), the purine-rich Shine-Dalgarno (SD) sequence complementary to the 3´-end region of 16S rRNA, and a spacer, of variable length, separating SD and the initiation triplet. An interaction that is important for translation initiation occurs at the 3'end of the 16S rRNA that base-pairs with the SD sequence of the mRNA as shown in Figure 1.5.

Myasnikov et al. 2005 also resolved the assembled 70S initiation complex comprising mRNA, fMet-tRNA^{fMet} and IF2 with either a non-hydrolyzable GTP analog or GDP as shown in Figure 1.6. Upon GTP-to-GDP transition, IF2 rotates counter-clockwise along its long axis (Figure 1.6 B) and also along a perpendicular axis (Figure 1.6A, central arrow), resulting in the G domain pointing upward and domain IV being partially retracted from the A site. This leads to a modified interaction pattern: upon transition from the GTP-bound state to the GDP-bound state, IF2 loses the contact with P-site tRNA, and interactions with decoding region and the ribosomal GTPase domain are reduced. The associated conformational change of the ribosome is a slight rotation of

the 30S subunit with respect to the 50S subunit. In addition, the classical position of the tRNA-EF-Tu complex on the ribosome (Figure 1.7A) (Valle et al., 2003) is not compatible with the presence of IF2 (Figure 1.7B), suggesting that IF2 release is required for the ribosome to enter the elongation phase. Myasnikov et al. proposed that EF-Tu induces the release of IF2 by shifting the reaction equilibrium from the mRNA-fMet-$tRNA^{fMet}$-IF2-GDP-70Sribosme complex through the mRNA-fMet-$tRNA^{fMet}$-70S ribosome initiation complex to the EF-Tu-70S ribosome elongation complex.

1.4 FLUORESCENCE RESONANCE ENERGY TRANSFER (FRET)

Fluorescence resonance energy transfer (FRET) as shown in Figure 1.8 is a distance-dependent interaction between the electronic excited states of two dye molecules in which excitation is transferred from a donor molecule to an acceptor molecule without emission of a photon. The efficiency of FRET is dependent on the inverse sixth power of the intermolecular separation, making it useful over distances comparable with the dimensions of biological macromolecules. The Förster distance, R_o, at which the efficiency is 50 %, is calculated by Equation 1.

Equation 1:

$$R = Ro\ (1/E - 1)1/6 \qquad (1)$$

Equation 2:

$$R_o\,(Å) = [8.8 \times 10^{-5} \cdot \kappa^2 \cdot n^{-4} \cdot \phi_D J(\lambda)]^{1/6} \qquad (2)$$

Here ϕ_D is the quantum yield of the donor, n is the refractive index of water, 1.33 (Grossman, 1983). κ^2 is the dipole orientation factor and is set to a value of 2/3 for donors and acceptors that randomize by rotational diffusion prior to energy transfer. $J(\lambda)$ represents the spectral overlap between the fluorescence emission spectra of the donor and the absorbance spectra of the acceptor.

Thus, FRET is an important technique for investigating a variety of biological phenomena that produce changes in molecular proximity.

1.5 THIOSTREPTON (ThS)

Recent studies have indicated that the position of IF2 on the ribosome is at least overlapping with that of EF-Tu and EF-G (La Teana et al. 2001; Marzi et al. 2003; Brandi et al. 2004; Allen et al., 2005; Myasnikiov et al., 2005). Like IF2, also these bacterial translation factors are GTPases and are involved in different steps of protein synthesis. A number of antibiotics that inhibit protein synthesis are thought to act by preventing structural changes of the ribosome occurring during translation. ThS, binding to the L11-binding region of the 23S rRNA, is one of them; this antibiotic is a potent inhibitor of translocation and its action has been the focus of several studies which have suggested different mechanisms of interference with translocation.

It has been reported by Rodnina et al. (1999), that ThS does not interfere with EF-G binding or with the single round of GTP hydrolysis, but in subsequent steps which are Pi release, tRNA translocation and dissociation of the factor from the ribosome. However, a

different mode of inhibition was proposed by Cameron et al. (2002). Based on their results, these authors concluded that ThS inhibited the proper interaction of EF-G·GTP with the ribosome, probably by blocking an essential conformational change within the binding region. Also, Seo et al. (2004) proposed that added ThS slows down the initial binding of EF-G, and prevents formation of the more stable EF-G complex.

Since, as mentioned above, IF2 is a GTPase which binds to a ribosomal site overlapping with that of EF-G, where upon GTP hydrolysis is triggered, the effect of ThS on IF2 functions was also investigated and the conclusions regarding its effect are controversial. In some studies, it has been concluded that ThS inhibits the recycling of IF2 off the ribosomes, either by freezing the factor on the 70S ribosome (Lockwood et al., 1972; Lockwood et al., 1974; Sarkar et al., 1974) or by blocking the binding site on the 50S subunit for 30S initiation complex (Naaktgeboren et al., 1976). However, a recent publication suggested that ThS decreases the stability of the IF2-70S and IF2-50S complexes without affecting the IF2-dependent binding of initiator tRNA to either the 30S ribosomal subunit or to the 70S ribosome nor preventing the adjustment of fMet-$tRNA^{fMe}$ in the P site sufficient to yield fMet-puromycin; however, formation of the initiation dipeptide was strongly inhibited by the presence of ThS (Brandi et al., 2004).

Furthermore, conflicting results were obtained for what concerns the IF2-dependent GTP hydrolysis; thus, in line with the report that thiostrepton prevents the coupling of ribosomal subunits, it was reported that ThS inhibits the IF2-dependent GTP hydrolysis (Naaktgeboren et al., 1976) while other publications have shown instead that this

antibiotic stimulates the GTPase activity of IF2, probably causing a more rapid turnover of the factor (Cameron et al., 2002).

1.6 SIGNIFICANCE

As described above, functional complexes of the bacterial ribosome undergo large conformational changes during the initiation of protein synthesis. Dramatic progress in the elucidation of ribosome structure by both X-ray crystallography and cryoelectron microscopy (cryo-EM) has provided some of the best evidence for such changes. At the same time, detailed rate studies of initiation, even though for the most part incomplete, have shown this process to be complex, multistep reactions, raising the question of the extent to which specific structural changes can be assigned to specific steps described in the proposed kinetic mechanism.

To answer this question, our work has the following goals: a) further elucidating the kinetic mechanism of initiation using fluorescence stopped-flow, quenched flow, and FRET approaches. In particular, a key step in initiation is the formation of a 70S initiation complex (70SIC) and we will elucidate the timing and magnitude of a key conformational change within the process of 70SIC formation (Chapter 3); b) characterize simultaneous binding of G-factor proteins to the ribosome. We will follow up our recent result showing that two G-proteins, IF2 and EF-Tu, can bind to the ribosome simultaneously during the transition from initiation to elongation by coupling collaborative studies, using modeling to obtain a structure of the complex, with

measurements designed to both capture the movement of IF2 as EF-Tu binds, and to determine the importance of the stoichiometry of ribosomal protein dimer L7/L12 for the process (Chapter 4); c) elucidate the mechanism of IF2 and fMet-tRNA^{fMet} interactionduring 30SIC formation using a FRET approach (Chapter 5) and d) using in vitro fluorescence assays developed in the course of this work to identify biologically active thiopeptide precursor compounds as potential new antibiotics (Chapter 6).

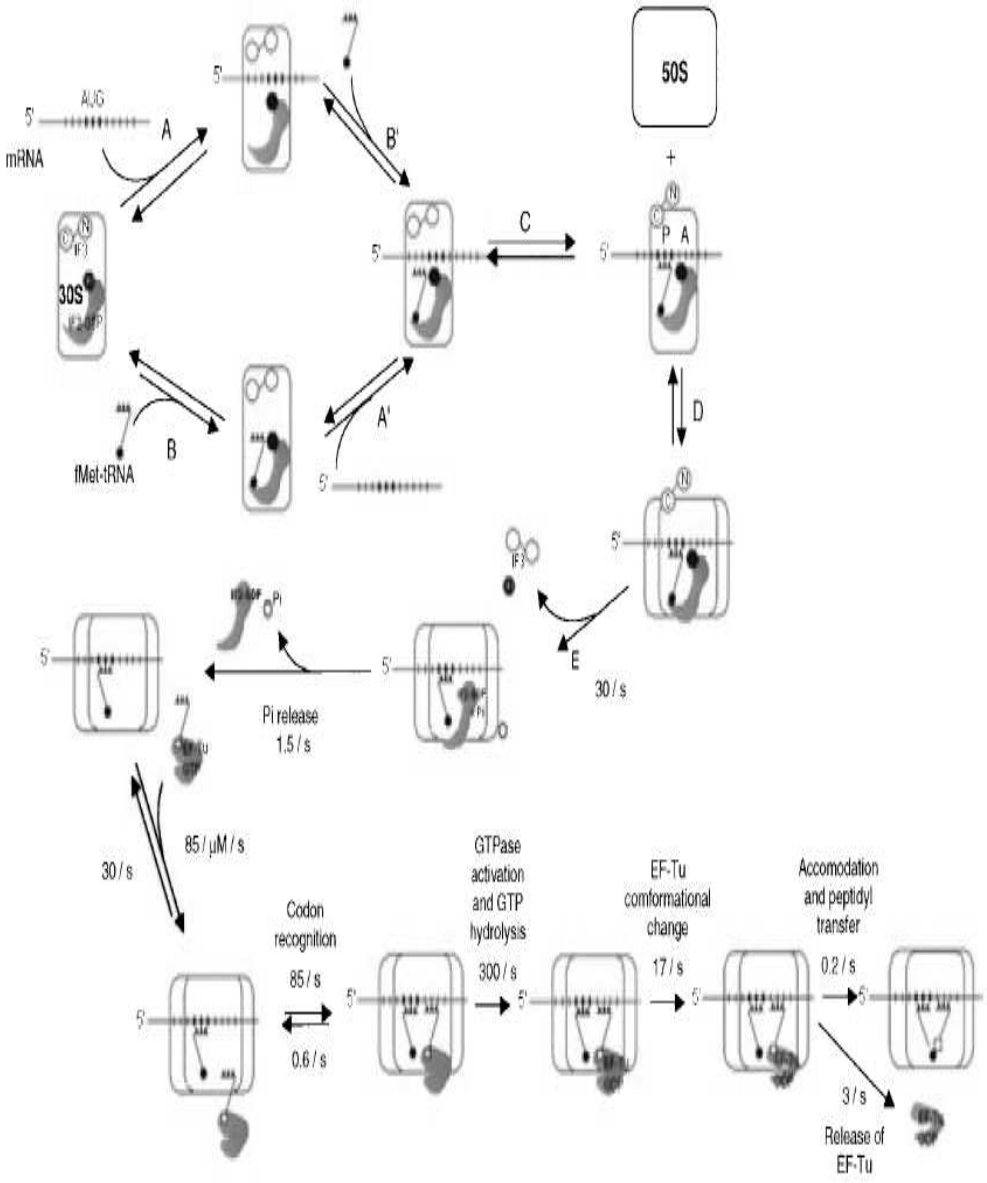

Figure 1.1. Scheme of the translation initiation events starting from "initiation competent" 30S and free ligands (mRNA and fMet-tRNA^{fMet}) and ending with the formation of the initiation dipeptide. Based on this model, the messenger RNA (mRNA)

and the initiator tRNA bind, independently and in random order (steps A, A', B, B'), to the ribosomal subunit 30S onto which the initiation factors IF1, IF2, IF3 and one molecule of GTP are bound, to form the "pre-initiation complex 30S". The interaction between codon and anticodon occurs after the ribosome undergoes a conformational change induced by the initiation factors (step C); that process signals the transition to the "initiation complex 30S". Steps A, A' B, B', are in rapid equilibrium between them and step C is the limiting step of the velocity of the entire process. Following this, a first-order kinetic step occurs that is controlled in both directions by the initiation factors, which guarantee the efficiency and the fidelity of the initiation of protein synthesis. The initiation complex 30S can either dissociate to its components or bind the 50S ribosomal subunit to form the "initiation complex 70S" (step D). This step is irreversible by the ejection of initiation factors IF1and IF3.

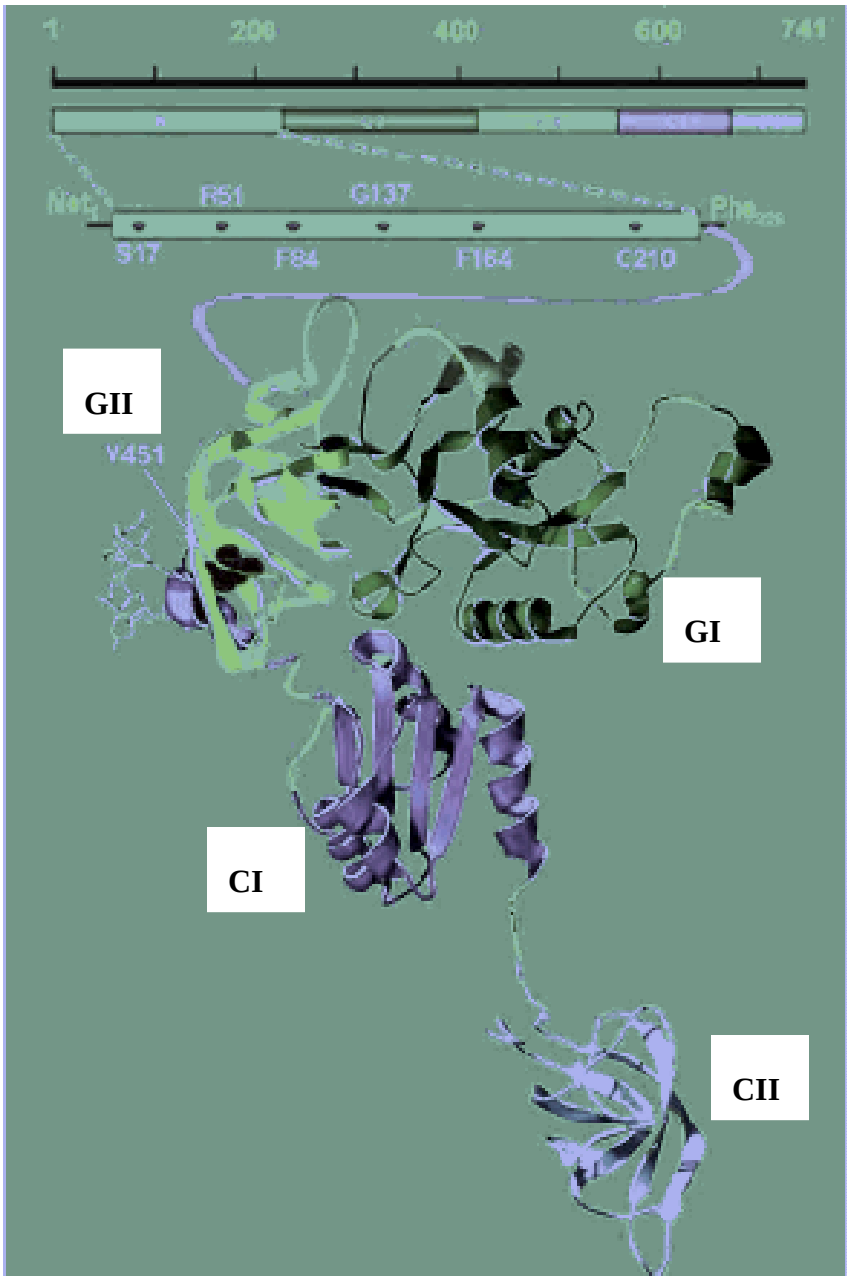

Figure 1.2. The three-dimensional structure of IF2 as predicted by homology modeling with the archaeal IF2/eIF5B three-dimensional structure (Roll-Mecak et al., 2000). The three-dimensional structure of the C-2 domain was taken from pdb file 1D1NA (Guenneugues et al., 2000). This figure is adapted from (Marzi et al., 2003)

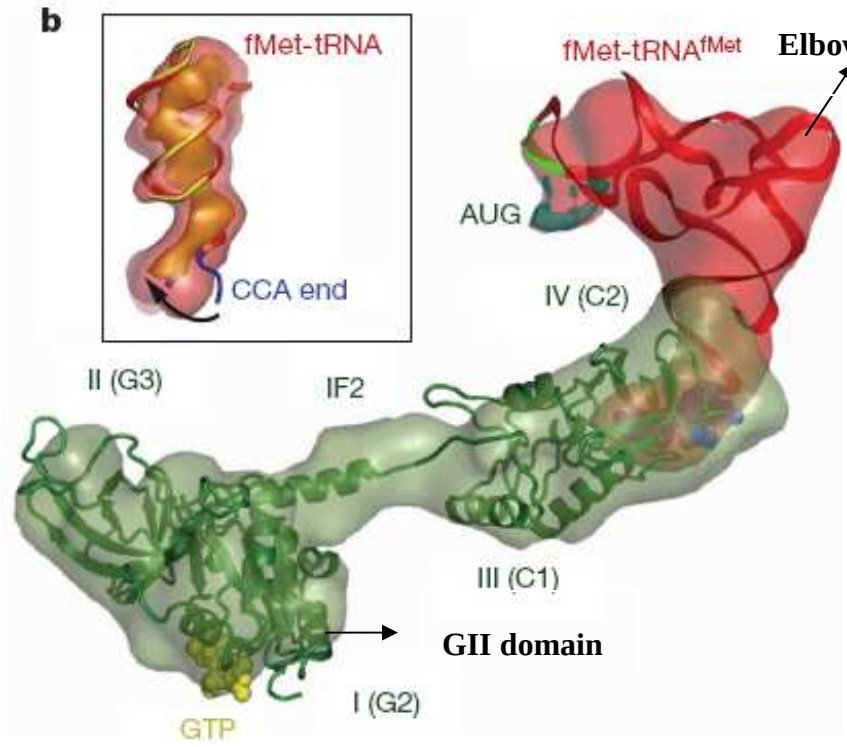

Figure 1.3. The interaction between IF2 and fMet-tRNA within the 30SIC.

The tRNA decoding stem is bent towards the mRNA (the anti-codon is shown in green; the residual density next to it corresponds to the AUG start codon shown in dark green).Notably, the 3' CCA end of the tRNA (insert, view from 50S side) is kinked towards IF2 domain IV (C2) compared to a classical tRNA (in yellow), as seen from differential protein/RNA density contouring levels (shown in pink and orange). (Simonetti 2008)

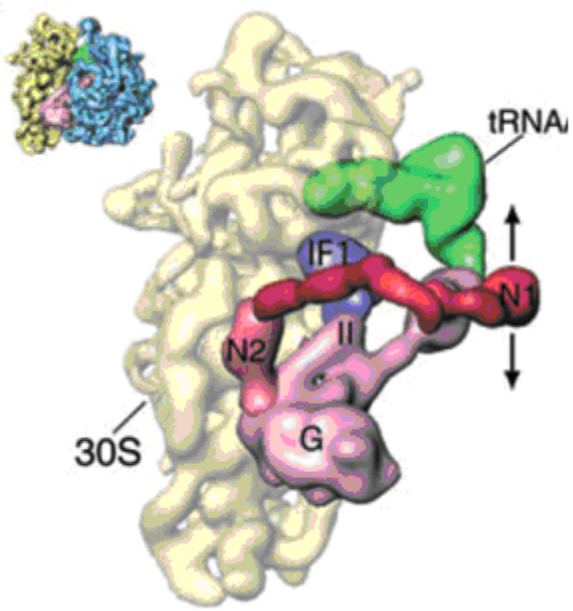

Figure 1.4. The *E. coli* 70S-IC (50S subunit removed for clarity) is shown with fitted X-ray structures of IF2 (red), IF1 (blue), fMet-tRNA^{fMet} (green) (Allen et al., 2007)**.** The cryo-EM map of the N2 domain is also depicted, as well as a model of the N1 domain based on the NMR structure (Laursen et al., 2004). The arrows on the model of the N1 domain indicate its inherent mobility.

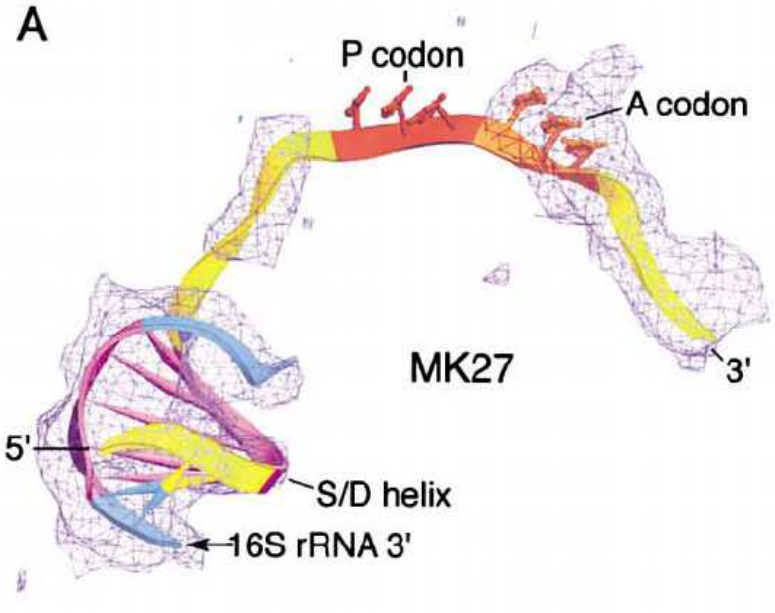

Figure 1.5. MK27 mRNA on the 70S ribosome with the mRNA model (yellow) docked. The Shine-Dalgarno (S/D) helix (magenta) and the A- and P-site codons (orange and red, respectively) are viewed from the top of the 30S ribo- (green). It is adapted from Yusupova et al., 2001.

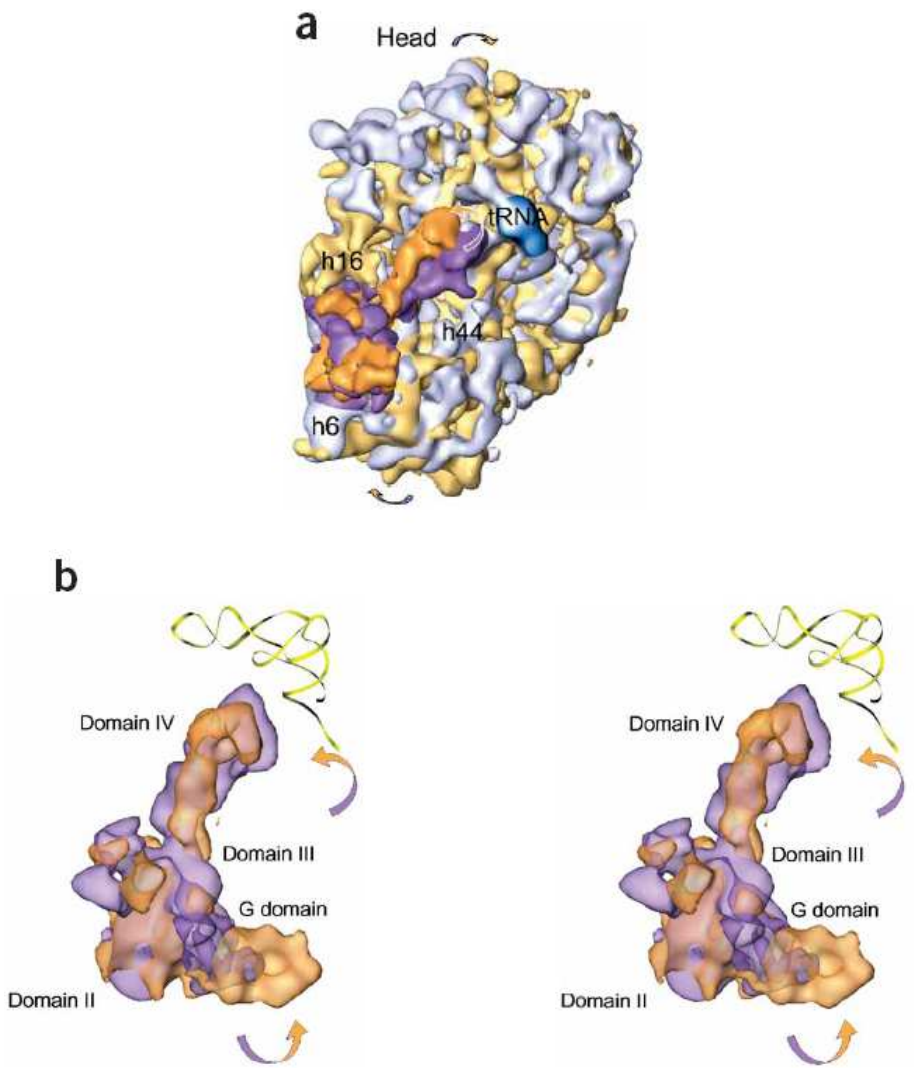

Figure 1.6. Comparison of the GTP- and GDP-bound states of IF2, illustrating the conformational change and spatial shift of IF2 and the associated conformational change of the ribosome upon GTP hydrolysis. (A) Superposition of the IF2-GMPPCP-30S subunit complex on the IF2-GDP-30S subunit complex. (B) Stereo representation of IF2 in the two superposed states; the tRNA is shown as a green ribbon (Myasnikov et al., 2005).

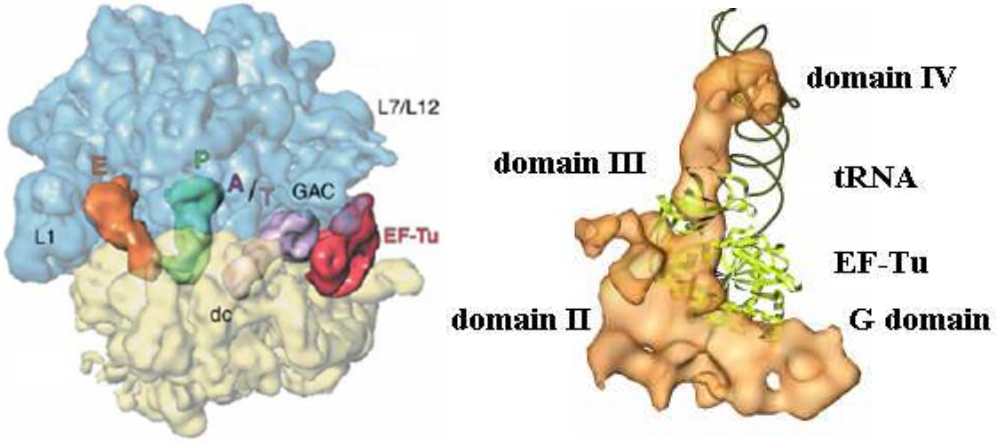

Figure 1.7. tNRA-EF-Tu complex on the ribosome (A) and the superimposed state of EF-Tu and IF2 (B)(Valle et al., 2003; Myaniskov et al., 2005). In (B), EF-Tu is in green and IF2 is in orange.

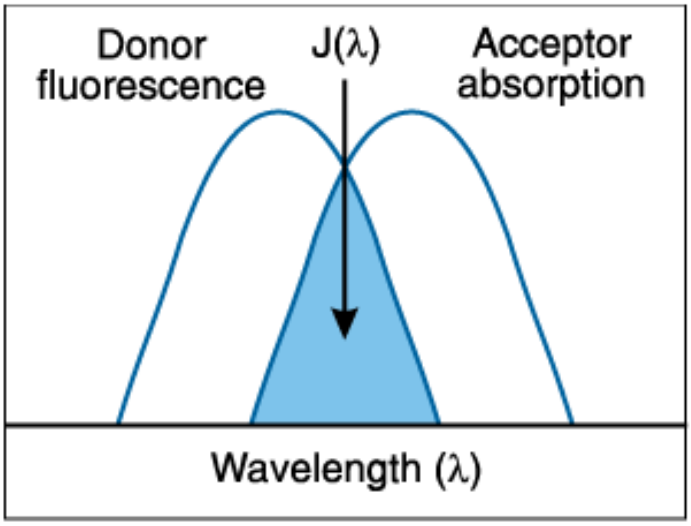

Figure 1.8. Schematic representation of the FRET spectral overlap integral.

CHAPTER 2

MATERIALS AND METHODS FOR CHAPTERS 3-5

2.1 PREPARATIONS

2.1.1 Preparations of the ribosomes and subunits

AM77 ribosome

60-70 grams frozen cells from rifampicin-resistant *E. coli* AM77 strain only containing ribosomes that lack L11 suspended in 200mL buffer (20 mM Tris-HCl pH7.5, 100 mM NH_4Cl, 10 mM $MgAc_2$, 0.5 mM EDTA, and 3 mM 2-mercaptoethanol/ βME) were opened by French press (10,000-12,000 psi) followed by two centrifugations at 15k rpm for 30 min and 60 min, respectively to obtain the supernatant S30. S30 was layered on top of 1.1 M sucrose in buffer 1 (20 mM Tris-HCl pH7.5, 500 mM NH_4Cl, 10 mM $MgAc_2$, 0.5 mM EDTA, and 3 mM βME) and centrifuged at 30k rpm (Beckman rotor Ti 45) for 21 hr.

The pellets were resuspended in 35 mL buffer 1 and loaded on top of 10 mL 1.1 M sucrose in buffer 1, ready for the centrifugation at 30k rpm for 21 hr. This step was repeated twice, and the final pellets were dissolved in buffer 2 (10 mM Tris-HCl pH7.5, 60 mM NH_4Cl, 8mM $MgAc_2$, 0.25 mM EDTA, 3 mM βME, and 5% sucrose). The tight couple 70S ribosomes were isolated by centrifugation in a Beckman Ti 15 rotor (20k rpm, 16 hr) on a gradient from 10% to 50% sucrose in buffer 2. The 70S peak was collected (Seo et al., 2004), and the ribosomes were pelleted (Beckman Ti 70.1, 40k rpm, 18 hr), resuspended in buffer (20 mM Hepes pH 7.5, 30 mM NH_4Cl, 30 mM KCl, 6 mM $MgCl_2$, and 4 mM βME), frozen in small aliquots by liquid nitrogen, and stored at -80 ^oC.

JE105 ribosome

JE105 ribosome with a single L12 dimer (a gift from Dr. Sanyal at Uppsala University) is a genetically recombined E. coli strain, for which the last 30 nucleotides of the L10 gene of the wild-type E.coli strain (MG1655) were replaced with AmpR gene. As a result, all the ribosomes from this strain contained L10 protein with 10 amino acids deleted from its C-terminus, which is the binding site for one L12 dimer (Mandava et al., 2007). The preparation of JE105 ribosomes grown in the presence of 80 ug/mL ampicillin was the same as for the AM77 ribosome except that 6 mM Mg^{2+} was used in the zonal sucrose gradient, as for normal tight-couple isolation.

L7/L12-depleted ribosome

500 pmole MRE600 70S ribosome in 500 µl buffer (10 mM Tris-HCl pH7.5, 1.0 M NH_4Cl, 20 mM $MgCl_2$, and 4 mM βME) was mixed with 250 µl cold ethanol with stirring on ice for 10 min, followed by the addition of an additional 250 µl ethanol and continued stirring on ice for another 5 min. The solution was centrifuged at 110k rpm for 40min. The process was repeated and the pellet was dissolved in buffer W (50 mM Tris-HCl pH7.5, 70 mM NH_4Cl, 30 mM KCl, 7 mM $MgCl_2$, and 1 mM dithiothreitol/DTT).

50S and 30S subunits

Tight couple 70S ribosome pellet was dissolved in buffer 3 (20 mM Tris-HCl pH 7.5, 200 mM NH_4Cl, 2 mM $MgCl_2$, and 2 mM βME) and the subunits were isolated by zonal

centrifugation in a Beckman Ti 15 rotor (20k rpm, 16 hr) on a gradient from 10% to 50% sucrose in buffer 3. Based on the O.D. 260 nm profile, 50S subunits were pooled and pelleted in Ti 45 rotor at 30k rpm for 21 hr. Separately 30S subunits were pooled and pelleted in Ti 70.1 rotor at 56.6k rpm for 18 hr.

Reconstituted 50S subunits

50S subunits containing Cy5-labeled L11 (denoted $50S^{Cy5}$) were prepared by incubating $L11^{Cy5}$ (1 nmol, measured as Cy5) with 1 nmol of 50S-L11 subunits in buffer 4 (25 mM Tris pH 7.6, 30 mM NH_4Cl, 70 mM KCl, 7 mM $MgCl_2$, and 1 mM DTT) for 15 min at 37°C. Unbound $L11^{Cy5}$ and any residual unincorporated dye were removed by ultracentrifugation for 18 h through a 1.1 M sucrose cushion in buffer 4 in rotor type 70.1Ti at 220000g, yielding $50S^{Cy5}$ which contained 1.0±0.2 Cy5/subunit. A control reconstitution experiment performed with wild-type MRE 600 50S subunits resulted in a Cy5:50S subunit ratio of <0.2. 50S subunits reconstituted from $50S^{-L11}$ subunits and unlabeled L11 (denoted $50S^{L11}$) were prepared similarly.

2.1.2 Protein preparations

E. coli IF1, IF2, IF3 and B. stearothermophilus IF2 (Bst IF2) (Figure 2.2)

Preparation of *E. coli* IF2 is as described in Pan et al., 2006.

~8 grams of transformed *E. coli* cell pellets for IF1, IF3 or *Bst* IF2 (Grigoriadou et al., 2007a) were suspended in buffer (10 mM Tris pH7.7, 60 mM NH_4Cl, 10 mM $MgAc_2$, 5 mM βME, 0.1 mM phenylmethylsulfonyl-fluoride/PMSF, and 0.1 mM benzamidine) was broken by French press (10,000-12,000 psi) and centrifuged in the SS-34 rotor at 14k rpm for 1hr. The solid ammonium chloride was added to the supernatant to bring its concentration to 1 M, followed by the centrifugation in a Beckman Ti 45 rotor at 25k rpm for 17 hr to get the S-150 supernatant.

The S-150 supernatant of IF1 or IF3 was diluted with 9 volumes of Buffer 5 (20 mM Tris-HCl pH7.1, 1.0 mM EDTA pH 7.0, and 10% glycerol, containing no NH_4Cl) and loaded onto a PC column (Whatman P11, cellulose phosphate) equilibrated with Buffer 5 0.1 M NH_4Cl. The column was washed by Buffer 5 containing 0.1 M NH_4Cl and eluted with a linear gradient from 0.1 M to 0.7 M NH_4Cl in buffer 5. Fractions containing IF1, as seen on a 17% SDS-PAGE gel, or fractions containing IF3, as seen on a 12.5% SDS-PAGE gel, were combined and dialysed against Buffer 5 containing 6 M Urea, 0.05 M NH_4Cl. The pool was then loaded onto a PC column equilibrated in Buffer 5 containing 6 M Urea, 0.05 M NH_4Cl, washed with the same buffer and eluted with a linear gradient from 0.05 M to 0.3 M NH_4Cl for IF1 or a linear gradient from 0.05 M to 0.4 M NH_4Cl for IF3 in the same buffer. The fractions containing IF1 or IF3, as seen by SDS-PAGE analysis, were combined, diluted with 3 volumes of Buffer 5 containing no NH_4Cl, and loaded onto a PC column of 1-2 ml bed volume, equilibrated with Buffer 5 containing

0.1M NH_4Cl, for concentration. The column was eluted with Buffer 5 containing 1 M NH_4Cl and fractions of about 2 mL were collected. Fractions were pooled on the basis of A_{280nm}, and further purified on either a Sephadex G50 column (IF1) or a Sephadex G75 column (IF3). In each case the column was pre-equilibrated with Buffer 5 containing 0.2 M NH_4Cl, and eluted with the same buffer.

The S-150 supernatant of IF2 was diluted with 9 volumes of Buffer 5 (containing no NH_4Cl) and loaded onto a PC column (~40 mL, Whatman P11, cellulose phosphate) equilibrated with Buffer 5 containing 0.1 M NH_4Cl. The column was washed by Buffer 5 containing 0.1 M NH_4Cl and eluted with a linear gradient from 0.1 M to 0.6 M NH_4Cl in Buffer 5. Fractions containing IF2, as seen on a 8% SDS-PAGE gel, were combined and dialysed against Buffer 6 (20 mM Tris-HCl pH 8, 0.1 mM EDTA pH 8.0, 60 mM KCl, 0.1 mM PMSF, and 0.1 mM Benzamidine). The pool was then loaded onto a Mono Q column (~1 mL) equilibrated in Buffer 6, washed with the same buffer and eluted with a gradient from 60 mM to 800 mM NH_4Cl in the same buffer. The fractions containing IF2, as seen by SDS-PAGE analysis, were combined and dialysed against the storage buffer (20 mM Tris-HCl pH 7.1, 200 mM NH_4Cl, 0.1 mM EDTA, 5% glycerol, and 5mM βME). Typical SDS-PAGE analyses of IF1, IF2 and IF3 are shown in Figure 2.2.

The activities of initiation factors were tested by the amount of ^{35}S-fMet-tRNA^{fMet} bound to 30S pre-initiation complexes as a function of added factor. All the initiation factors promoted the binding of fMet-tRNA^{fMet} with a plateau value of 0.8-1.0 fMet per ribosome. These assays also helped to establish the right concentrations of initiation

factors used in the experiments to reach saturating levels of fMet-tRNA^{fMet} bound. Sample data are shown in Figure 2.5.

L11

The method was as described in Seo et al., 2006 with a modification. In the Ni-NTA resin purification step under the native condition as described in QIAGEN handbook, the S100 protein in Buffer 7 (50 mM NaH_2PO_4, 300 mM NaCl, 10 mM imidazole, 4 mM βME) from ~8 g cell pellets (The N-terminus His-tagged L11 was engineered in Pet-14b vector and was transformed into BL21(DE3)pLysS host strain and the sequence is shown in Figure 2.4) was loaded to ~3 ml bed volume of Ni-NTA column (2×1cm). The His-tagged-L11with impurities (about 6 mg) was eluted by buffer 7 containing 250 mM imidazole, followed by the two dialyses, first against Buffer 8 (20 mM Tris-HCl pH7.1, 1 mM EDTA, 6 M Urea, 100 mM NH_4Cl) without $MgCl_2$ to get rid of PO_4^{3-} and to prevent the precipitation of $Mg_2(PO4)_3$, when then against Buffer 8 with 20 mM $MgCl_2$ added. The sample was finally loaded onto a MonoS FPLC column (~1mL) using the linear gradient buffer (20 mM Tris-HCl pH7.1, 1 mM EDTA, 6M Urea, 100-800 mM NH_4Cl) to separate the target His-tagged L11 from the higher molecular-weight protein. The His-tagged L11 (~3 mg) elutes out around 150 mM NH_4Cl. SDS-PAGE analysis showed L11 to be the major protein (Figures 2.3A and B).

L7/L12

The supernatant from the preparation of L7/L12-depleted ribosome was precipitated by acetone (the volume ratio of acetone: supernatant is 5:1) on ice for 10 min and centrifuged at 15k rpm for 20 min. The pellet was dissolved in buffer (50 mM Tris pH7.6, 30 mM NH_4Cl, 70 mM KCl, 7 mM $MgCl_2$, and 1 mM DTT). The L7/L12 can be visualized on a 16.5% SDS-PAGE gel (Figure 2.3C).

2.1.3 Preparation of mRNA

mRNA (Figure 2.1) was prepared from JM109 cells transformed with pTZ18 plasmid containing the 022 sequence under a T7 promoter, which were provided by Dr. C. Gualerzi (University of Camerino). The plasmid was extracted from the cell using the Qiagen Plasmid Maxi kit, and linearized by the restriction enzyme HindIII. *In vitro* transcription was conducted using the EPICENTRE Ampliscribe T7 Flash Transcription Kit. mRNA was isolated from other components in the reaction mixture by precipitation with 2.5 M LiCl on ice (30 min), followed by two ethanol precipitation (2.5 volume of 100% ethanol and 1/10 volume of 0.3 M NaAc pH5.2, 1 h at -20 ºC). The purity was confirmed by urea-PAGE gel (Figure 2.3D), and the concentration was determined by absorption at 260 nm using extinction coefficient of 0.04 mg/A260. The activity of mRNA was tested by the amount of fMet-$tRNA^{fMet}$ bound to the ribosome as a function of mRNA concentration (Figure 2.5).

2.1.4 Fluorescence labeling of proteins and tRNA

L11^{Cy5}

The L11 was concentrated to 2-5 mg/mL (Centricon YM-10), exchanged into the 50 mM Tris-HCl pH 7.5, 400 mM NH_4Cl buffer by a NAP-5 column (Sephadex G-25 medium, 0.9×2.8cm) at a final concentration of 1mg/ml L11. 1 mL of this solution was reacted at 37 ^oC with 50 ul of ~10 mM Cy5 (Figure 2.3, GE Healthcare) in DMF, added dropwise with stirring. After incubation for 1h at 37 ^oC, the reaction was quenched with 3 µL 14 M 2-mercaptoethanol and excess dye was removed by gel filtration on G-25 column (1cm X 35cm, Sigma), pre-equilibrated in buffer (20 mM Hepes pH7.6, 20 mM $MgAc_2$, 400 mM NH_4Cl, 1 mM EDTA, and 4 mM βME), and concentrated using Centricon-10 filters with membrane YM10.

IF2^{Cy3}

The *Bst* G378C-IF2 mutant was concentrated in buffer (50 mM Tris–HCl pH7.5, 800 mM NH_4Cl, 2 mM tris(2-carboxyethyl)phosphine/TCEP, and 1 mM EDTA pH8.0), and labeled in buffer (50 mM Tris–HCl pH 7.5, 800 mM NH_4Cl, 0.01% (v/v) Triton X-100) at a concentration of ~15 µM with a 50-fold molar excess of Cy3 maleimide (Figure 2.3, GE Healthcare). After incubation for 2 h with stirring at room temperature, the reaction mixture was kept in the cold room overnight. The reaction was terminated by adding βME to a final concentration of 35 mM. Excess dye was removed by gel filtration on G-25 column (1cm X 35cm, Sigma) pre-equilibrated in buffer (20 mM Tris–HCl pH 7.5, 200 mM NH_4Cl, 1 mM DTT, 0.1 mM EDTA pH8.0, and 5 % (v/v) glycerol), and

concentrated using Centricon filters with membrane YM30. Labeled protein had a stochiometry of 0.9 to 1.0 Cy3/protein, calculated using a $\varepsilon_{550,\ Cy3}$ of 150,000 $M^{-1}cm^{-1}$ (GE Healthcare). IF2 concentration was estimated by the Bradford assay.

Cy5-fMet-tRNA^{fMet}

tRNA^{fMet} from *E. coli* acquired from Chemical Block (Moscow) was fluorescently labeled with Cy5 hydrazide (Figure 2.6)(GE Healthcare) via reduction of D-loop dihydrouridines with $NaBH_4$ and replacement of the resulting ureidopropanols with Cy5 hydrazide (Figure 2.7). The procedure is similar to the one described for preparation of yeast tRNA^{Phe}(prf16/17) (Wintermeyer and Zachau, 1979; Wintermeyer and Zachau, 1974). My colleague Stanislav Kirrillov refined the protocol. 20 µL of $NaBH_4$ (100 mg/mL in 0.01 M KOH) was added to 10 A260 unit of tRNA dropwise, followed by incubation on ice for 60 min. The reaction was stopped by lowering the pH to 4-5 by gradually adding 6 M acetic acid. After precipitating this mixture twice with 2.5 volume of 100% ethanol and 1/10 volume of 20 % KAc (pH 5) at -20 ºC, the pellet was dissolved in 20 µL NaAc pH 3.7 and mixed with 5 µL of Cy5 (~200 mM) in DMSO and incubated at 37 ºC for 2 hr. To increase the labelling efficiency, the reaction mixture was dried by lyophilyzer for 15 min and redissolved in 100 µL water. Then the pH was adjusted to 7.5 by Tris-HCl, and the mixture was extracted with phenol three times to remove extra dye. The resulting sample was precipitated by 2.5 volume of 100% ethanol and 1/10 volume

of 20 % KAc (pH6.5) at -20 ºC for two times (pH6.5 was used instead of pH5.0 to prevent the dissociation of Cy5), and was dissolved in water.

2.1.5 Aminoacylation (charging) of tRNAs

Unlabeled and Cy5-labeled *E. coli* $tRNA^{fMet}$ were charged and formylated with partially purified *E. coli* tRNA synthetase containing MetRS and formyl transferase by incubating 20 μM $tRNA^{fMet}$, 80 μM [^{35}S]–methionine (2000 dpm/pmol), 720 μM folinic acid (as a formyl donor), and 1/10 volume of crude *E.coli* aminoacyl-tRNA synthetases in 100 mM Tris-HCl pH7.8, 4 mM ATP, 20 mM $MgCl_2$, 1 mM EDTA, 10 mM KCl, and 7 mM βME at 37 ^{o}C for 30 min. The reaction was ended by addition of 1/10 volume of 20% KAc (pH5.0). The samples were extracted by 1 volume of phenol (saturated with Tris buffer, pH4.3, from Fisher) to remove proteins and other components, with the second extraction by 1 volume of chloroform to remove phenol. Then ethanol precipitation was carried out (2.5 volume of 100% ethanol, -20 ºC overnight). The pellets after centrifugation were dissolved in 50 mM NaAc (pH5.0), and further purified by an FPLC MonoQ chromatography using 0 – 1 M NaCl in 50 mM NaAc (pH5.0) (Rodnina et al., 1994). The tRNA was eluted at about 0.7 M NaCl.

2.2 COMPLEX FORMATION

All complexes were made up in Buffer A (25 mM Tris-HCl pH 7.5, 70 mM NH_4Cl, 30 mM KCl, 7 mM $MgCl_2$, 1 mM DTT) at 37 ^{o}C unless otherwise specified.

30S Initiation complex (30SIC) was always formed by incubation of 1.0 equiv of 30S subunits with 1.5 equiv of IF1, IF3, and fMet-tRNA^{fMet}, 3.0 equiv of mRNA, and various amounts of IF2. 30SICs made up with Eco-IF2, Bst-IF2, and Bst-IF2^{Cy3} are denoted 30SIC^{Eco}, 30SIC^{Bst}, and 30SIC^{Cy3}, respectively.

Ternary complex (TC) was formed by incubation of 1.0 equiv of [^{3}H] Phe-tRNA^{Phe} with 1.5 equiv of EF-Tu, 200 μM GTP, phosphoenolpyruvate (Roche Diagnostics) (1.5 mM), and pyruvate kinase (Roche Diagnostics) (0.5 mg/L) for 15 min unless otherwise specified. The TC concentration was calculated as the concentration of [^{3}H] Phe-tRNA^{Phe}.

70S Initiation complex (70SIC) was preformed by incubation of 30SIC (0.3 μM) with 50S subunits (0.5 μM) in buffer A.

2.3 KINETICS

All concentrations specified in the text and figure legends refer to final concentrations after mixing unless otherwise specified, and were performed at 20 ^{o}C in buffer A (25 mM Tris, pH7.6, 30 mM NH4Cl, 70 mM KCl, 7 mM MgCl2, and 1 mM DTT) or polyamine buffer (20 mM Hepes pH7.6, 150 mM ammonium acetate, 4.5 mM $MgAc_2$, 0.05 mM spermine, and 2 mM spermidine)

2.3.1 Instrumentation

Two rapid mixing devices frequently used in my kinetic studies are quenched flow and stopped flow (Figure 2.8). In a quenched flow apparatus, two solutions are

rapidly mixed and the reaction is stopped by a quenching reagent after a certain amount of time. The samples can then be analyzed by various means. In a stopped flow apparatus two solutions are rapidly mixed, and the reaction over time can be monitored by observation techniques such as UV-Vis absorption, fluorescence, and light scattering. Our quenched flow (Kintek) and stopped flow (SX.18MV stopped-flow spectrofluorometer (Applied Photophysics) have dead times of 5 ms and 1 – 2 ms, respectively, giving sufficient time resolution for most of the changes we monitor.

2.3.2 Equilibrium Fluorescence

Solutions were excited at 540 nm, and emission was monitored from 560 to 720 nm (SPEX Fluorolog-3, Jobin Yvon Inc.). 70SIC compositions are indicated in the legends. All solutions were pre-incubated 5 min. at 20 ^{o}C before spectra were recorded.

2.3.3 Light scattering, IF2^{Cy3} fluorescence, 50S^{Cy5} fluorescence, and Pi release

Measurements were performed in either an SX.18MV (Applied Photophysics) or a KinTec SF-2004 stopped-flow spectrophotometer by rapid mixing of 30S complexes with 50S subunits. For light scattering, the excitation was at 395 nm and output was monitored using a KV455 nm long-pass filter (Schott). For IF2^{Cy3} fluorescence and 50S^{Cy5} fluorescence, excitation was at 540 nm and output was monitored at 567 nm and either at 670 nm or using a 680 ± 10 nm bandpass filter, respectively. In Pi release, phosphate released during 70S initiation complex formation was monitored on the stopped flow

apparatus using MDCC-PBP. 30SIC complex was rapidly mixed with 50S subunit. The 30SIC solution also contained MDCC-PBP (2.5 μM), Pi MOP (7-methyl guanosine, 0.6 mM), and purine nucleoside phosphorylase (0.9 unit/mL) in Pi release experiments (Brune et al., 1994). MDCC was excited at 436 nm and monitored using a 455 nm long pass filter.

2.3.4 GTP hydrolysis

GTPase measurements used [γ-^{32}P] GTP. Aliquots were quenched with 0.6 M $HClO_4$, 1.8 mM KH_2PO_4 solution, and [^{32}P] Pi was extracted into ethyl acetate as a dodecamolybdate complex. (Rodnina et al., 1999; Wahler and Wollenberger, 1958) Background due to the ribosome-independent GTPase activity of *Bst* IF2 was subtracted (Severini et al., 1991). In these experiments, 50 S subunits in one syringe were mixed with IF2.GTP alone, or with IF2.GTP as part of the 30SIC in the other. We attribute the lower GTPase/IF2 stochiometry in the 50 S experiment to surface inactivation of IF2 in the syringe before mixing. One would expect this effect to be reduced in the 70 S experiment, since much of the IF2 surface would be buried within the 30SIC

2.3.5 Poly(U)-dependent poly (Phe) synthesis

The assay was carried out as described (Wang et al., 2007), except that 70S ribosomes were formed by pre-incubation of 50S subunits (0.5 μM) with 30S subunits (1.0 μM) for 15 min at 37 ^{o}C.

2.3.6 Formation of fMet-puromycin

All kinetics experiments were carried out at in buffer A at 25 ºC unless otherwise specified. Given below are concentrations after mixing. 0.5 µM initiation complex was rapidly mixed with 10 mM puromycin on the quench flow apparatus. Reactions were quenched with 0.3 M NaAc pH 5.2. [^{35}S]-fMet-puromycin was extracted into ethyl acetate and radioactivity was determined.

2.3.7 fMetPhe formation

Ternary complex was formed by pre-incubating 5 µM EF-Tu, 1 mM GTP, 1.5 mM phosphoenolpyruvate, and 0.5 mg/L pyruvate kinase for an additional 3 min and then incubating with 1 µM [^{3}H]-Phe-tRNA^{Phe} for 3 min at 37 ºC. 0.2 µM ternary complex (defined by [^{3}H]-Phe-tRNA^{Phe} concentration) was rapidly mixed with 0.4 µM initiation complex on a Kintek quench flow apparatus at 25 ºC. Reactions were quenched with 5 M NH_4OH, lyophilized, taken up in 500 µl of water, and eluted with water from an analytical grade cation exchange column (Bio-Rad 50W-X8, 400 µl) that had been prewashed with 0.01 M HCl and water. Dipeptide eluted in the flow-through and ~5 column volumes and radioactivity was determined in a scintillation counter.

2.3.8 Formation of fMet-Phe-puromycin

For fMetPhe-puromycin formation, 30SIC was rapidly mixed with 50S, TC, and EF-G for varying times, followed by rapid addition of puromycin and further incubation for 5

seconds. Reaction was quenched by addition to ice-cold tubes pre-filled with 0.3 M sodium acetate (pH 5.2), fMetPhe-puromycin was extracted into ethyl acetate, and ^{3}H-radioactivity was determined.

2.3.9 Co-sedimentation and SDS-PAGE analysis experiments

SDS-PAGE analyses were performed on i) 70SIC complexes, ii) PRE complexes and iii) POST complexes. In each case, the final solution was loaded onto a 1.1M sucrose cushion and centrifuged for 40 min at 110 krpm using a micro-ultracentrifuge (Sorvall Discovery M120SE). The pellet was then dissolved in Buffer A and subjected to SDS-PAGE analysis. 70SIC complexes were formed by mixing 70S, 1 µM; IF1, IF2, IF3, fMet-tRNA^{fMet}, 1.5 µM; 022mRNA, 3 µM; GTP 200 µM and incubating at 37 ^{o}C for 15 min. TC was formed by mixing EF-Tu, 6 µM; Phe-tRNA^{Phe}, 3 µM; phosphoenolpyruvate, 1.5mM; pyruvate kinase, 0.0005 mg/ml; and GTP 200 µM at 37 ^{o}C for 15 min. PRE complex was formed by adding 70SIC (0.30 µM) to TC (0.60 µM) (both final concentrations), followed by incubation at 37 ^{o}C for 2 min. In experiments containing kirromycin, kirromycin was added to 70SIC and incubated for 5 min prior to TC addition. POST complexes were formed by mixing 70SIC complexes with TC and EF-G in the presence of GTP. The stoichiometries of IF2 and EF-Tu co-sedimenting with ribosomes were determined by comparison with standard samples.

2.3.10 Western blotting

Running SDS-PAGE gel: The protein sample was run on a 16.5% SDS-PAGE gel at 100 volts for ~3 hr in the cold room in which the pre-stained protein markers (Invitrogen) were used to indicate the approximate molecular mass of bands observed on the membrane. The inner chamber of the apparatus was filled with Tris-glycine running buffer containing the antioxidant NuPAGE, (Invitrogen) which is added to minimize degradation of the proteins.

Transfer: A PVDF membrane (LC2005, Invitrogen) was soaked in methanol for 30 sec and rinsed for three times with distilled water. The 4 blotting pads, the resolving gel, the PVDF membrane and the filter paper (LC2005, Invitrogen) equilibrated with transfer buffer(25 mM Tris-HCl, 192 mM Glycine and 10% methanol) were assembled in the following order, on the cathode side of the apparatus: two blotting pads, filter paper, equilibrated gel, equilibrated membrane, filter paper, and two blotting pads. A glass pipette could be used to squeeze the bubbles out. The transfer module was tightly placed in the tank in which the inner chamber was filled with the transfer buffer and the outer chamber was filled with the cold water. The transferring was conducted at 30 volts for 1 hr in the cold room.

Probing: After the apparatus was disassembled, the membrane was incubated in blocking buffer (10% milk powder in 100 mM Tris-HCl pH7.5, 150 mM NaCl, and 0.1% Tween 20) at room temperature (RT) for 1 hr. The blocking solution was poured off and the diluted primary anti-L7/I12 antibody (a gift from Dr. Wilson, University of Alberta) in blocking buffer was added to incubate at RT for 1 hr or in the cold room overnight.

The membrane was rinsed by TBST buffer (100 mM Tris-HCl pH 7.5, 150 mM NaCl, and 0.1% Tween 20) four times by incubating it for 10 min with agitation at RT each time. The use of larger volumes of TBST would reduce the background. The secondary Ab(Rabbit anti-sheep IgG-HRP, Santa Cruz Biotechnology) in blocking buffer was poured over the membrane and incubated for 1 hr at RT with agitation. The wash steps were repeated and the blot from the membrane was ready to be developed.

Enhanced Chemiluminescence Development: Two solutions (Luminol/Enhancer and stable peroxide buffer, both obtained from Thermo Fisher) were mixed in equal parts and the blot was incubated in the above solution for about 1 min. The blot was wrapped in a plastic sheet and exposed to film (Fujifilm LAS-3000).

2.3.11 Native 0.5% agarose/3% acrylamide gel

A 15 mL solution containing 6% acrylamide, 50 mM Tris-HCl pH 8.0, 0.2 mM $MgCl_2$, and 0.2% ammonium persulfate(APS) was pre-incubated at 45 ^oC for 20 min and then mixed with 15 mL 1% agarose, followed by the 1 min incubation at 45 ^oC. Prior to pouring into the gel assembly, tetramethylethylenediamine(TEMED) was added to promote gel formation. The whole assembly was kept in the cold room for 10 min and taken out to the RT for 1 hr. Samples were loaded onto the gel and run in buffer (25 mM Tris-HCl, pH 8.0 and 0.1 mM $MgCl_2$) at 100 volts in the cold room for 2 hr. The gel was stained with 0.2% methylene blue in 7.5% acetic acid and destained in 1% acetic acid (Griaznova and Traut, 2000).

2.3.12 Data analysis

Apparent rate constants and microscopic constants for specific kinetic schemes were determined using the programs Igor-Pro (Wavemetrics) and Scientist (MicroMath Research, LC), respectively. The latter allows global fitting of multiple experimental parameters to a specific scheme, and requires setting of initial values of rate constants.

The Förster distance R_o was calculated from eq 1, where ϕ_D is the quantum yield of $30SIC^{Cy3}$, η is the refractive index of water (= 1.33; *30*), κ^2 is a dipole orientation factor, and was set equal to 2/3 assuming random orientations of the fluorophores (Lakowicz, 1999; dos Remedios and Moens, 1995) and $J(\lambda)$ is the spectral overlap integral. ϕ_D was determined by comparing the integrated fluorescence of $30SIC^{Cy3}$ to that of a standard, Rhodamine B, as described (Lakowicz, 1999), yielding a value of 0.57 ± 0.03. $J(\lambda)$, equal to 4.66 x 10^{-13} $M^{-1}cm^3$, was determined from the fluorescence and absorption spectra of $30SIC^{Cy3}$ and $50S^{Cy5}$, respectively (Seo et al., 2006). These values permit calculation of R_o equal to 60 ± 5 Å, in good agreement with other reported values of 50 – 60 Å for the Cy3:Cy5 pair (*33, 34*).

$$R_o\ (\text{Å}) = [8.8 \times 10^{-5} \cdot \kappa^2 \cdot \eta^{-4} \cdot \phi_D \cdot J(\lambda)]^{1/6} \quad (1)$$

FRET efficiency, *E*, was calculated from eq 2, where F_{DA} and F_A are the background-corrected fluorescences of the donor/acceptor pair and the acceptor alone, respectively, on irradiation at the excitation wavelength (λ_{ex}) of the donor (540 nm) and detection at

the emission maximum of the acceptor, λ_A (670 nm), f_D is a fractional labeling of donor (equal to 1.0), and ε_A and ε_D are the extinction coefficients of donor and acceptor at λ_{ex}.

$$E = \left(\frac{\varepsilon_A(\lambda_{ex})}{\varepsilon_D(\lambda_{ex})}\right)\left(\frac{F_{DA}(\lambda_A)}{F_A(\lambda_A)} - 1\right)\left(\frac{1}{f_D}\right) \quad (2)$$

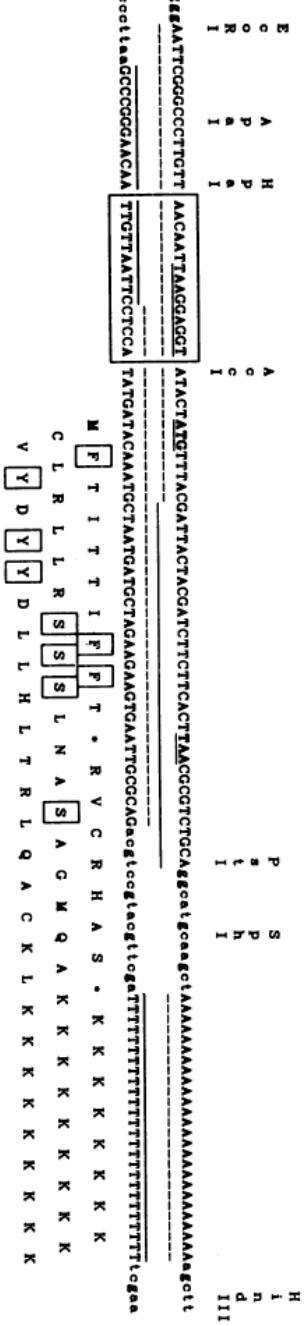

Figure 2.1. The sequence and restriction map of the synthetic gene encoding 022mRNA (Calogero et al., 1988).

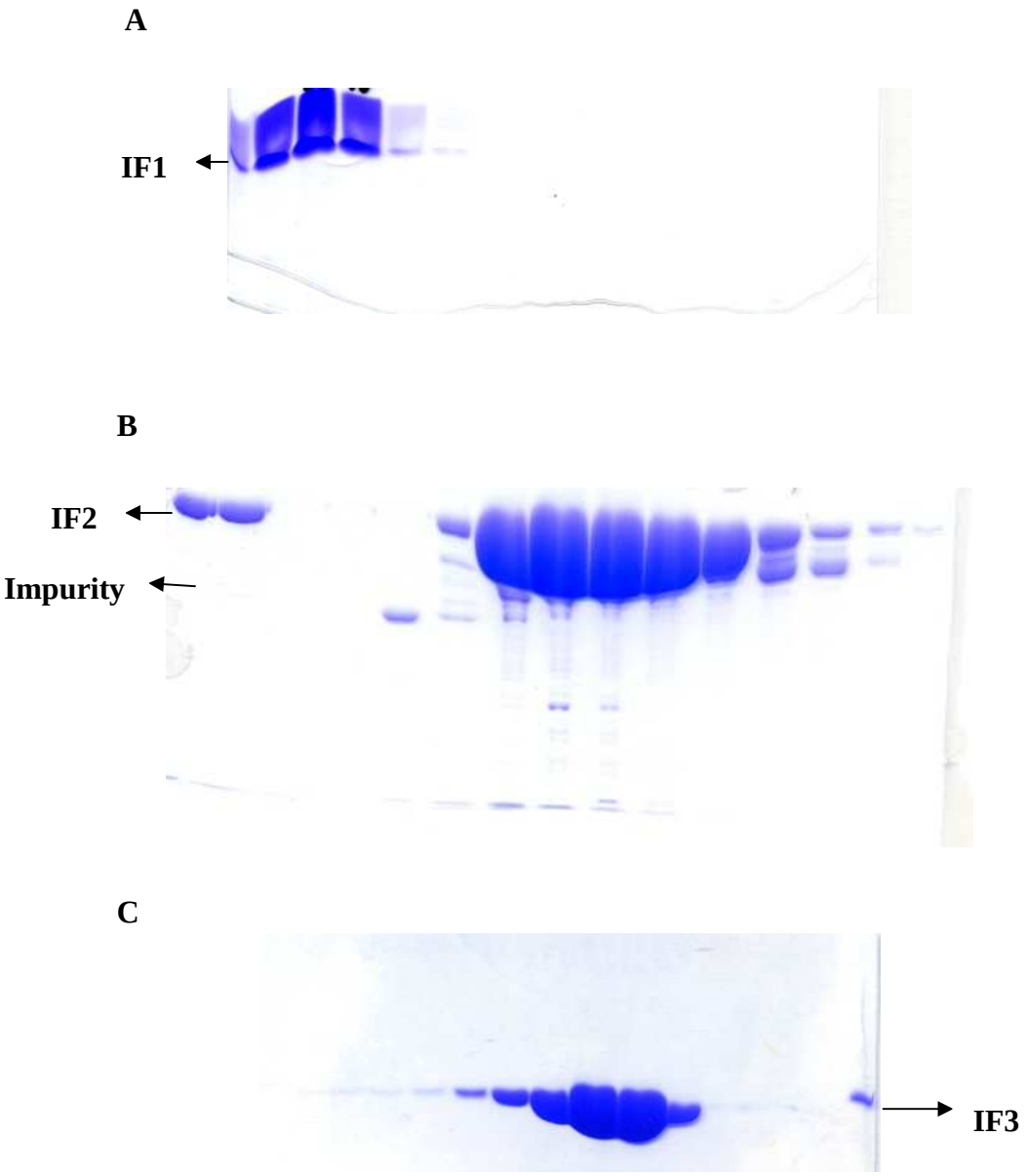

Figure 2.2 SDS-PAGE analyses of *E. coli* IF1 (A) and IF3 (C) and *Bst* IF2 (B). (A) The fractions from the Sephadex G50 column are run on a 17% gel. (B) The fractions from the MonoQ column are run on an 8% gel. The first lane is a purified IF2 sample and the second lane is a partially purified sample prior to MonoQ chromatography. The Mono Q step removes a minor impurity barely visible in lane 2**.** (C) The fractions from the Sephadex G75 column are run on a 12.5% SDS-PAGE gel.

A


L11

B

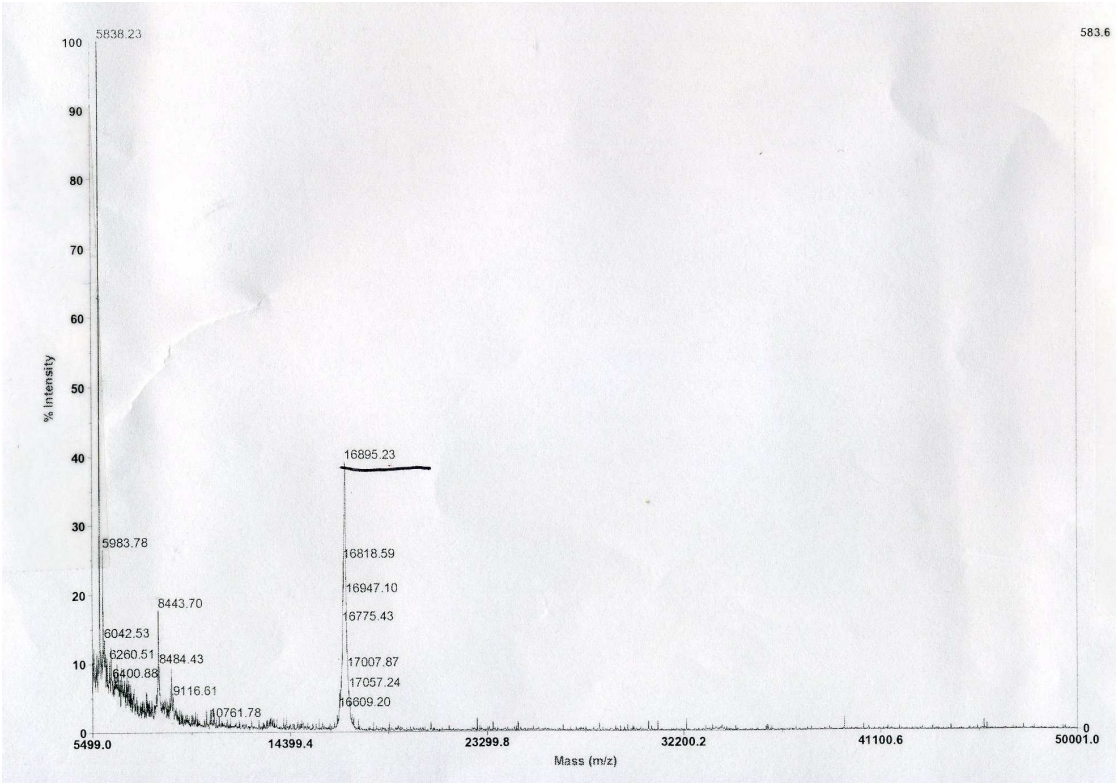
5838.23
583.6
100
90
80
70
60
50
40
30
20
10
0
% Intensity
16895.23
5983.78
16818.59
16947.10
8443.70
16775.43
6042.53
6260.51
8484.43
17007.87
6400.88
17057.24
9116.61
16609.20
10761.78
0
5499.0
14399.4
23299.8
32200.2
41100.6
50001.0
Mass (m/z)

C

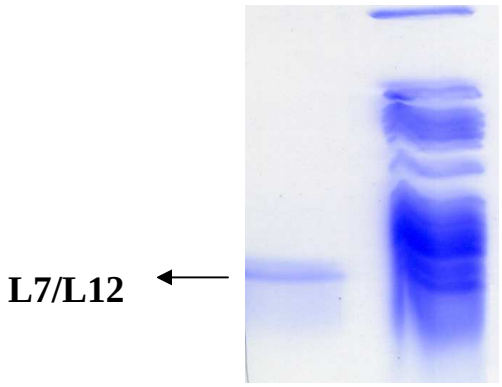

D

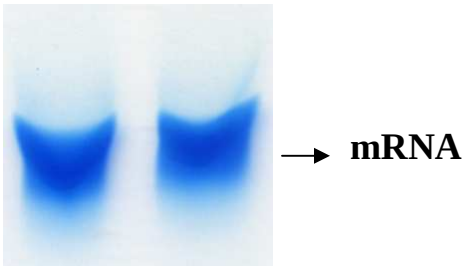

Figure 2.3. PAGE and MALDI analyses. For the PAGE analyses, the bands shown for the purified samples were the only ones seen in the full gel**.** (A) 14% SDS-PAGE analysis of L11 protein after MonoS column. The first lane is the initial sample, the second lane is the flow-through, and the subsequent lanes are the collected L11-containing fractions. The dual bands might be due to proteolysis of L11 during preparation of sample for PAGE analysis because only one peak at 16895 a.m.u (calculated His-tagged L11 MW 16.922 kD) was observed by MALDI analysis of the MonoS-purified fractions (B). (C) 16.5% SDS-PAGE analysis of L7/L12 protein (left lane) stripped from wild type ribosome (right lane). (D) Urea-PAGE analysis of 022AUGmRNA.

M G S S H H H H H H S S G L V P R G S H M A K K V Q A Y V K L Q V A A G M A N P S P P V G P A L G Q Q G V N I M E F C K A F N A K T D S I E K G L P I P V V I T V Y A D R S F T F V T K T P P A A V L L K K A A G I K S G S G K P N K D K A G K I S R A Q L Q E I A Q T K A A D M T G A D I E A M T R S I E G T A R S M G L V V E D

Figure 2.4. The sequence of His-tagged L11.

A

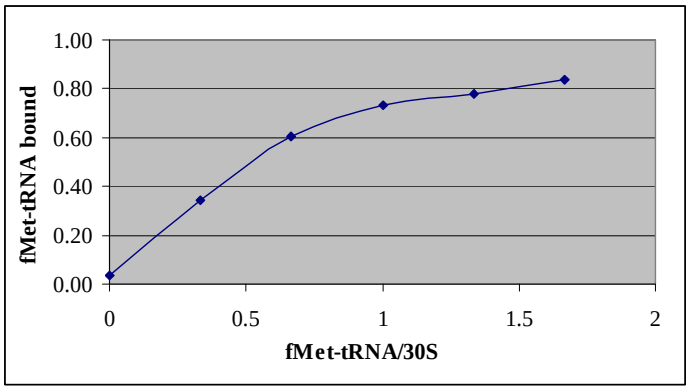
1.00
0.80
0.60
0.40
0.20
0.00
fMet-tRNA bound
0
0.5
1
1.5
2
fMet-tRNA/30S

B

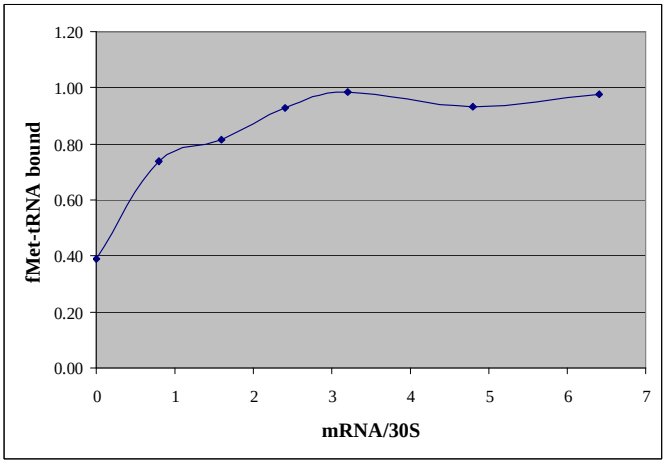
1.20
1.00
0.80
0.60
0.40
0.20
0.00
fMet-tRNA bound
0
1
2
3
4
5
6
7
mRNA/30S

C

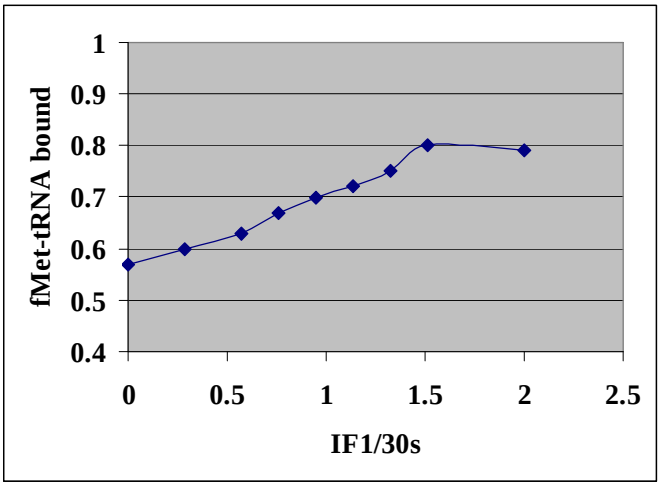
1
0.9
0.8
0.7
0.6
0.5
0.4
fMet-tRNA bound
0
0.5
1
1.5
2
2.5
IF1/30s

D

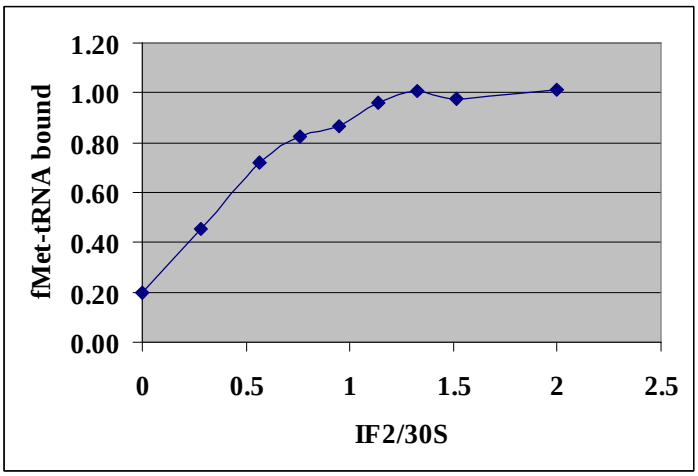

E

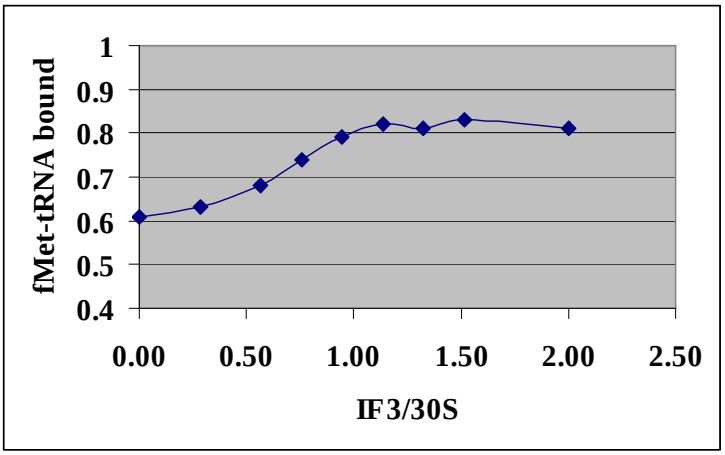

Figure 2.5. The activities of fMet-tRNA^{fMet} (A), mRNA (B), IF1 (C), IF2 (D) and IF3(E) binding to pre-30S initiation complex. [^{35}S]-fMet-tRNA^{fMet} was incubated with 30S subunit, IF1, IF2, IF3, GTP in buffer A at 37 ºC for 15 min followed by filtration on nitrocellulose filters. The experiments used different concentrations of fMet-tRNA^{fMet} (A), mRNA (B), IF1 (C), IF2 (D), or IF3 (E). For the components that were not varied, the concentrations were 0.30 µM 30S, 0.45 µM IF1, 0.45 µM IF2, 0.45 µM IF3, 0.9 µM mRNA, 0.45 µM [^{35}S]-fMet-tRNA^{fMet}.

A

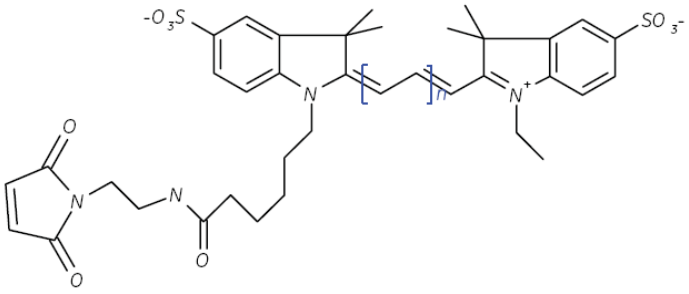

where n = 1 or 2 for Cy3 or 5

B

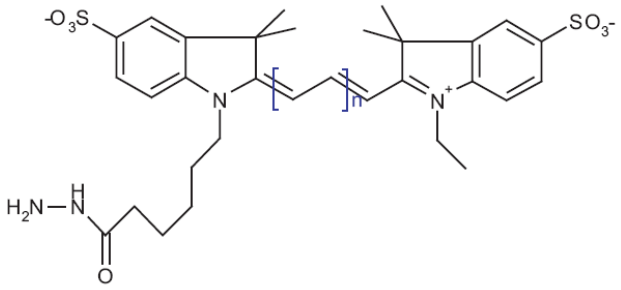

where n = 1 or 2 for Cy3 or 5

Figure 2.6. Structures of Cy3 and Cy5. (A) Cy3 or Cy5 maleimide. (B) Cy3 or Cy5 hydrazide.

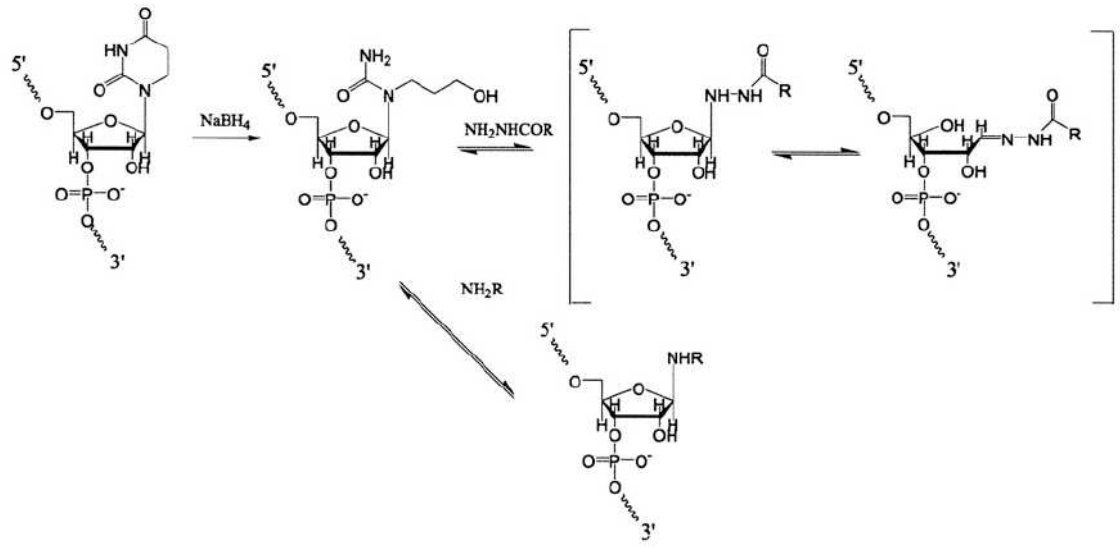

Figure 2.7. The labeling scheme (Pan et al., 2009). Reductive cleavage of dihydrouridine by sodium borohydride, yielding 3-ureidopropanol, has been described by Cerutti and Miller (1967).

A

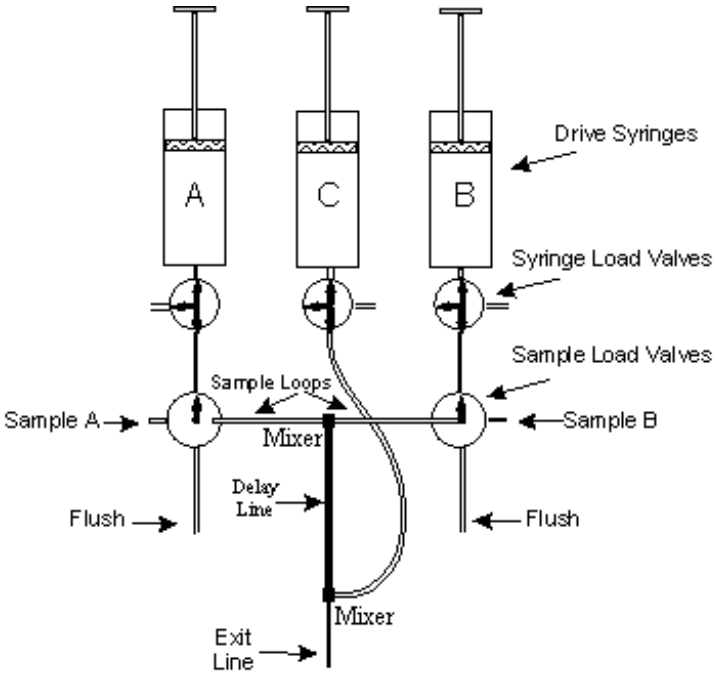

B

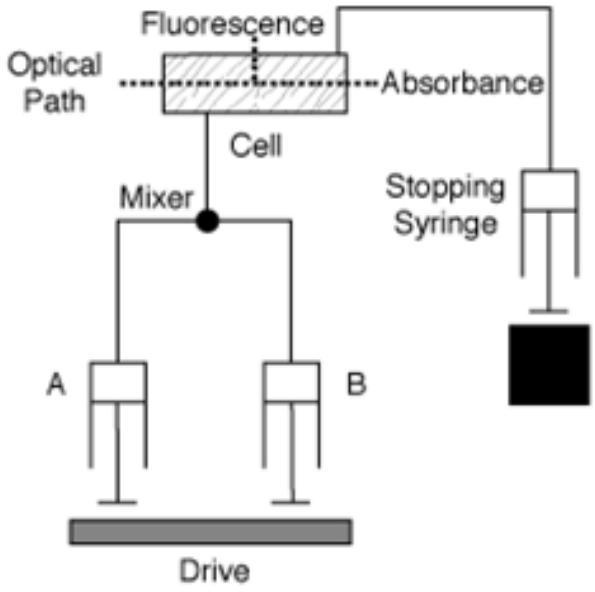

Figure 2.8. Diagrams of rapid kinetic instruments. (A) Quench flow. (B) Stopped flow.

CHAPTER 3

IF2 INTERACTION WITH THE RIBOSOMAL GTPASE-ASSOCIATED CENTER DURING 70S INITIATION COMPLEX FORMATION

3.1 ABSTRACT

Addition of an E. coli 50S subunit containing a Cy5-labeled L11 N-terminal domain (L11-NTD) within the GTPase-associated center (GAC) to an E. coli 30S initiation complex containing Cy3-labeled B. stearothermophilus initiation factor 2 (Bst-IF2), leads to rapid development of a FRET signal. FRET efficiency increases as the initially-formed 70S ribosome is converted to the 70S initiation complex (70SIC) (Grigoriadou et al., 2007), demonstrating the ability of IF2 to induce conformational change within the inherently flexible GAC. Movement of IF2 toward L11-NTD following initial 70S ribosome formation is analogous to movement of EF-G following its binding to the ribosome (Seo et al., 2006). However, the rate with which such movement occurs has a much weaker dependence on GTP hydrolysis for IF2 than for EF-G, perhaps reflecting the more critical role of GTP hydrolysis in translocation than in 70SIC formation. The increase in FRET efficiency can also be used to monitor the fidelity function of initiation factor IF3 during 70SIC formation and provides evidence that conformational changes in the ribosome resulting from IF2-GTPase modulate IF3 function. While Bst-IF2 is fully functional as a substitute for E. coli IF2 in formation of E. coli 70SIC, relative reactivities toward dipeptide formation of 70SICs formed with the two IF2s suggests that Bst-IF2.GDP is more difficult to displace from the GAC than E. coli IF2.GDP.

3.2 INTRODUCTION

Initiation factor 2 (IF2) is a G-protein that plays a crucial role in the initiation of procaryotic protein synthesis, interacting directly with fMet-tRNA^{fMet}, favoring its decoding in the P-site, and physically linking the 30S and 50S subunits in the 70S initiation complex (70SIC) (Gualerzi and Pon, 1990; Boelens and Gualerzi, 2002; Ramakrishnan, 2002; Laursen et al., 2005; Gualerzi et al., 2001). It shares a common binding locus on the ribosome, the GTPase associated center (denoted GAC), with other G-proteins utilized in protein synthesis, such as elongation factor G (EF-G). The GAC includes 23 S rRNA helices 42-44, the associated proteins L11, L10, and at least one L7/L12 protein (Li et al., 2006; Connell et al., 2007). Cryoelectron microscopy (cryo-EM) studies have indicated that both EF-G·GTP and IF2·GTP binding to the ribosome are accompanied by large conformational changes in the ribosome, and that, in both cases, further conformational changes in the ribosome·G-protein complex are seen following GTP hydrolysis (Agrawal et al., 1999; Agrawal et al., 2001; Myasnikov et al., 2005; Allen et al., 2005).

The N-terminal domain of L11 (L11-NTD) is a particularly mobile portion of the ribosome that, following GTP hydrolysis, approaches the G' domain of EF-G (Agrawal et al., 2001; Diaconu et al., 2005; Schuwirth et al., 2005). In earlier work utilizing single-turnover fluorescence resonance energy transfer (FRET) measurements, we determined that rapid movement of the G' domain toward L11-NTD within the *E. coli* ribosome requires prior GTP hydrolysis and, via branching pathways, either precedes Pi release

(major pathway) or occurs simultaneously with it (minor pathway) (Seo et al., 2006). In this latter work fluorescent groups were placed on the Cys 38 within L11-NTD and on a suitable residue within the G' domain.

Here we utilize a similar approach to determine whether there is a comparable movement toward L11-NTD of the G1-domain of IF2 (IF2 lacks a G' domain) during 70SIC formation from 30S initiation complex (30SIC) and 50S subunit. The cryo-EM structures of 70S complexes containing fMet-tRNA^{fMet}, mRNA and either IF2.GDPCP (a nonhydrolyzable analogue of GTP) or IF2·GDP (*11*) result in an estimated distance of 50 – 55 Å between the α-carbons of residue 378 in IF2 and residue 38 in L11 (Figure 4.1), quite suitable for probing by measurement of FRET efficiency. Accordingly, we employ 50S subunits containing protein L11 labeled with Cy5 at position 38 (denoted L11^{Cy5}) and *B. stearothermophilus* IF2 (Bst-IF2) labeled with Cy3 at position 378 (denoted Bst-IF2^{Cy3}) (Marzi et al., 2003).

Substituting Bst-IF2 for Eco-IF2 has been shown to facilitate the characterization of translation intermediates, due to the higher stability of the complexes that Bst-IF2 forms with *E. coli* ribosomes and ribosomal subunits as compared with Eco-IF2 (Marzi et al., 2003; La Teana et al., 1996). Such substitution is reasonable in view of substantial evidence that Bst-IF2 is functionally interchangeable with Eco-IF2 in *E. coli* protein synthesis. Thus, Bst-IF2 complements an *E. coli infB* null mutation *in vivo* (E. Caserta and C. Gualerzi, private communication). In addition, *in vitro* studies demonstrate the near equivalence of Eco-IF2, Bst-IF2, and Bst-IF2^{Cy3} in binary complex formation with

E. coli fMet-tRNA^{fMet} (Wu and RajBhandary, 1997), in stimulating of AUG-dependent fMet-tRNA^{fMet} binding to *E. coli* 30S subunits and 70S ribosomes (Brombach et al., 1986) and in kinetic measures of 70SIC formation (La Teana et al., 1996; Grigoriadou et al., 2007; work reported herein).

We find that FRET efficiency increases as the 70S ribosomes formed initially from 30SIC and 50S subunits are transformed into the 70SIC, and that the rate of such increase depends on GTP hydrolysis, paralleling results obtained with EF-G. We further demonstrate that the increase in FRET efficiency can be used to monitor the fidelity function of the initiation factor IF3 during 70SIC formation.

3.3 RESULTS

In the work described below we use the FRET signal between a 30SIC containing Bst-IF2^{Cy3} and a 50S subunit containing L11^{Cy5} to monitor the relative movement of IF2 with respect to L11 during 70SIC formation. Below we first demonstrate that, with minor qualifications, Bst-IF2^{Cy3} and L11^{Cy5} are acceptable functional analogues of Eco-IF2 and unlabeled L11, respectively, before presenting our FRET results.

3.3.1 Bst-IF2 and Bst-IF2^{Cy3} as functional analogues of Eco-IF2 with respect to 70SIC formation and reactivity

In the presence of IF3, 30S association with 50S subunits to form 70SIC is completely dependent on the presence of IF2 (Grigoriadou et al., 2007). Here we carry

out four rapid kinetics measures (increase in light scattering, IF2-dependent single turnover GTP hydrolysis and subsequent Pi release, increase in fMet-tRNA^{fMet} (prf20) fluorescence) that we previously employed in formulating a detailed quantitative kinetic scheme for 70SIC formation from 30SIC and 50S subunit (Grigoriadou et al., 2007) to compare the functionalities of Eco-IF2 (30SIC^{Eco}), BSt-IF2 (30SIC^{Bst}), and Bst-IF2^{Cy3} (30SIC^{Cy3}) in this process. We also compare the reactivities of the three 70SICs formed in dipeptide formation. Our results show that all three 30SICs have similar rates of 70SIC formation, but that the reactivity of the 70SIC in dipeptide formation is somewhat faster in the presence of Eco-IF2 vs. either of the Bst-IF2s.

The increase in light-scattering on addition of 30SIC to 50S subunit is well described as a 2-phase process (Figure 3.2A), with the first corresponding to initial binding of the 50S subunit to 30SIC to form a labile 70S complex and the second reflecting conversion to the more stable 70SIC. These two phases have apparent rate constants LS1 and LS2. Initial 70S formation is followed by GTP hydrolysis (Figure 3.2B), with an apparent rate constant (GTP1) that is similar to or somewhat smaller than LS1. Pi release proceeds via a lag phase, with an apparent rate constant Pi1, similar in magnitude to LS2, followed by the Pi release step, with an apparent rate constant Pi2 (Figure 3.2C). The increase in fluorescence of fMet-tRNA^{fMet}(prf20) on 70SIC formation, which could not be measured for Bst-IF2^{Cy3} because of fluorophore interference, is also preceded by a lag phase (Figure 3.2D), with apparent rate constants for both phases, fMet1 and fMet2, that are similar in magnitude to the values of Pi1 and Pi2.

Values for each of the apparent rate constants mentioned above are collected in Table 1. From these values, as well as by direct inspection of Figures 3.2A-D, we conclude that 70SIC formation proceeds in a very similar manner with either $30SIC^{Eco}$, $30SIC^{Bst}$, or $30SIC^{Cy3}$. Some small quantitative differences include larger overall light scattering changes falling in the order Bst-$IF2^{Cy3}$ > Bst-IF2 > Eco-IF2, and GTP1 values decreasing in the order Eco-IF2>BSt-IF2> Bst-$IF2^{Cy3}$.

The functionality of the three 70SIC complexes in fMetPhe-$tRNA^{Phe}$ formation following addition of the Phe-$tRNA^{Phe}$.EF-Tu.GTP ternary complex was determined either following rapid mixing of each of the pre-formed 30SICs with 50S subunits and the cognate TC, or following rapid mixing of each of the pre-formed 70SICs with cognate TC (Figure 3.2E, Table 3.2). Comparable reactivities (k'_{dp}) were found following the first protocol, with apparent rate constants falling in the order $30SIC^{Eco}$ ($0.28 \pm 0.06\ s^{-1}$) > $30SIC^{Cy3}$ ($0.18 \pm 0.06\ s^{-1}$) ~ $30SIC^{Bst}$ ($0.14 \pm 0.03\ s^{-1}$). On the other hand, the second protocol, while leaving the apparent rate constant (k^*_{dp}) for $30SIC^{Bst}$ essentially unchanged ($0.12 \pm 0.02\ s^{-1}$), leads to a marked increase k^*_{dp} found with $30SIC^{Eco}$ ($1.6 \pm 0.2\ s^{-1}$).

The latter difference may be related to the more stable binding within the 70SIC of Bst-IF2·GDP than Eco-IF2·GDP (La Teana et al., 1996; Qin et al., in preparation). Thus, productive binding of TC leading to dipeptide formation requires, at a minimum, movement of IF2 away from its canonical position within the 70SIC (Myasnikov et al., 2005), allowing TC binding to the GAC, if not full IF2 dissociation from the ribosome.

Such movement (or dissociation) might be partially rate-determining for dipeptide formation when 50S subunit and TC are added simultaneously to 30SIC, consistent with earlier results of Tomsic et al. (Tomsic et al., 2000), but might already be completed, at least for the more weakly bound Eco-IF2, when TC is added to pre-formed 70SIC, resulting in more rapid dipeptide formation.

3.3.2 $50S^{Cy5}$ as a functional analogue of wt-50S with respect to 70SIC formation and reactivity

Having established the functionality of $30SIC^{Cy3}$, we next use $30S^{Cy3}$ to compare $50S^{Cy5}$ with wt-50S with respect to three single-turnover kinetic (GTP1 and the apparent rate constants for dipeptide and fMet-puromycin formation) and three single-turnover stoichiometric (GTPase, dipeptide, fMet-puromycin) measures of 70SIC formation and reactivity. The results, as displayed in Figure 3.3A,B and Table 3.2 (along with more limited results for $50S^{L11}$ and $50S^{-L11}$) show $50S^{Cy5}$ to be a good functional analogue of wt-50S, with the only significant difference in these six measures being found for the value of k'_{dp} (fMet-Phe formation), 0.18 ± 0.06 s^{-1} and 0.07 ± 0.01 s^{-1} for wt-50S and $50S^{Cy5}$, respectively. Furthermore, pre-formed 70S ribosomes have virtually identical activities in poly(U)-dependent poly(Phe) synthesis, whether made with wt-50S or $50S^{Cy5}$ subunits (Figure 3.3C).

There is a significant decrease in the GTPase stoichiometry obtained with $50S^{-L11}$ subunits (Figure 3.3A, Table 3.2), consistent with earlier results showing that $50S^{-L11}$

subunits are somewhat defective in forming 70SIC from 30SIC (Naaktgeboren et al., 1976; Gütz et al., 1989). However, even the $50S^{-L11}$ subunits show appreciable activity in polyPhe synthesis (Figure 3.3C), in agreement with earlier results (Cundliffe et al., 1979, Cohlberg et al., 1976).

3.3.3 FRET changes accompanying 70SIC formation from $30SIC^{Cy3}$ and $50S^{Cy5}$

The experiments described above establish the basic functionality of $30SIC^{Cy3}$ and $50S^{Cy5}$ in 70SIC formation, making it likely that the FRET experiments described below that measure FRET during the combination of these modified subunits will be relevant for understanding the process of 70SIC formation from native, unmodified subunits. Long term incubation (15 min, 37 ^{o}C) of $30SIC^{Cy3}$, containing a fluorescent donor (D), with $50S^{Cy5}$ subunits containing a fluorescence acceptor (A) results in formation of the double-labeled 70SIC (DA sample) and the generation of a strong FRET signal (Figure 3.4A), with considerable decreases and increases in donor and acceptor fluorescence signals, respectively, as compared with the fluorescence of the D ($30SIC^{Cy3}$ plus $50S^{L11}$) and A ($30SIC^{Bst}$ plus $50S^{Cy5}$) samples. In fact, the donor decrease shown in Figure 3A underestimates FRET efficiency, given the intrinsic rise in donor fluorescence that accompanies 70SIC formation when $30SIC^{Cy3}$ is rapidly mixed with unlabeled $50S^{L11}$ subunits (Figure 3.4B). By contrast, there is no corresponding change in acceptor fluorescence when $30SIC^{Bst}$ replaces $30SIC^{Cy3}$ (Figure 3.4B). The similarity in acceptor fluorescence intensity at the two $30SIC^{Cy3}$ concentrations employed in Figure 3.4A

indicates that essentially all of $50S^{Cy5}$ is taken up within the 70SIC at the higher 30SIC concentration. These results permit calculation of a FRET efficiency in the 70SIC complex of ~50% by application of eq 2 (Chapter 2).

3.3.4 Changes in FRET vs. changes in light scattering during 70SIC formation

Strong evidence that the FRET signals seen in Figure 3.4 are a direct consequence of 70SIC formation is provided by results in Figure 3.5 A showing no such appearance of a FRET signal, measured as the increase in Cy5 fluorescence, when fMet-$tRNA^{fMet}$ is omitted from the reaction mixture. This is in accord with recent results showing that, in the presence of IF3, fMet-$tRNA^{fMet}$ is required for 70SIC formation (Grigoriadou et al., 2007; Antoun et al., 2004; Antoun et al., 2006).

The increase in light scattering on formation of 70SIC from 30SIC and 50S subunit provides another measure of 70SIC formation (Grigoriadou et al., 2007). Comparison of the time dependence of the increase in FRET efficiency for the complete system (i.e., including fMet-$tRNA^{fMet}$) with the corresponding increase in light scattering, measured on identical samples (Figure 3.5A), clearly shows that both increases proceed in more than one phase, with both showing an initial rapid phase that is somewhat more pronounced for the light scattering change (Grigoriadou et al., 2007) than for the FRET change. As with FRET change, the rapid increase in light scattering is abolished when fMet-$tRNA^{fMet}$ is omitted.

The experiments shown in Figure 3.5A were conducted with both $IF2^{Cy3}$ and $50S^{Cy5}$ subunits present in excess over 30S subunits. Under these conditions, the time courses of FRET and light scattering increases are directly comparable, with virtually all 30S subunits in the sample containing $IF2^{Cy3}$ as part of the 30SIC and all $30SIC^{Cy3}$ interacting with $50S^{Cy5}$. Other conditions, such as those employed in Figure 5B (30S > $IF2^{Cy3}$ > $50S^{L11}$; 50S > 30S > $IF2^{Cy3}$), lead to multiphasic increases in light scattering that reflect sample heterogeneity and are unsuitable for directly comparing increases in FRET and light scattering. Thus, slow phases of light scattering are observed when either 50S subunit concentration is limiting, due to the presence of a minor fraction (< 20 %) of 50S subunits that lack L11 ($50S^{-L11}$) and form 70SIC complexes only very slowly (data not shown –see also Naaktgeboren et al., 1976; Gütz et al., 1989), or when $IF2^{Cy3}$ is limiting, since 30S initiation complexes formed in the presence of IF3 but lacking IF2 also form 70SIC very slowly (Grigoriadou et al., 2007). Such sample heterogeneity is not a problem for FRET measurements, which only measure rapid 70SIC formation events between 30SICs containing Bst-$IF2^{Cy3}$ and 50S subunits containing $L11^{Cy5}$. The rate of Pi release is also shown in Figure 3.5B for direct comparison with the rate of FRET increase.

The results in Figures 5A and 5B can be globally fit to the minimal Scheme 1 (Figure 3.5C), in which an initial binding reaction to form $70S_I$ ribosomes (step 1), giving rise to a FRET signal with concomitant GTP hydrolysis (Figures 3.2B, 3.3A), is followed by a conformational change (step 2), resulting in formation of $70S_{II}$ ribosomes, from which Pi is released (step 3). In carrying out this fitting the light scattering increase due to $70S_I$,

$70S_{II}$, or 70SIC formation is assumed to be identical (Antoun et al., 2004). Constraining the FRET efficiencies to also be the same for all three 70S species led to poor fits to the FRET data. However, setting the relative FRET efficiency (RFE) for 70SIC equal to 1.0 and allowing the RFEs of the other 70S species to be different led to best-fit values of 0.57 and 1.00 for $70S_I$ and $70S_{II}$, respectively. This point is made graphically in the inset to Figure 5A which shows that the ratio, normalized FRET change: normalized light scattering change, increases as $70S_I$ is converted to $70S_{II}$ and does not change thereafter. We conclude that the L11-NTD gets closer to the G1 domain of IF2 as $70S_I$ is converted to $70S_{II}$, and that this movement follows GTP hydrolysis and precedes Pi release.

3.3.5 GTP hydrolysis accelerates the increase in FRET efficiency following 70S formation

The previous conclusion led us to examine whether GTP hydrolysis was required for the increase in FRET efficiency within the 70S complex by replacing GTP with its nonhydrolyzable analogue GDPNP. We initially attempted to compare light scattering and FRET changes in the presence of GDPNP under conditions (50S > IF2 >30S) exactly paralleling those we had used in the presence of GTP (Figure 3.5A). As seen in Figure 6A, replacement of GTP by GDPNP during 70SIC formation leads to only a small decrease in the magnitude of light-scattering increase, with little change in the rate of such increase. However, these conditions are not suitable for measuring FRET changes during 70SIC formation, since a rapid and significant change in FRET signal is seen even

in the absence of 70S formation (i. e., with fMet-tRNA^{fMet} omitted, Figure 3.6B), presumably reflecting direct binding of Bst-IF2^{Cy3}.GDPNP to 50S^{Cy5}. No such signal is seen in the presence of GTP (Figure 3.5A), because of the rapid hydrolysis of GTP within the 50S.IF2·GTP complex, and the relatively weak binding of IF2·GDP to 50S subunits (Grigoriadou et al., 2007).

Accordingly FRET experiments were carried out under conditions (30S > IF2 > 50S) minimizing 50S.IF2.GDPNP formation, as seen by the very small FRET change when fMet-tRNA^{fMet} is omitted (Figure 3.6C). Under these conditions, the total FRET change seen with GDPNP is similar to that seen with GTP, but the time development is different, with the initial rise occurring slightly faster with GDPNP and the full FRET change occurring much more slowly.

The light scattering results in the presence of GDPNP were well fit assuming biphasic kinetics. In contrast, fitting the FRET results required three phases, and show an approximate doubling in the apparent FRET efficiency during the slow third phase (k_{app} ~0.2 s^{-1}) when, on the basis of the light scattering results, little additional 70S formation would be expected. Taken together, the results in Figure 3.6A and 3.6C are consistent with a kinetic scheme for 70SIC formation in the presence of GDPNP that is similar to Scheme 1 for GTP (Figure 3.5C), except that step 3 would be reversible and the increase in FRET efficiency following 70S formation occurs later in the process. It would thus appear that GTP hydrolysis accelerates, but is not essential for, the movement of L11-

NTD toward the G1 domain of IF2 as the initial 70S complex formed is converted to 70SIC.

3.3.6 FRET monitoring of the fidelity function of IF3

Earlier we showed that the rate and magnitude light scattering increase provided a sensitive measure of the ability of IF3 to discriminate between a canonical (AUG) and a non-canonical (AUU) initiation codon in 70SIC formation (Grigoriadou et al., 2007b). The increase in FRET efficiency accompanying 70SIC formation also provides a sensitive probe of such discrimination (Figure 3.7). Thus, in the presence of IF3, substituting AUU (trace 3) for AUG (trace 1) leads to large decreases in both the rate and extent of FRET efficiency increase, whereas in the absence of IF3 the apparent rate is little affected, and the extent of increase is somewhat increased (traces 2 and 4). Identical trends were observed for light scattering changes (Grigoriadou et al., 2007b).

3.4 DISCUSSION

IF2 is a G-protein that is part of the 30SIC, and is retained within the 70SIC that is formed following reaction of the 30SIC with the 50S subunit (Myasnikov et al., 2005; Allen et al., 2005). Here we show that FRET measurement of IF2 interaction with L11-NTD can be used to monitor the relative motions of IF2 and the GTPase activation center during the process of 70SIC formation. We measure a FRET efficiency of 50% for the 70SIC complex, corresponding to an approximate fluorophore-fluorophore distance of 60

Å, equal to R_o (see Chapter 2). This value is in reasonable accord with the distances of 50 – 55 Å between the α-carbons of residue 378 in Bst-IF2 and residue 38 in L11 that can be estimated from cryo-EM structures of 70S complexes containing fMet-tRNA^{fMet}, mRNA and either IF2.GDPCP (another nonhydrolyzable analogue of GTP) or IF2·GDP (Myasnikov et al., 2005), since the distances between the dyes would be expected to be somewhat greater than the distances between the α-carbons to which they are attached.

Although IF2·GDP binds to 70S ribosomes less tightly than IF2·GTP (Grigoriadou et al., 2007), consistent with the cryo-EM results of Myasnikov et al. (Myasnikov et al., 2005) that indicate substantial differences in the overall interaction of IF2 with the 70S ribosome following GTP hydrolysis and Pi release, the results presented in Figure 5 indicate that the G1 domain of IF2 moves closer toward L11-NTD as part of the process by which the complex initially formed from 50S association with the 30SIC, $70S_I$·GDP·Pi in Scheme 1 (Figure 3.5C), is converted into the $70S_{II}$·GDP·Pi complex, preceding Pi release and 70SIC formation. We estimate this distance reduction as ~ 12 Å (eq 3); i.e., from 72 Å to 60 Å.

$$R = R_o\left(\frac{1}{E} - 1\right)^{1/6} \quad (3)$$

Scheme 1 is a minimal kinetic scheme that accounts quantitatively for the results presented in Figure 3.5. It is fully consistent with the more complete scheme for 70SIC formation that we proposed earlier (Grigoriadou et al., 2007; Grigoriadou et al., 2007b), with the one minor change that the binding of 30SIC^{Cy3} to 50S^{Cy5} is 2 - 3 fold weaker than to wt-50S. This earlier work, which employed a coumarin derivative of Bst-IF2,

labeled at position 451, and fMet-tRNA^{fMet}(prf) (Figure 3.2D), demonstrated that conversion of the initially formed 70S complex to 70SIC required two conformational changes, corresponding approximately to steps 2 and 3 in Scheme 1, with step 2 involving a change in IF2 fluorescence and step 3 involving a change in fMet-tRNA^{fMet} fluorescence.

Results presented in Figure 3.7 show that FRET changes can be used to demonstrate the ability of IF3 to discriminate between a canonical (AUG) and a non-canonical (AUU) initiation codon in 70SIC formation and are consistent with the notion, proposed by us earlier (Grigoriadou et al., 2007b), that such discrimination occurs during 70SIC formation. This notion has recently received direct support from some rate measurements of Milon et al. 2008 showing that 70S formation from 30SIC precedes IF3 dissociation, and contrasts with results of Antoun et al. (Antoun et al., 2006) indicating that IF3 dissociation from 30SIC precedes 70S formation. It is likely that the reason for this apparent disagreement has to do with the strong dependence of the rates of these two processes on mRNA sequence. Thus, both our earlier (Grigoriadou et al., 2007b) and current studies and those of Milon et al. 2008 employed ribosomes programmed with 022mRNA, which has a relatively short Shine–Dalgarno sequence (4 nt) separated from the AUG initiation codon by a long spacer (9 nt) and affords relatively rapid 70SIC formation. However, Milon et al. also found that use of 002mRNA, which has a long Shine–Dalgarno sequence (9 nt) and a shorter spacer (5 nt), leads to much slower 70S formation, which proceeds at the same rate as IF3 dissociation, consistent with the results

of Antoun et al. 2006, who used an mRNA similar to 002mRNA.

The 70S ribosome is a labile structure that undergoes conformational changes on the binding of the G-proteins EF-G and IF2. Cryoelectron microscopy studies (Myasnikov et al., 2005; Allen et al., 2005) have shown not only that G-proteins bind to the same site on the 70S ribosome via their G(GTPase)-domains, but also that the conformational changes that result from G-protein binding as a GTP complex and from hydrolysis of the ribosome-bound GTP to GDP are similar for such proteins. This has led to the suggestion that ribosomal GTPases take advantage of the intrinsic flexibility of the ribosome to induce conformational changes that promote movement of mRNA and tRNA across the ribosome surface during the various steps of the protein synthesis cycle (Myasnikov et al., 2005; Frank et al., 2007; Cornish et al., 2008).

Our current and earlier related studies provide strong evidence that the analogy between the structures of the complexes that at least two G-proteins, IF2 and EF-G, make with the ribosome is maintained on a dynamic level as well. In particular, the kinetics of FRET efficiency increase between fluorescent derivatives of L11-NTD and either IF2 (labeled in the G1 domain, this work) or EF-G [labeled in the G'-domain (Seo et al., 2006) have two important points in common: 1) FRET efficiency increases, indicating a movement of the G-proteins toward L11-NTD, following GTP hydrolysis and prior to Pi release (Figure 3.5); and 2) the rate of attainment of the higher FRET efficiency state is considerably decreased on substitution of a nonhydrolyzable analogue for GTP, although the total increase in FRET efficiency is maintained (Figure 3.6C). These two points

provide strong evidence that at least some of the conformational changes attributed to GTPase activity are triggered by the hydrolysis step itself, in accord with earlier suggestions (Tomsic et al., 2000; Rodnina et al., 1997; Savelsbergh et al., 2003), that the high FRET efficiency state is the preferred mode of G-protein binding to the 70S ribosome, and that the conformational change necessary for the attainment of that state is accelerated by GTP hydrolysis rather than by Pi release.

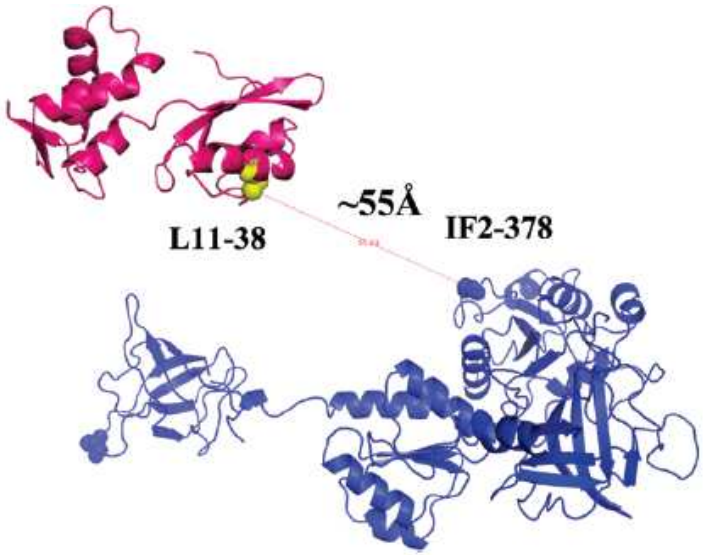

Figure 3.1. Distance between L11 residue 38 and IF2 residue 378 in a 70S.IF2.GMPPCP fMet-tRNA^{fMet}.mRNA complex. According to a cryoelectron microscopy structure (EMD-1172, Myaniskov et al., 2005).

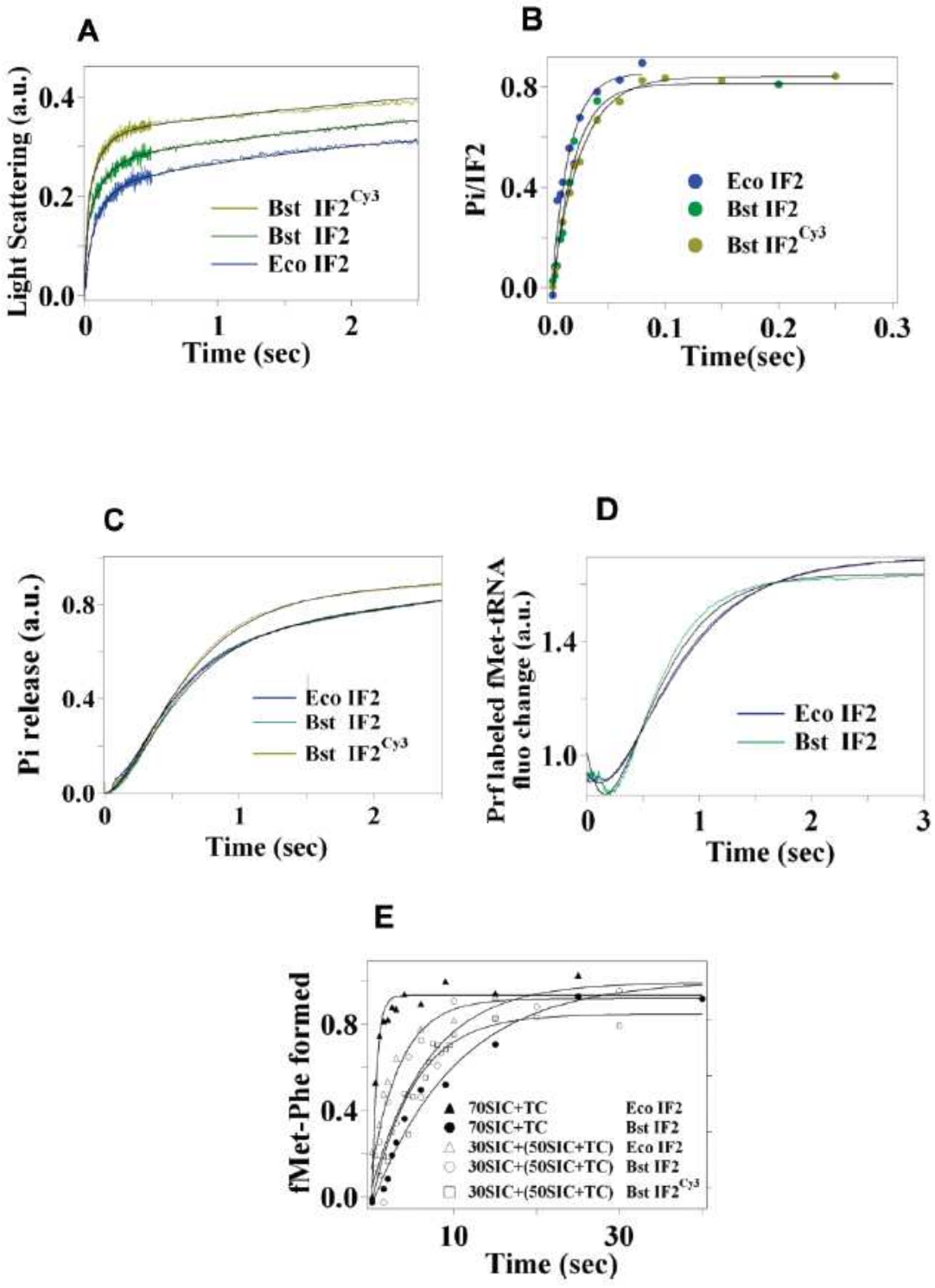
A
Light Scattering (a.u.)
0.0
0.2
0.4
0
1
2
Time (sec)
Bst IF2Cy3
Bst IF2
Eco IF2
B
Pi/IF2
0.0
0.4
0.8
0.0
0.1
0.2
0.3
Time(sec)
Eco IF2
Bst IF2
Bst IF2Cy3
C
Pi release (a.u.)
0.0
0.4
0.8
0
1
2
Time (sec)
Eco IF2
Bst IF2
Bst IF2Cy3
D
Prf labeled fMet-tRNA fluo change (a.u.)
1.0
1.4
0
1
2
3
Time (sec)
Eco IF2
Bst IF2
E
fMet-Phe formed
0.0
0.4
0.8
10
30
Time (sec)
70SIC+TC Eco IF2
70SIC+TC Bst IF2
30SIC+(50SIC+TC) Eco IF2
30SIC+(50SIC+TC) Bst IF2
30SIC+(50SIC+TC) Bst IF2Cy3

Figure 3.2. Measures of 70SIC formation and reactivity using different 30SICs. (A) Light scattering. (B) GTP hydrolysis; (C) Pi release; (D) fMet-tRNA^{fMet}(prf) fluorescence; (E) fMetPhe-tRNA^{Phe} formation. Experiments in (A), (C), and (D) were carried out by rapid mixing of the various 30SICs with wt-50S subunits in a stopped-flow spectrofluorometer. In all experiments except those in (E) with pre-formed 70SIC, 30S and 50S subunits were present in final concentrations of 0.3 µM and 0.5 µM, respectively. Preformed 70SIC in (E) was present at 0.3 µM. Other final concentrations were: IF2: 0.15 µM (A), (E); 0.45 µM (B) – (D). GTP: 100 µM (A), (C), (D); 36 µM (B); 200 µM (E). TC: 1.0 µM (E).

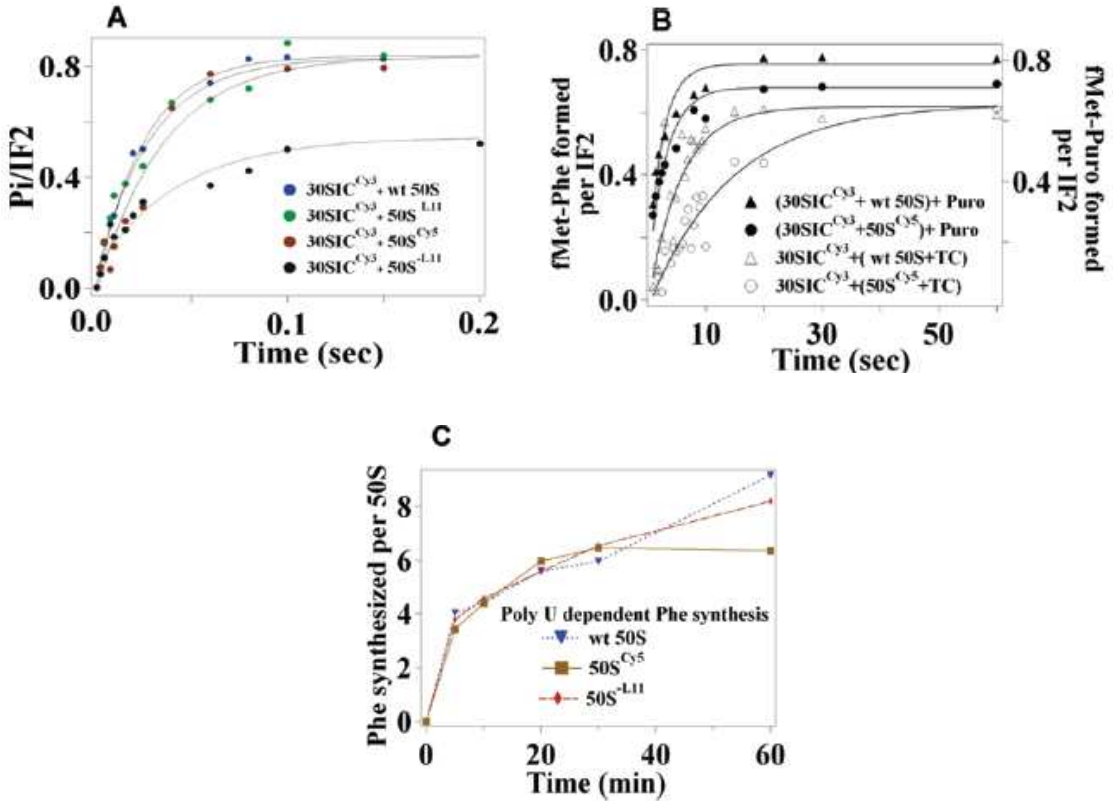

Figure 3.3. Measures of 70SIC formation and reactivity using different 50S subunits. (A) GTP hydrolysis; (B) fMetPhe-tRNA^{Phe} and fMet-puromycin formation; (C) Poly (U)-dependent polyPhe synthesis. fMetPhe-tRNA^{Phe} formation was carried out by rapid mixing of 30SIC^{Cy3} with 50S subunits and Phe-tRNA^{Phe}EF-Tu.GTP ternary complex. Final concentrations were: 50S, 0.5 µM; 30S, 0.3 µM; IF2, 0.15 µM. Other final concentrations were: GTP: 36 µM (A); 200 µM (B); puromycin, 2.5 mM (B). (C) see Materials and Methods. Results with wt-50S and 50S^{-L11} parallel those reported earlier.

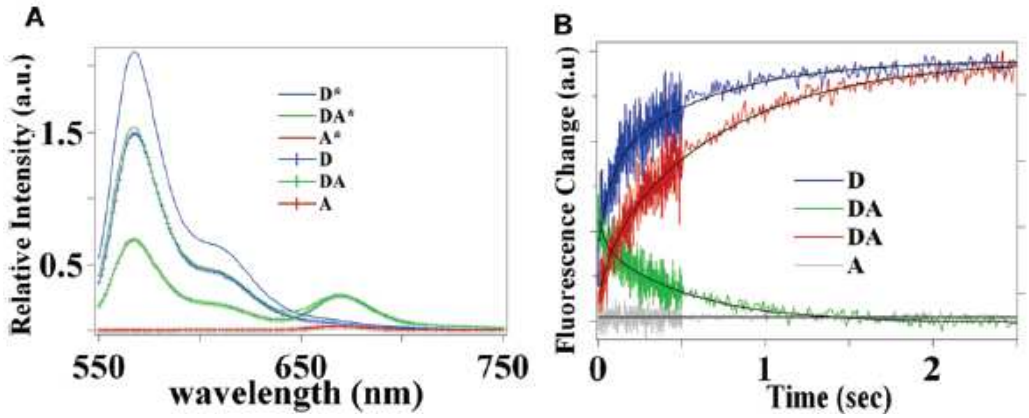

Figure 3.4. FRET between L11^{Cy5} and Bst-IF2^{Cy3} in the 70SIC complex. (A) After 70SIC formation. (B) During 70SIC formation. Excitation was at 540 nm. DA samples contain 30SIC^{Cy3} and 50S^{Cy5}; D samples contain 30SIC^{Cy3} and 50S^{L11}; A samples contain 30SIC^{Bst} and 50S^{Cy5}. In (A) 30SIC and 50S subunits were incubated at 37 ^{o}C for 15' prior to the taking of fluorescence spectra. Final concentrations were: 30S, 0.3 µM (hatched lines) or 0.6 µM (smooth lines); Bst-IF2 or Bst-IF2^{Cy3}, 0.15 (hatched lines) or 0.3 µM (smooth lines); 50S^{L11} or 50S^{Cy5}, 0.14 µM; GTP, 100 µM. In (B) 30SICs were rapidly mixed with 50S subunits. The D and A samples were monitored at 567 nm and 670 nm, respectively. The DA samples were monitored at both wavelengths, as indicated. Final concentrations were: 30S, 0.30 µM; IF2, 0.25 µM; 50S, 0.18 µM; GTP, 100 µM.

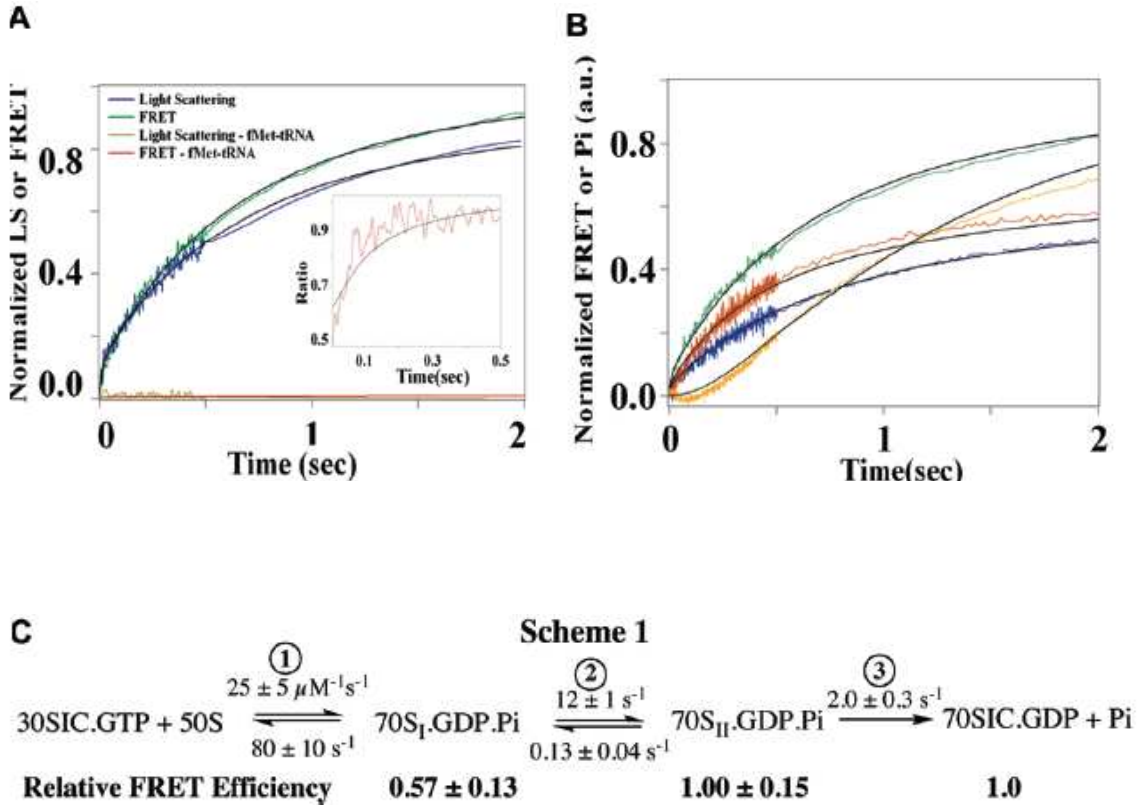

Figure 3.5. Measures of 70SIC formation on combining 30SIC^{Cy3} and 50S^{Cy5}: FRET, light scattering, and Pi formation. (A) Direct comparison of FRET (green trace, acceptor fluorescence – excitation 540 nm; monitoring 670 nm) and light scattering (blue trace – irradiation at 436 nm; monitoring via a 455 nm cutoff filter) changes during 70SIC formation. Both traces were determined for an identical solution having the following final concentrations: 30S, 0.3 μM; Bst-IF2^{Cy3}, 0.45 μM; 50S^{Cy5}, 0.60 μM. For ease of comparison, the changes in each value were normalized to the total

change seen at the plateau for each measurement (~ 10 s). The ratio of normalized FRET change to normalized light scattering change is plotted in the inset. When fMet-tRNA^{fMet} was omitted, virtually no changes were seen in either FRET (red trace) or light scattering (yellow trace). (B) FRET changes (green, red, and blue traces) and Pi formation (orange trace). Final concentrations employed: green and orange traces: 30S, 0.3 μM; Bst-IF2^{Cy3}, 0.45 μM; 50S^{Cy5}, 0.60 μM; blue trace: 30S, 0.6 μM; Bst-IF2^{Cy3} 0.50 μM; 50S^{Cy5}, 0.18 μM; red trace: 30S, 0.3 μM; Bst-IF2^{Cy3} 0.25 μM; 50S^{Cy5}, 0.50 μM. FRET changes are normalized for the total change seen at the plateau for the green trace, as in (A). The Pi release is normalized for the total change seen at the plateau, achieved at ~ 5s. Final GTP concentration in (A) and (B), 100 μM. All solid black lines are fits of the data to Scheme 1. (C) Scheme 1, the minimal scheme accounting quantitatively for 70SIC formation in the presence of GTP.

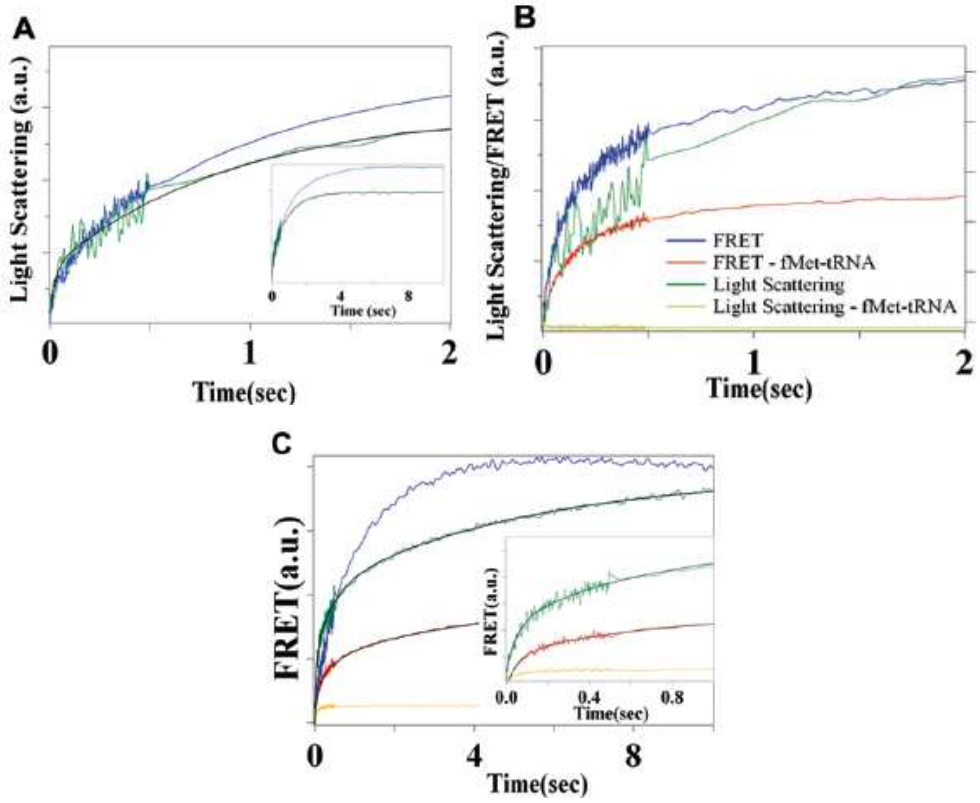

Figure 3.6. Measures of 70SIC formation when GDPNP replaces GTP. (A) Light scattering increase during 70SIC formation (blue trace, GTP; green trace, GDPNP). Inset: extension of results to 10 s. (B) FRET efficiency and light scattering increases during 70SIC formation measured in the presence of GDPNP. FRET efficiency, blue and red traces in the presence or absence of fMet-tRNA^{fMet}, respectively. Light scattering, green and yellow traces in the presence or absence of fMet-tRNA^{fMet}, respectively. (C) FRET efficiency increases during 70SIC formation. Blue trace: higher 30SIC concentration in the presence of GTP; green and orange traces, higher 30SIC concentration in the presence of GDPNP in the presence or absence of fMet-tRNA^{fMet},

respectively; red trace, lower 30SIC concentration in the presence of GDPNP. Inset: Expanded time scale. Final concentrations in (A) and (B) were 30S, 0.3 μM; Bst-IF2^{Cy3}, 0.45 μM; 50S^{Cy5}, 0.60 μM. Final concentrations in (C) were 30S, 0.6 μM; Bst-IF2^{Cy3}, 0.5 μM; 50S^{Cy5}, 0.18 μM (blue and green traces –higher 30SIC) or 30S, 0.3 μM; Bst-IF2^{Cy3}, 0.25 μM; 50S^{Cy5}, 0.18 μM (red trace – lower 30SIC). Final GTP or GDPNP concentration in (A) – (C), 100 μM. Solid black lines are fits of the GDPNP results to either a two-phase (light scattering) or three-phase (FRET) reaction. Fitted parameter values are: light scattering - k_{app1}, 35 ± 5 s^{-1}, k_{app2}, 1.10 ± 0.03 s^{-1}; FRET, higher 30SIC - k_{app1}, 20 ± 1 s^{-1}, k_{app2}, 2.2 ± 0.1 s^{-1}, k_{app3}, 0.19 ± 0.01 s^{-1}: relative FRET efficiency amplitudes; phase 1, 0.46 ± 0.05: phase 2, 0.51 ± 0.05: phase 3, 1.00. FRET, lower 30SIC - k_{app1}, 16 ± 1 s^{-1}, k_{app2}, 1.9 ± 0.1 s^{-1}, k_{app3}, 0.19 ± 0.01 s^{-1}: relative FRET efficiency amplitudes; phase 1, 0.64 ± 0.08: phase 2, 0.47 ± 0.06: phase 3, 1.00.

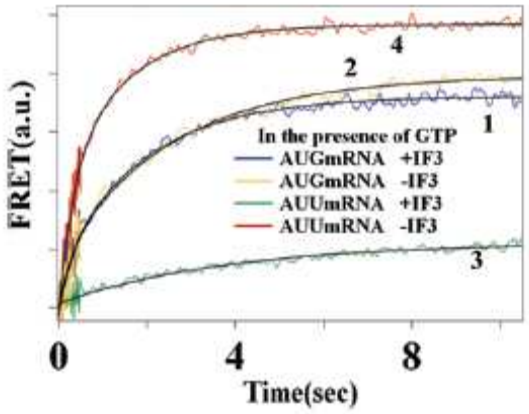

Figure 3.7. FRET monitoring of the fidelity function of IF3. The effect of IF3 on the rate and extent of FRET efficiency increase when the AUG initiation codon is replaced by AUU. 022AUG-mRNA, +IF3, blue trace; 022AUG-mRNA, -IF3, orange trace; 022AUU-mRNA, +IF3, green trace; 022AUU-mRNA, -IF3, red trace. Final concentrations were: $IF2^{Cy3}$, 0.15 µM; 30S, 0.3 µM; $50S^{Cy5}$, 0.14 µM; GTP, 100 µM.

Table 3.1. Functionality of different 30SICs with respect to 70SIC formation and reactivity[a]

Apparent rate constant (s^{-1})	$30SIC^{Eco}$	$30SIC^{Bst}$	$30SIC^{Cy3}$
LS1	61 ± 5	82 ± 5	65 ± 3
LS2	10 ± 1	8 ± 1	10 ± 1
GTP1	64 ± 13	53 ± 8	40 ± 2
fMet1	4.1± 0.4	5.2 ± 0.5	-
fMet2	1.6 ± 0.3	2.1 ± 0.2	-
Pi1	7.0 ± 0.5	7.0 ± 0.5	7.0 ± 0.5
Pi2	1.5 ± 0.1	1.3 ± 0.1	1.4 ± 0.1
k'_{dp}[b]	0.28 ± 0.06	0.14±0.03	0.18±0.06
k^*_{dp}[c]	1.6 ± 0.2	0.12±0.02	-

[a] reaction conditions as described in the legend to Figure 3.2

[b] dipeptide formation, rapid mixing of 30SIC with 50S subunits and cognate TC

[c] dipeptide formation, rapid mixing of 70SIC with cognate TC

Table 3.2. 50S subunit function in 70SIC formation: apparent rate constants and reaction stoichiometries

Parameter	wt-50S	$50S^{-L11}$	$50S^{L11}$	$50S^{Cy5}$
GTP1 (s^{-1})	41 ± 3	23 ± 6	37 ± 9	29 ± 6
Pi/IF2	0.85 ± 0.05	0.48± 0.04	0.83 ± 0.07	0.83± 0.04
$k_{,'dp}(s^{-1})$	0.18 ± 0.06	-	-	0.07 ± 0.01
fMetPhe/IF2	0.65 ± 0.07	-	-	0.66± 0.04
$k'_{puro}(s^{-1})$	0.42 ± 0.05	-	-	0.33 ± 0.04
fMet-puro/IF2	0.75 ± 0.03	-	-	0.65 ± 0.03

CHAPTER 4

SIMULTANEOUS BINDING OF G-PROTEINS TO THE RIBOSOME

4.1 ABSTRACT

Procaryotic ribosomal protein synthesis is carried out with the aid of four G-proteins (IF2, EF-Tu. EF-G, RF3) which share a common binding locus within the 70S ribosome that includes protein L11. Such sharing has lead to the commonly held view that simultaneous stable binding of two G-proteins to the ribosome is impossible, and that a ribosome-bound G-protein must dissociate before a second G-protein can bind. Here we use FRET experiments that measure IF2–L11 interaction within the ribosome as well as ribosome:G-factor co-sedimentation experiments to demonstrate that IF2 and EF-Tu can coexist stably on the ribosome, and that IF2 and EF-G can coexist at least transiently. We present a three-dimensional model demonstrating how such coexistence could be achieved and consider the role that multiple copies of ribosomal protein L7/L12 may play in multiple G-protein binding to the ribosome and G-factor exchange during polypeptide elongation.

4.2 INTRODUCTION

Procaryotic ribosomal protein synthesis is carried out with the aid of four G-proteins, initiation factor 2 (IF2), elongation factors EF-Tu and EF-G, and ribosomal release factor 3 (RF3). These factors participate in each of the four distinct stages of protein synthesis: initiation (IF2), culminating in the formation of 70S initiation complex (70SIC); elongation, proceeding via an alternation between pre-translocation (PRE) complex formation (EF-Tu) and post-translocation (POST) complex formation (EF-G); termination (RF3), involving the hydrolytic cleavage of complete polypeptide from peptidyl tRNA bound to the ribosome; and ribosome recycling (EF-G), resulting in the reformation of 50S and 30S subunits, the latter capable of re-initiation on a new mRNA. Cryoelectron microscopic (cryo-EM) structures (Agrawal et al., 1998; Klaholz et al., 2004; Stark et al., 2000; Stark et al., 2002; Valle et al., 2003a,b; Myasnikov et al., 2005; Allen et al., 2005) show these four protein factors to share a common binding locus, mainly located at the intersubunit space of the 70S ribosome and spanning two adjacent but distinct sites on the 50S subunit, the so-called GTPase associated center (denoted GAC and including 23S rRNA helices 42-44 and the associated proteins L11, L10, and at least one of the four L7/L12 proteins) and the sarcin-ricin loop (SRL) comprising 23S rRNA nucleotides (2646-2674) (Li et al., 2006; Connell et al., 2007).

An important and currently unresolved question is the mechanism by which one G-protein is exchanged for another as protein synthesis moves between these four stages, or,

during the elongation stage, as EF-Tu and EF-G bind alternatively to the ribosome. It has long been accepted that simultaneous stable binding of two G proteins to the ribosome is impossible. Thus, the failure of early attempts to obtain evidence for a stable complex containing both EF-Tu and EF-G (Richman and Bodley, 1972; Mesters et al., 1994) and the strong overlap between the binding sites for EF-G and EF-Tu seen by cryo-EM (Agrawal et al., 1998, 1999a; Stark et al., 2000; Valle et al., 2003a,b; Mitra and Frank, 2006; Connell et al., 2007) have led to current models of the elongation stage [e. g., Sergiev et al., 05a; Berk and Cate, 2007] in which EF-G must dissociate from the ribosome before EF-Tu, in the form of a ternary complex (TC) (aa-tRNA.EF-Tu.GTP) can bind. Similarly, the release of IF2 from the 70S ribosome following GTP hydrolysis has been deemed essential by some workers for formation of the first peptide bond (Lockwood et al., 1972; Caldas et al., 2000; Myasnikov et al., 2005), which requires TC binding, with comparison of cryo-EM structures of initiation and elongation complexes indicating an incompatibility for simultaneous binding of IF2 and EF-Tu (Myasnikov et al., 2005).

Each of the four G-protein proteins binds to the ribosomes more tightly as a GTP complex than as a GDP complex **(**IF2: La Teana et al., 1996; Luchin et al., 1999; Myasnikov et al., 2005; Grigoriadou et al., 2007**), (**EF-Tu: Pape etal., 1998**) (**EF-G: Pan et al., 2007**) (**RF3: Gao et al., 2007, Zavialov et al., 2003**),** leading to the plausible hypothesis that such weakened binding allows dissociation of one G-protein from the

ribosome prior to the association of another. Cryo-EM structures of ribosome complexes containing either IF2.GDPCP (a non-hydrolyzable analog of GTP) or IF2.GDP are consistent with this hypothesis (Myasnikov et al., 2005).

On the other hand there is some evidence that two G proteins can bind simultaneously to the 70S ribosome, IF2 and EF-G, from the work of Lockwood and Maitra (1974), and two copies of EF-G, from rapid kinetics results of our own (Seo et al., 2004). In addition, the fact that the first peptide bond can be formed regardless of GTP hydrolysis (Tomsic et al., 2000) led Brandi et al. (2004) to speculate that IF2 and EF-Tu could be bound simultaneously to the ribosome, with IF2 sliding or turning so as to occupy a position in which no steric clash with EF-Tu would occur.

Here we use results from FRET and co-sedimentation experiments to demonstrate that neither added TC nor EF-G displaces IF2 from the ribosome as it transitions from the 70S initiation complex (70SIC) to the elongation stage of polypeptide synthesis, and that EF-Tu and IF2 are able to bind simultaneously in a stable fashion to the ribosome. The implications of these findings for the general question of G-protein factor exchange are considered.

4.3 RESULTS

4.3.1 FRET evidence for simultaneous binding to 70S ribosomes of Bst-IF2 and either EF-Tu or EF-G

Elsewhere (Qin et al., 2009) we have shown that formation of functional 70SIC from 30SIC complexes containing Bst-IF2 labeled with Cy3 (Bst-IF2^{Cy3}) at position 378 in the G1 domain (Marzi et al., 2003), denoted 30SIC^{Cy3}, with 50S subunits containing ribosomal protein L11 labeled in position 38 within the N-terminal domain (L11-NTD), denoted 50S^{Cy5}, is accompanied by the generation of a FRET signal, diagnostic of IF2 interaction with L11-NTD within the 70S ribosome, which persists even after GTP bound to Bst-IF2 is hydrolyzed and Pi is released, with an estimated fluorophore-fluorophore distance of ~ 60 Å. Sample results demonstrating decreased donor (Cy3) fluorescence coupled with enhanced acceptor fluorescence (Cy5) are shown in Figure 1A. These results indicate that Bst-IF2^{Cy3}.GDP is stably bound to 70SIC, consistent with recent direct visualization of this complex obtained by cryo-EM (Myasnikov et al., 2005). Ribosome-bound Bst-IF2^{Cy3} can be readily exchanged with Bst-IF2 in solution, as evidenced by the large increase in donor fluorescence and decrease in acceptor fluorescence on Bst-IF2 addition (Figure 4.1B). However, both donor and acceptor fluorescence change to only minor extents, on addition of even large molar excesses of Phe-tRNA^{Phe}.EF-Tu.GTP ternary complex (TC) (Figure 4.1B, Figure 4.4). Although such addition has been shown to afford dipeptide formation (Qin et al., 2009), leading to PRE complex formation, the results in Figure 4.1B do not rule out the possibility that IF2 first dissociates from the ribosome, permitting TC binding, and then reassociates with the ribosome following EF-Tu.GDP dissociation.

To investigate this point further, we determined the dynamics of both FRET change, as monitored by acceptor fluorescence, on rapid mixing of $30SIC^{Cy3}$ with solutions of $50S^{Cy5}$ containing varying quantities of TC and EF-G, and, in parallel, of fMetPhe and fMetPhe-puro formation, using rapid quench assays. These experiments were conducted in two buffers that have been used extensively in studies of ribosome function, Buffer W (Figure 4.1C), a relatively high Mg^{2+} (7 mM) buffer which allows for high stoichiometries of tRNA binding **(**Pape et al., 1998; Savelsbergh et al., 2003; Pan et al., 2006, 2007**)** and polyamine buffer (Figure 5.1D), which employs a lower Mg^{2+} concentration in the presence of spermine and spermidine, and increases the accuracy of tRNA recognition (Rheinberger and Nierhaus 1987) and stabilizes the binding of E-site tRNA (Agrawal et al., 1999b; Dinos et al., 2005).

In the experiment shown in Figure 4.1C in Buffer W, the rapid rise in acceptor fluorescence corresponding to 70SIC formation, seen in the absence of TC, is followed by a small decrease for reactions carried out in the presence of saturating TC, which results in fMetPhe formation and PRE complex formation. The apparent rate constant for this decrease, $0.076 \pm 0.003\ s^{-1}$, is essentially identical to the apparent rate constant for fMetPhe formation, $0.08 \pm 0.01 s^{-1}$, suggesting that Bst-$IF2^{Cy3}$ re-orients within the 70S ribosome on TC binding, permitting dipeptide formation and PRE complex formation. Added TC has almost no effect on the rise in acceptor fluorescence in the first phase of reaction, and does not lead to a sharp transient drop in fluorescence thereafter, strongly

suggesting that IF2 remains bound to the ribosome throughout the process. For experiments conducted in polyamine buffer (Figure 4.1D), neither added TC, nor the combination of added TC and EF-G, which moves fMetPhe-tRNA^{Phe} to the puromycin-reactive P- position as a result of POST complex formation, have appreciable effects on the change in acceptor fluorescence that accompanies 70SIC formation. These results strongly suggest that IF2 remains bound to the ribosome throughout the first elongation cycle, which involves 70SIC conversion to PRE complex, which is in turn converted to POST complex.

Overall, the experiments presented in Figure 4.1 presenting compelling evidence that either EF-Tu or EF-G can coexist on 70S ribosomes with IF2, at least transiently, but leave open the question of whether either EF-Tu or EF-G can stably co-exist with IF2 on the ribosome. This point is addressed directly below.

4.3.2 Co-sedimentation evidence for stable simultaneous binding to 70S ribosomes of IF2 and EF-Tu

Direct evidence for stable simultaneous binding of IF2 and EF-Tu to the ribosome was obtained by sucrose cushion co-sedimentation experiments, in which quantitative SDS-PAGE analysis was performed on the proteins extracted from ribosomal pellet. Shown in Figure 4.2 are results from 5 separate experiments, in which the pre-incubated ribosomal sample, prior to ultracentrifugation, contained: 1) 70SIC; 2) 70SIC + TC; 3)

70SIC + TC + kirromycin; 4) 70SIC + TC + EF-G.GTP; and 5) 70SIC + TC + EF-G.GTP + fusidic acid + puromycin. Here, kirromycin or the combination of fusidic acid and puromycin is added to stabilize EF-Tu.GDP (Wolf et al., 1977; Parmeggiani et al., 1985) or EF-G (Seo et al., 2006) binding to the ribosome, respectively. In the absence of these added antibiotics, neither EF-Tu nor EF-G is bound to the ribosome stably enough to be retained on ultracentrifugation. These experiments permit the conclusions that i) IF2 within 70SIC is bound tightly enough to cosediment with the ribosome (lane 1); ii) EF-Tu binding to the ribosome in the presence of kirromycin does not displace bound IF2 (lane 3); and iii) EF-G binding in the presence of fusidic acid leads to a weakening of IF2 binding but not a complete removal (lane 5).

More quantitative conclusions can be made for these and related experiments from the results summarized in Table 4.1. The results show that using ≥ 1.5-fold excess of Bst-IF2 in forming 70SIC results in stoichiometric retention of Bst-IF2 in the pelleted ribosome (experiment #9) and this stoichiometry is little affected by addition of excess TC in either the presence or absence of kirromycin (experiment #s 3, 4, 10). Futhermore, the sum of the stoichiometries of Bst-IF2 and EF-Tu that co-sediment with the ribosome clearly exceeds 1.0 (1.3 – 1.6 for experiment #s 2 – 4), demonstrating clearly that at least some of the sedimented ribosomes must contain both bound EF-Tu and bound Bst-IF2. The failure of added TC to displace Bst-IF2 from the ribosome in the co-sedimentation assay contrasts with the ability of Bst-IF2 added from solution to displace ribosome

bound Bst-IF2. This is shown by a large reduction in the amount of Bst-IF2^{Cy3} co-sedimenting with ribosomes, as determined by $\mathbf{A_{554nm}}$, in the presence of added Bst-IF2 (Table 4.2), in results paralleling those presented in Figure 4.1B.

In contrast to the high retention of Bst-IF2 (experiment #1), no detectable IF2 co-sediments with 70SIC made with Eco-IF2.GTP, with or without added TC and kirromycin (experiment #s 5 and 6). Since GTP bound with IF2 is rapidly hydrolyzed to GDP with release of Pi (Tomsic et al., 2000; Grigoriadou et al., 2007), the co-sedimentation results clearly demonstrate that Bst-IF2.GDP is more stably bound to 70S ribosomes than Eco-IF2.GDP, as suggested by other studies (La Teana et al. 1996; Qin et al., 2008). However, when 70SIC is made with GDPNP in place of GTP, Eco-IF2 is stoichiometrically retained (0.9 per ribosome). This result recalls those of Luchin et al. (1999) showing that, although wt-IF2 does not cosediment with 70S following GTP hydrolysis, such co-sedimentation is found for Eco-IF2 variants with inhibited GTPase activity. Strikingly, the high stoichiometry of co-sedimenting IF2.GDPNP is not reduced in the presence of added TC and kirromycin, which results in the co-sedimentation of 0.5 equivalents of EF-Tu (experiment # 8). Thus, Eco-IF2 or Bst-IF2 can be bound to the 70S ribosome simultaneously with EF-Tu.

Although binding of EF-G.GTP to the ribosome during translocation has no apparent effect on the IF2-L11 FRET signal (Figure 4.1D), it does lead to a clear decrease in the stoichiometry of co-sedimenting IF2 (experiment #s 11, 12 and 13). We

interpret the two sets of results as indicating that IF2 and EF-G can bind concurrently to the ribosome, but that bound EF-G weakens IF2 binding such that it is not fully retained during ultracentrifugation through a sucrose cushion. This interpretation is supported by the lack of effect on retained IF2 of using a large excess of EF-G (experiment #s 12 and 13), or of adding fusidic acid and puromycin (experiment #13). However, because EF-G is less well retained during ultracentrifugation than is EF-Tu in the presence of kirromycin, we lack the clear-cut proof of this interpretation that would be provided by a combined stoichiometry of co-sedimented IF2 and EF-G in excess of 1.0/ribosome.

4.3.3 A model for simultaneous binding of IF2 and EF-Tu to the ribosome.

Comparison of the observed 70S binding sites of EF-Tu (as a kirromycin-stalled complex, Valle et al., 2003a) and IF2.GDP (Myasnikov et al., 2005) shows there to be substantial steric overlap, leading the the conclusion that their mutual positions on the ribosome are incompatible (Figure 4.3A). However, there are several possibilities for how the binding site of IF2 might be rearranged to allow coexistence with EF-Tu in a mixed complex on the ribosome. One attractive model is shown in Figure 3B, in which the electron density map obtained by Valle et al. (2003a) (emd-1055 in the EM-Database) is used as a framework in which to position IF2 so as to avoid steric clashes with either ribosomal components or EF-Tu. Here, relatively minor movements of the IF2 G2-G3, C1 and C2 domains (for IF2 nomenclature see Simonetti et al., 2008) allow IF2 to be

bound simultaneously with EF-Tu, while retaining its general position within the intersubunit space. Such minor movements are consistent with the at most minor changes seen in $IF2^{Cy3}$-$L11^{Cy5}$ FRET efficiency on either TC or EF-G binding (Figure 4.1). In the model EF-Tu makes strong contacts with the GAC, the SRL, and presumably at least one CTD of L7/L12 (Valle et al., 2003a). IF2 retains its strong contacts with the 30S subunit via its NTD (Caserta et al., 2006) and contacts several regions of the 50S subunit, including H69, L14, and L19/H95 via the C2, C1, and G domains, respectively.

H69 of 23S rRNA is believed to assist tRNA movement from A- to P- and P- to E-site during translocation (Yusupov et al., 2001; Valle et al., 2002; Valle et al., 2003a; Schuwirth et al., 2005; Korostelev et al., 2006; Selmer et al., 2006; Yusupova et al., 2006; Li and Frank, 2007). Within the A/T site tRNA, adopting a bent conformation, contacts only the tip of H69 via its hinge region between the D and anticodon stems (Valle et al., 2003a). A particularly interesting feature of the model is that it positions the C2 domain of IF2 as a virtual continuation of H69, where it is well-positioned to assist movement of tRNA from the A/T site to the A site following GTP hydrolysis and EF-Tu dissociation. Here the charge distribution of IF2-C2, in which a continuous negative surface is surrounded by patches of positive residues (Figure 4.3C), would allow sliding of the tRNA in place.

4.4 DISCUSSION

The experiments displayed above provide compelling evidence that IF2 and EF-Tu can coexist stably on the ribosome, and that IF2 and EF-G can coexist at least transiently. Stable coexistence of IF2 and EF-Tu, in the presence of the antibiotic kirromycin, is demonstrated by the co-sedimentation experiments in Figure 4.2. Transient coexistence for both elongation factors is demonstrated by the failure of either the TC or EF-G.GTP to substantially decrease the IF2-L11 FRET signal, which occurs exclusively via IF2 interaction with L11 as part of a 70S complex (Qin et al., 2009), while at the same time affording both EF-Tu-dependent fMetPhe formation and EF-G dependent translocation (Figures 4.1C, 4.1D). Here it is worth emphasizing that the co-sedimentation assay, though quite rigorous in providing clear stoichiometric evidence for G cofactor coexistence on the ribosome, is likely to be overly stringent as an indicator of what complexes exist in solution, since more labile and/or thermodynamically weaker complexes that do not survive ultracentrifugation will not be seen in this way. Thus, a longer-lived ribosome complex containing both IF2 and EF-G is not excluded by our results.

The FRET experiments demonstrating transient coexistence were carried out with a Cy3-labeled variant of Bst-IF2 rather than of Eco-IF2. However, Bst-IF2 is functionally interchangeable with Eco-IF2 in *in vitro* assays (Brombach et al., 1986; Qin et al., 2009), and has recently been shown to complement an *E. coli infB* null mutation *in vivo* (E. Caserta and C. Gualerzi, private communication). Thus, although the complexes that Bst-

IF2 forms with *E. coli* ribosomes and ribosomal subunits are somewhat more stable than those formed by Eco-IF2, they are unlikely to be artifactual, and in fact allow translation intermediates involving IF2 to be studied more easily, both in the present case and in earlier studies (La Teana et al., 1996; Marzi et al., 2003).

Since IF2 remains bound to the ribosome during at least one complete elongation cycle, it is reasonable to expect that it may survive several such cycles, raising the question of the functional significance of such binding. The model presented in Fig. 3 shows how bound IF2 could facilitate tRNA movement from the A/T- to the A-site during elongation. In addition, Caserta et al. (2006) have hypothesized that anchoring IF2 to the ribosome could ensure the exercise of its functions in favoring 70S formation initiator and fMet-tRNA^{fMet} binding to the P-site (Grigoriadou et al., 2007 and references therein), even when the number of ribosomes in the cell is drastically reduced, as in time of famine. It has also been shown that IF2, acting in concert with IF1, catalyzes peptidyl-tRNA release from the P-site of ribosome, an activity which decreases with increasing length of nascent polypeptide and is especially marked in the presence of low concentrations of TC cognate for the codon in the A-site (Karimi et al., 1998). Such activity could liberate ribosomes trapped at the initial stages of protein synthesis elongation by ``hungry codons" or for other reasons (Karimi et al., 1998), and would be expected to be enhanced by IF2 already bound to the ribosome as compared with IF2 coming from the cytosol.

The structural model shown in Figure 5.3B shows one possibility for how the ribosome could accommodate both IF2 and EF-Tu (parallel models could be constructed for simultaneous binding of IF2 and EF-G), but leaves open the question of the mechanism by which such accommodation is achieved. Here the results of Kothe et al. (2004) and Diaconu et al. (2005) are pertinent. These workers have obtained strong evidence that the highly mobile L7/12 C-terminal domains [CTDs] that are proximal to the GAC promote recruitment of G-protein factors to the ribosome. Helgstrand et al. (2007) has shown that these CTDs, of which there are four copies on an *E. coli* ribosome, can each bind to all four G-protein translation cofactors, possibly via interaction with a site or sites that the G proteins have in common, although this latter point has been questioned (Nechifor et al., 2007). Ultimately, these cofactors form additional contacts with the GAC and the SRL, as well as with other regions of the ribosome that might be specific for each factor, such as the 30S binding site of the N-terminus of IF2 (Marzi et al., 2003; Allen et al., 2005, 2007; Caserta et al., 2006) and the A-site interaction of domain IV of EF-G (Valle et al., 2003b) Helgstrand et al. (2007) have suggested that some copies of L7/L12 could potentially interact with G-protein factors not yet positioned in their final binding sites on the ribosome.

Taking this suggestion one step further, we hypothesize that binding of an incoming TC to a 70SIC proceeds via an initial contact with an L7/L12 CTD not involved in IF2 binding. *In vivo*, where ribosome concentration is ~ 20 µM (Lambert et al., 1983; Caldas

et al., 2000), even weak binding should suffice for substantial complex formation. Displacement of IF2 from the GAC and SRL to allow “canonical” EF-Tu binding in the position seen by cryo-EM (Figure 4.3B) would then take place via a concerted series of reactions from this initially formed complex. Experiments are underway to test this hypothesis, as well as to determine whether, during normal protein elongation, when both EF-Tu and EF-G binding to the ribosome are transient, EF-G binding precedes EF-Tu release (and vice-versa), via initial contact with an L7/L12 CTD as described above.

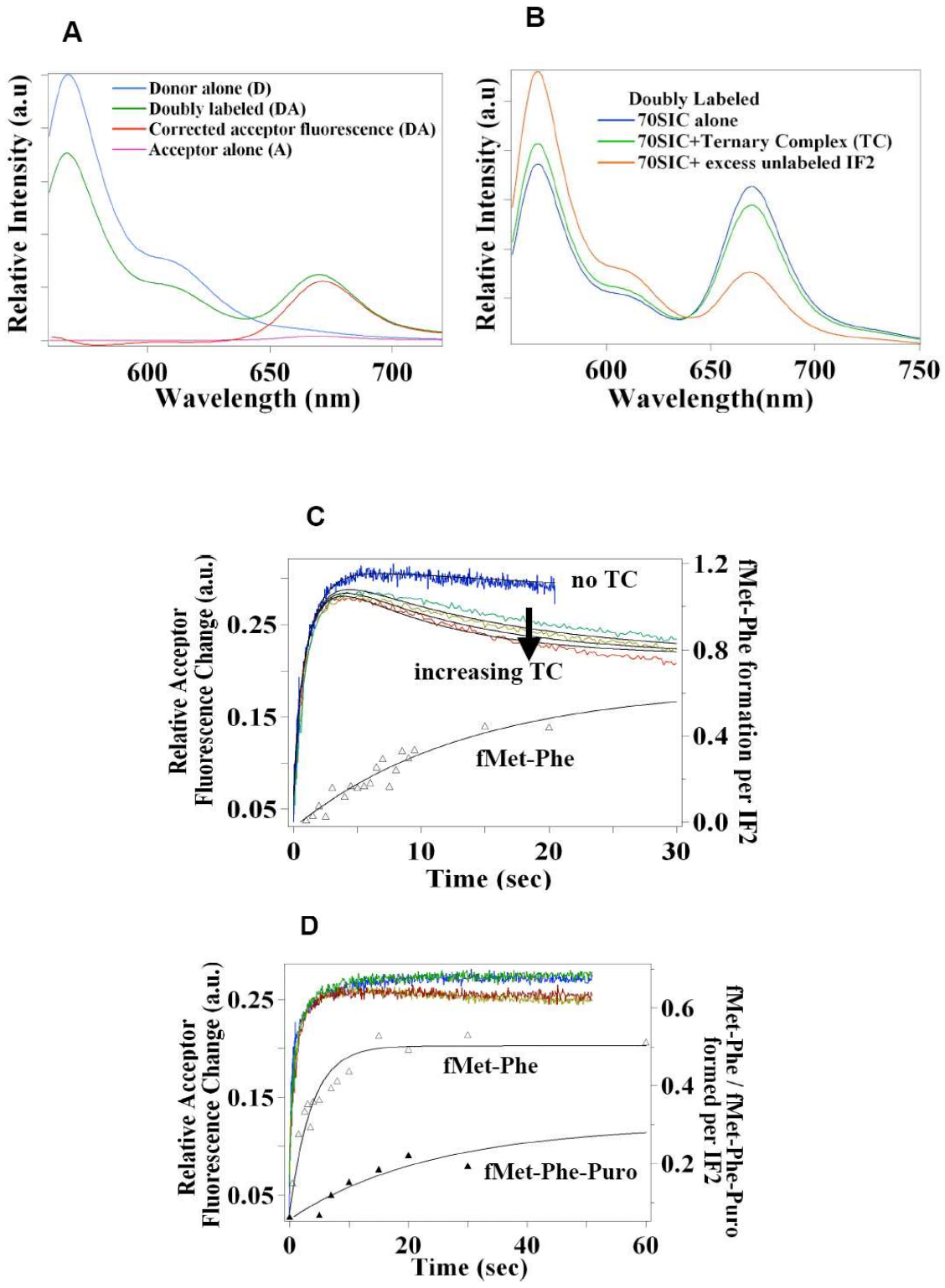
A
Donor alone (D)
Doubly labeled (DA)
Corrected acceptor fluorescence (DA)
Acceptor alone (A)
Relative Intensity (a.u)
600
650
700
Wavelength (nm)
B
Doubly Labeled
70SIC alone
70SIC+Ternary Complex (TC)
70SIC+ excess unlabeled IF2
Relative Intensity (a.u)
600
650
700
750
Wavelength(nm)
C
no TC
increasing TC
fMet-Phe
Relative Acceptor Fluorescence Change (a.u.)
0.25
0.15
0.05
1.2
0.8
0.4
0.0
fMet-Phe formation per IF2
0
10
20
30
Time (sec)
D
fMet-Phe
fMet-Phe-Puro
Relative Acceptor Fluorescence Change (a.u.)
0.25
0.15
0.05
0.6
0.4
0.2
fMet-Phe / fMet-Phe-Puro formed per IF2
0
20
40
60
Time (sec)

Figure 4.1. Monitoring IF2 binding to the ribosome by FRET between L11^{Cy5} and IF2^{Cy3} A. In the 70SIC. FRET is indicated by the decrease in donor emission and the increase in acceptor emission in the doubly-labeled (*DA*, donor-acceptor) sample, as compared with the singly labeled samples, *D*, donor alone or *A*, acceptor alone on excitation at 540 nm. The corrected acceptor fluorescence due to FRET is obtained by subtracting out contributions from the D and A samples to the DA sample (Seo et al., 2006). **B.** Effect of added TC (0.375 µM) or excess Bst-IF2 (1.0 µM) on the *DA* FRET signal seen in part A. Further increases in TC concentration up to 1.5 µM led to only slight additional decreases in FRET efficiency (Figure 5.4). **C. and D.** Kinetics of FRET acceptor fluorescence change, fMetPhe formation (Δ), and fMetPhe-puromycin formation (▲) during formation of 70SIC, PRE and POST complexes. A split time scale is employed in part D to make clear the persistence of acceptor emission during fMetPhe-puromycin formation. 30SIC^{Cy3} was rapidly mixed with 50S^{Cy5} and varying TC and EF-G concentrations, as indicated. Experiments in parts A – C and D were carried out in W and polyamine buffers, respectively. All experiments contained: IF1, IF3, fMet-tRNA^{fMet} 0.45µM; 022mRNA 0.9 µM; 30S 0.3 µM. In addition, experiments in parts A and B contained Bst-IF2^{Cy3} or Bst-IF2, 0.25 µM; 50S^{Cy5} or 50S, 0.18 µM; GTP 100 µM: experiments in parts C and D contained IF2^{Cy3} 0.15 µM; 50S^{Cy5}, 0.5 µM; GTP, 200 µM. In part D in the absence of EF-G, similar fluorescence traces were obtained at 0.5 µM or 2.0 µM TC. fMetPhe formation was carried out at 1 µM TC. fMetPhe-puromycin formation was carried out at 1 µM of both TC and EF-G and 2.5 mM puromycin.

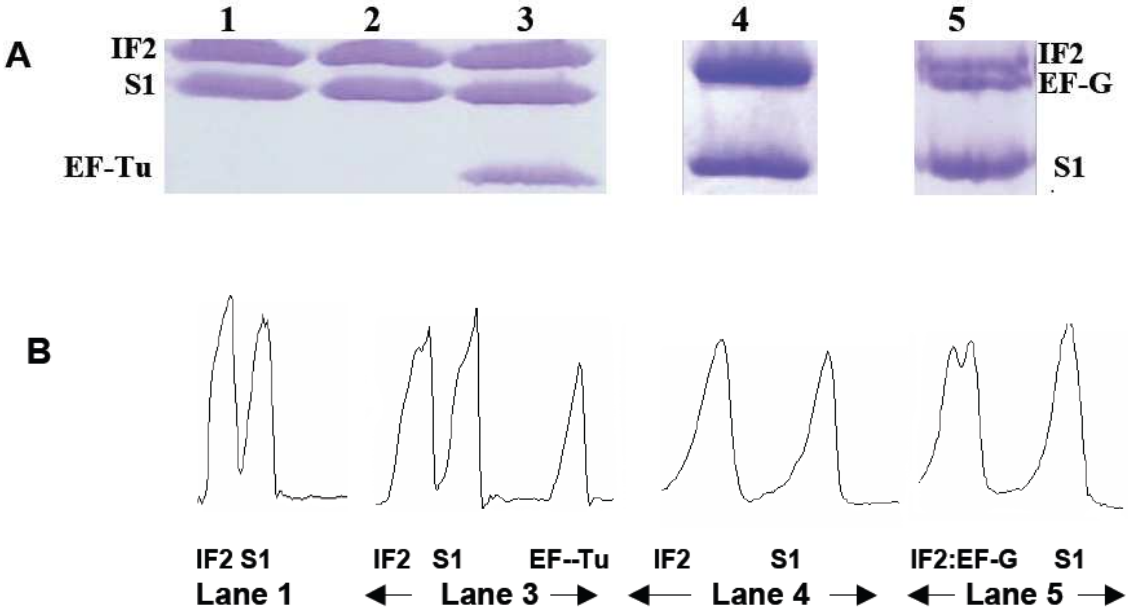
A
1
2
3
4
5
IF2
S1
EF-Tu
IF2
EF-G
S1
B
IF2 S1
Lane 1
IF2 S1 EF--Tu
Lane 3
IF2 S1
Lane 4
IF2:EF-G S1
Lane 5
C
Scanned Intensity (a.u.)
6000
4000
2000
0
IF2
S1
EF-Tu
0
20
40
60
80
Protein pmoles

Figure 4.2. Cosedimentation of ribosomes and factors through a sucrose cushion. A. SDS-PAGE analysis of pelleted samples. Lanes 1 and 4: 70SIC alone; Lanes 2 and 3: 70SIC preincubated with TC in the absence and presence of kirromycin (0.2 mM), respectively; Lane 5: 70SIC preincubated with TC and EF-G (3 µM) in the presence of fusidic acid (1 mM) and puromycin (0.3 mM). All preincubations contained, in Buffer W: IF1, IF3, fMet-tRNAfMet, 0.45 µM; mRNA 0.9 µM; 70S 0.3 µM, GTP 200 µM, TC 0.6 µM, and either 0.33 µM Bst-IF2 (lanes 1 – 3) or 0.45 µM Bst-IF2 (lanes 4, 5). Lanes 1 – 3, 14% acrylamide gel, lanes 4 and 5, 8% acrylamide gel. B. Lanes 1 and 3 -5 scanned using ImageJ. Lane 2 gave results identical to Lane 1. C. Sample standard lines from intensity of gel staining for proteins Bst-IF2 (square), EF-Tu (diamond) and S1 (triangle), giving the following values (in arbitrary units) per pmol, based on three independent measurements: Bst-IF2, 93 ± 7; S1, 57 ± 6; EF-Tu, 46 ± 8. The value for Eco-IF2 was essentially identical to that for Bst-IF2. The concentrations of proteins were determined as follows: Bst-IF2 and Eco-IF2, Bradford assay (Bradford ,1976); S1, set equal to the ribosome concentration from which protein was extracted (1A260 unit equals 26 pmole); EF-Tu, determined from the EF-Tu:[3H-GDP] binding filter assay (Arai et al., 1972). This value corresponds to about 60% of the value obtained by Bradford assay.

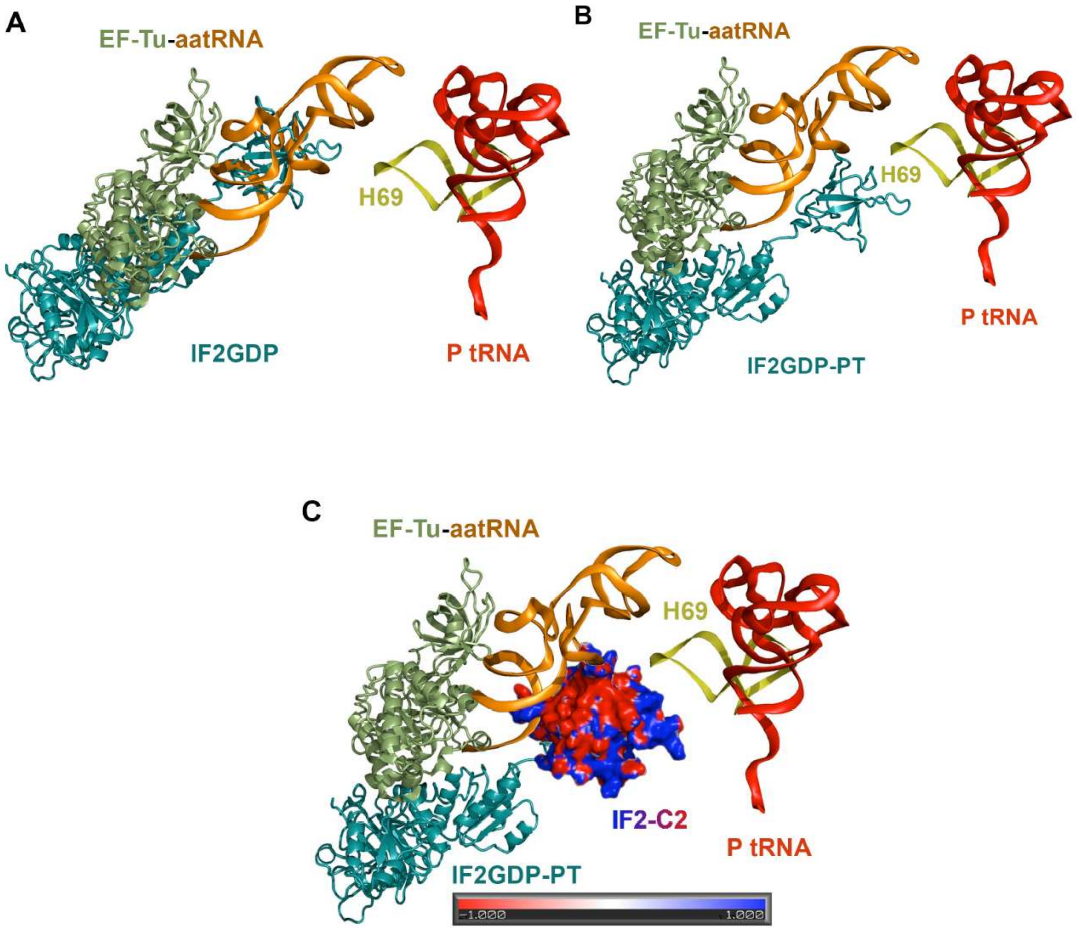
A
EF-Tu-aatRNA
H69
IF2GDP
P tRNA
B
EF-Tu-aatRNA
H69
P tRNA
IF2GDP-PT
C
EF-Tu-aatRNA
H69
IF2-C2
P tRNA
IF2GDP-PT
-1.000
1.000

Figure 4.3. A plausible model for simultaneous binding of EF-Tu and IF2 to the 70S ribosome. A. Steric clash between IF2.GDP and kirromycin-stabilized TC bound to the 70S complex, using previously determined positions of IF2.GDP and P-site tRNA (Myasnikov et al., 2005) and of the TC complex (Valle et al., 2003a). B. A plausible model for simultaneous binding of both factors, in which the position of TC and P-site tRNA are unchanged from A., and IF2, while relocated within the 70S, with movements of the order of 10 - 30 Å of the G1-G2-G3, C1 and C2 domains, is still retained within the intersubunit space. C. As for B with the surface charge distribution of the C2 domain of IF2 colored from red-negative to blu-positive. The C2 domain in this position forms an ideal prolongation of H69. This may help the A/T tRNA to be accommodated into the A/A site. The figure has been produced using Pymol (DeLano, W.L. "PyMOL" (2002) www.pymol.org) and the pdb files 2HGR_C for the fMet-tRNA (Yusupova et al., 2006), 2HGU_A for the H69 and 1LS2 for the EF-Tu-Phe-tRNA complex (Valle et al., 2002).

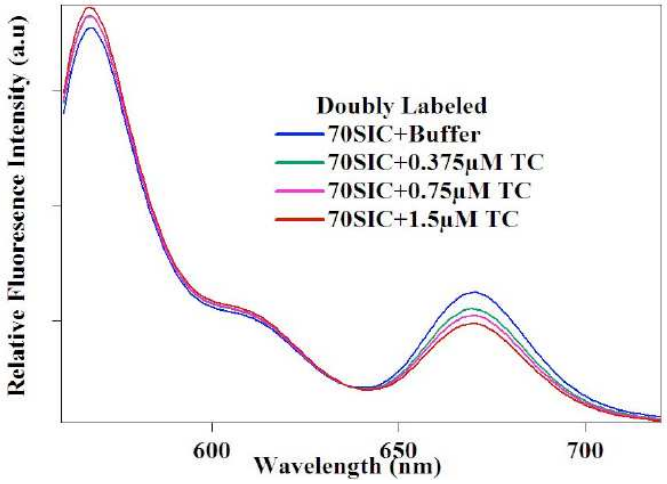

Figure 4.4. Titration of DA FRET signal with excess added TC, as indicated. All experiments contained: IF1, IF3, fMet-tRNAfMet 0.45μM; 022mRNA 0.9 μM; Bst IF2Cy3 or BSt IF2, 0.25 μM; 30S 0.3 μM; 50SC5 or 50S, 0.18 μM; GTP 100 μM in Buffer W.

Table 4.1. Co-sedimentation of IF2 and EF-Tu with 70S ribosomes[a]

Experi-	Preincubation						Co-sedimentation	
ment #	IF2	GXP	IF2/70S	TC/70S	EF-G/70S	Antibiotic(s)[b]	IF2/70S	EF-Tu/70S
1	*Bst*	GTP	1.0	-	-	-	0.7	-
2	*Bst*	GTP	1.0	3.0	-	kirro	0.7	0.6
3	*Bst*	GTP	2.0	3.0	-	kirro	0.9	0.5
4	*Bst*	GTP	3.0	3.0	-	kirro	1.1	0.6
5	*Eco*	GTP	3.0	-	-	-	n.d.[c]	-
6	*Eco*	GTP	3.0	3.0	-	kirro	n.d.	0.5
7	*Eco*	GDPNP	2.0	-	-	-	0.9	-
8	*Eco*	GDPNP	2.0	3.0	-	kirro	0.9	0.5
9	*Bst*	GTP	1.5	-	-	-	1.0	-
10	*Bst*	GTP	1.5	3.0	-	-	0.8	n.d.
11	*Bst*	GTP	1.5	3.0	3.0	-	0.5	n.d.
12	*Bst*	GTP	1.5	3.0	9	-	0.5	n.d.
13	*Bst*	GTP	1.5	-	9	puro + FA	0.4	-

[a] Samples of 70SIC, formed as described in Materials and Methods, were preincubated with varying amounts of EF-Tu, EF-G, and antibiotics and complexes formed were collected by ultracentrifugation through a sucrose cushion. IF2 and EF-Tu contents of complexes were determined by SDS-PAGE analysis (Figure 4.2).

[b] kirro: kirromycin, 0.2mM; puro: puromycin 0.3 mM; FA: fusidic acid 1.0mM

[c] not detectable

Table 4.2: Co-sedimentation results from Bst-IF2^{Cy3} chasing by TC or Bst-IF2[a].

Experiment	Preincubation			Co-sedimentation
	IF2^{C3}/70S	TC/70S	IF2/70S	IF2^{C3}/70S
1	1.5	-	-	0.94
2	1.5	2.0	-	0.85
3	1.5	-	4.5	0.33

[a] 70SIC was made as in Materials and Methods except that Bst-IF2^{Cy3} was used in place of Bst-IF2. Subsequently either TC or Bst-IF2 was added as indicated prior to pelleting.

CHAPTER 5

IF2 INTERACTION WITH INITIATIOR tRNA DURING 30S AND 70S INITIATION COMPLEX FORMATION

5.1 ABSTRACT

How the interaction between IF2 and fMet-tRNA^{fMet} dynamically changes during the formation of 30S initiation complex and 70S initiation complex remains elusive. Here I present stopped flow FRET experiments between Cy3-IF2 as a donor and Cy5- fMet-tRNA^{fMet} designed to answer this question. A FRET signal arising from Cy3-IF2 and Cy5- fMet-tRNA^{fMet} demonstrated that IF2 and fMet-tRNA^{fMet} forms as a binary complex. The decrease of FRET signal seen upon the binary complex mixing with 30S-preinitiation complex indicated an adjustment of the interaction during this process. Future studies looking at 70SIC formation would be worth pursing.

5.2 INTRODUCTION

IF2 forms a well-characterized binary complex with the acceptor end of fMet-tRNA^{fMet} via its C2 domain (Figure 5.1) (Guenneugues et al., 2000; Meunier et al., 2000). This interaction is maintained during part of the process of 70S initiation complex (70SIC) formation (Allen et al., 2005; Allen et al., 2007), but is lost within the fully formed 70SIC as fMet-tRNA^{fMet} occupies the 70S P-site, permitting reaction with aa-tRNA to form dipeptide as part of elongation cycle. We have shown that during 70SIC formation, fMet-tRNA^{fMet}(prf20) undergoes a marked increase in fluorescence (Figure 5.2) and fluorescent IF2 (IF2^{C}) undergoes a small decrease in fluorescence, both with a rate constant of 2.3 s^{-1}, a value that is consistent with step 4 in Scheme 1 (Figure 5.3) being essentially rate-limiting for dipeptide formation (Grigoriadou et al., 2007a; Qin et al., 2009). The questions that remain open are whether step 4 or a preceding step corresponds to the required separation of IF2 from fMet-tRNA^{fMet}, and, if so, how large a separation is entailed.

Ultimately we plan to carry out stopped-flow FRET experiments to answer this question, using IF2 Cys derivatives labeled in positions that are close to the interaction region between IF2 and fMet-tRNA^{fMet}. According to Marzi et al. 2003, in the binary IF2: fMet-tRNA^{fMet} complex, the residues within GII peptide Asn 611-Arg 645 of *E. coli* IF2, corresponding to Asn 464-Glu 498 of *Bst* IF2, are close to the elbow region of fMet-

tRNA^{fMet}. Consequently Cy5-D20- fMet-tRNA^{fMet} and Cy3-V451C-IF2 were chosen as a FRET pair and utilized in the following studies.

5.3 RESULTS

5.3.1 Initial work from fMet-tRNA^{fMet} (rhd) and Cy3-660C-IF2

Before the Cy5 hydrazide was successfully attached to initiator tRNA, the prepared fluorescent derivatives fMet-tRNA^{fMet}(prf) and fMet-tRNA^{fMet}(rhd) were used as fluorescent donors to the S660C-IF2 labeled with Cy3, within the CII domain. The time dependencies of the fluorescence changes of these two tRNAs and of Cy3-S660C-IF2 during 70SIC formation were similar to the published data (Figure 5.4) (Grigoriadou et al., 2007a; Qin et al., 2009). However, due to the significant interference with the donor's emission from Cy3 fluorophore, as shown in Figure 5.5, it was hard to reliably analyze the signal generated between fMet-tRNA^{fMet}(prf) or fMet-tRNA^{fMet}(rhd) and Cy3-S660C-IF2. We thus switched to fMet-tRNA^{fMet}(cy5) when this material became available. However, no significant FRET signal was observed between fMet-tRNA^{fMet}(cy5) and Cy3-S660C-IF2 studied as the binary complex. As a result, a second switch was to replace Cy3-S660C-IF2 with Cy3-V451C-IF2, which did yield a FRET signal with fMet-tRNA^{fMet}(Cy5) when studied as the binary complex, as described below.

.5.3.2 Characterizations of Cy5-fMet-tRNA^{fMet} derivative and Cy3 labeled IF2 derivative

The 30SIC consists of a 30S subunit containing bound mRNA, charged and formylated initiator tRNA (fMettRNA^{fMet}), and initiation factors IF1, IF2, and IF3. We have shown that the rate of 30SIC formation can be monitored by changes in fluorescence on ligand binding to the 30S subunit, using either a proflavin derivative of fMet-tRNA^{fMet}, prf-fMet-tRNA^{fMet} (Grigoriadou et al. 2007a,b), or a coumarin (Grigoriadou et al. 2007a) or Cy3 (Qin et al., 2009) derivative of IF2. Here, using Cy5-fMet-tRNA^{fMet} we obtained a rate of 30SIC formation essentially the same as that measured with IF2^{Cy3} (Fig. 5.6), suggesting that Cy5-fMet-tRNA^{fMet} is fully functional in formation of 30SIC.

V451C in the GII domain of Bst IF2 is proximal to the Asn 464-Glu 498 region of Bst IF2, experimentally shown to be near the elbow region of fMet-tRNA^{fMet} (Marzi et al., 2003). This variant was labeled by Cy3 maleimide as described in Chapter 2, to a stoichiometry of 1.0/protein. The activity of Cy3-V451C-IF2 was examined by formation of 30S initiation complex, giving an apparent rate constant of 21 ± 2 sec^{-1}, as shown in Figure 5.6.

5.3.3 Interaction of IF2 and fMet-tRNA^{fMet} as a binary complex

The experiments described above establish the basic functionality of IF2^{Cy3} and Cy5-fMet-tRNA^{fMet} in 30SIC formation, making it likely that the FRET experiments described

below that measure FRET during the combination of these derivatives will be relevant for understanding the process of 30SIC formation from native, unmodified components. A fluorescence donor $IF2^{Cy3}$ (D), with a fluorescence acceptor Cy5-fMet-$tRNA^{fMet}$ (A) results in formation of the double-labeled binary complex (DA sample) and the generation of a strong FRET signal (Figure 5.7A), with considerable decreases and increases in donor and acceptor fluorescence signals, respectively, as compared with the fluorescence of the D ($IF2^{Cy3}$ plus fMet-$tRNA^{fMet}$) and A (IF2 plus Cy5-fMet-$tRNA^{fMet}$) samples. As the fMet-$tRNA^{fMet}$ is a limiting factor in the experiment, the corrected acceptor fluorescence change was considered as a reflection of FRET signal. As indicated in Figure 5.7B, the addition of two equivalents of $IF2^{Cy3}$ was enough to lead to a saturated FRET signal at the equilibrium state, with a K_d ~0.1μM.

The fast kinetic study was further performed to reveal how IF2 interacts with the initiator tRNA. Figure 5.8 clearly shows that the FRET change is biphasic: a rapid initial binding with an apparent rate constant of 170 ± 6 sec^{-1} followed by a slow conformational change with an apparent rate of 0.34 ± 0.01 sec^{-1}. The experiments were repeated using the new KinTek stopped flow instrument. This instrument allows tracking the donor and acceptor fluorescence changes at the same time, as shown in Figure 5.9. As a consequence of no noticeable fluorescence change in the D or A sample, the fluorescence changes at 580 nm and 680 nm in the DA sample directly reflected the FRET change, with similar first apparent rate constants of 76 ± 2 sec^{-1} and 89 ± 3 sec^{-1}, respectively, and second apparent rate constants of 0.67 ± 0.01 s^{-1} and 0.61 ± 0.02 s^{-1}, respectively. The

lower concentrations of materials used in the new instrument account for the lower initial binding rates. The same second apparent rate constant from both donor and acceptor fluorescence changes in DA sample (Figure 5.9) supported that the second phase was induced by a conformational change between IF2 and initiator tRNA.

5.3.4 Interaction of IF2 and fMet-tRNA^{fMet} during 30SIC formation

The kinetic pathway of 30S initiation complex formation hasn't been fully explored. It was reported that the 30S ribosomal subunit with a full complement of each initiation factor interacts in stochastic order with the first ligand, either mRNA or fMet-tRNA, to yield two binary complexes which, upon binding the second ligand, form an unstable "pre-ternary complex" consisting of a 30S subunit bearing two noninteracting ligands (mRNA and initiator tRNA) (Gualerzi et al., 2001, Figure 1.1). This complex is a kinetic intermediate of the bona fide 30S initiation complex which is formed through a ribosomal conformational rearrangement that induces the mRNA start codon and the anticodon of fMet-tRNA to base-pair in the P site (Gualerzi and Pon 1990; Gualerzi et al. 2000). All the steps preceding the formation of the 30S initiation complex are believed to be in rapid equilibrium, and its formation occurs through an isomerization of the preternary complex. This isomerization consists of at least two first-order rearrangements kinetically controlled by the initiation factors.

To find out how the interaction of IF2 and fMet-tRNA^{fMet} changes during 30SIC formation, the binary complex of IF2^{Cy3} and fMet-tRNA^{fMet}(cy5) was rapidly mixed with

pre-30S initiation complex containing IF1, IF3, mRNA and 30S subunit in the presence of GTP. A significant decrease of FRET signal was observed (Figure 5.10), which may be triggered by an adjustment of fMet-tRNA^{fMet} within the P site of the ribosome (Gualerzi and Pon 1990). The decrease of FRET signal was also consistent with the latest reported 30SIC structure (Figure 5.11), showing IF2 and fMet-tRNA^{fMet} were getting further, compared to the structure of a free binary complex (Figure 5.1).

The experiments were also conducted in the stopped flow instrument. The acceptor fluorescence in the doubly labeled sample dramatically decreased upon rapid mixing with the pre-30SIC with an initial apparent rate constant of 46 ± 1 sec^{-1} and a second phase constant of 0.90 ± 0.04 s^{-1} (Figure 5.12). When the concentration of the binary complex was kept the same, doubling the concentration of the pre-30SIC had little effect on these constants and led to only with a slight increase in amplitude (Figure 5.12, Table 5.4). The phenomenon indicated that the experimental condition is saturated for the binary complex binding the pre-30SIC and that neither the first or second step seen in Figure 5.12 corresponds to a binding event.

5.4 DISCUSSION AND FUTURE WORK

It was proposed that fMet-tRNA^{fMet} and mRNA randomly bound to pre-30SIC without direct interaction and then with help of initiation factors the active 30SIC was formed (Figure 1.1). Our data has provided another possible route to form 30SIC. Based on Figure 5.12, IF2 and fMet-tRNA^{fMet} as a binary complex bind to pre-30SIC and,

during this binding process, IF2 and fMet-tRNA^{fMet} quickly come apart and rearrange themselves within the 30S subunit to form a functional 30SIC.

In light of the preliminary work here, the following work should be conducted in the future. The interaction of IF2 and fMet-tRNA^{fMet} during 70SIC formation should be investigated to determine whether the FRET signal would further decrease or increase due to the rearrangement of IF2 and fMet-tRNA^{fMet} on the 70S initiation complex.

It is known that IF1 can aid IF2 in facilitating fMet-tRNA^{fMet} binding to the P site of the ribosome and that IF3 is a fidelity factor and an anti-70S association factor that is important for supplying the subunit pool. But how these two factors kinetically impact the formations of 30SIC and 70SIC remain unclear. Implementation of the FRET system would provide insight into how IF1 and IF3 modulate 30SIC and 70S formation.

The non-cognate messenger RNA such as 022 AUU mRNA can replace the canonical AUG mRNA to explore how sensitive the interaction of IF2 and fMet-tRNA^{fMet} would be when the system encounters AUU starting codon. It is reported that no appreciable difference was observed during 30SIC formation but distinct difference was captured during 70S formation (Grigoriadou et al., 2007b). Therefore, it would be intriguing to track the underlying changing by means of FRET.

From a different perspective, the effects of antibiotics of FRET change kinetics may be investigated to determine how these compounds modulate 30SIC and 70SIC formation.

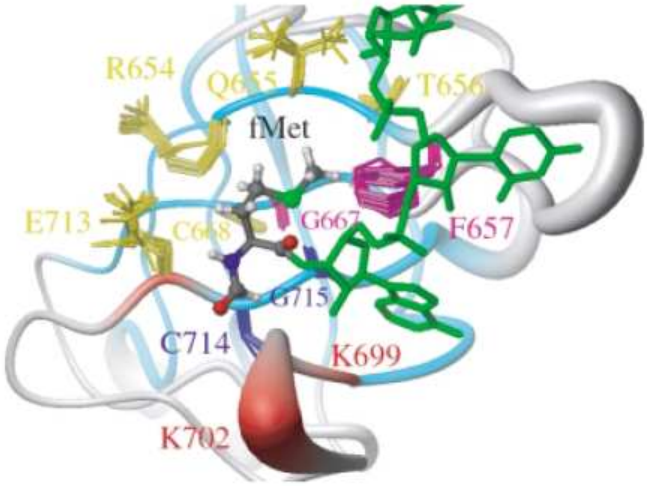

Figure 5.1. The modeled structures of C2 domain and CCA acceptor of fMet-tRNA (Meunier et al., 2000). The β-strands are coloured in cyan and the coils and turns in grey. The size of the ribbon is proportional to the r.m.s.d. of the ensemble of 20 structures when superimposed on the mean structure. The side chain of the residues that might be involved in the recognition are displayed for the 20 structures. The conserved residues C714 and G715 are indicated in blue. The residues surrounding the pocket are indicated in yellow.

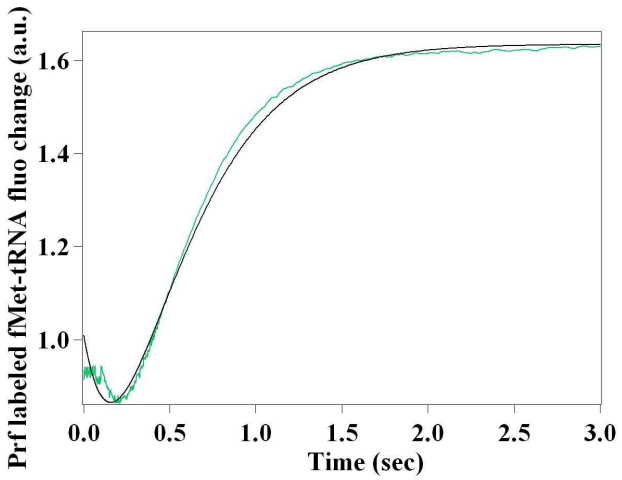

Figure 5.2. The fMet-tRNA^{fMet}(prf20) fluorescence change during 70SIC formation. 30S initiation complex containing fMet-tRNA^{fMet}(prf20) was rapidly mixed with 50S subunit. IF1, IF2, IF3, 0.45 µM; fMet-tRNA^{fMet} (prf20) 0.18 µM; mRNA, 0.9 µM; 30S, 0.3 µM; 50S, 0.5 µM; GTP, 100 µM.

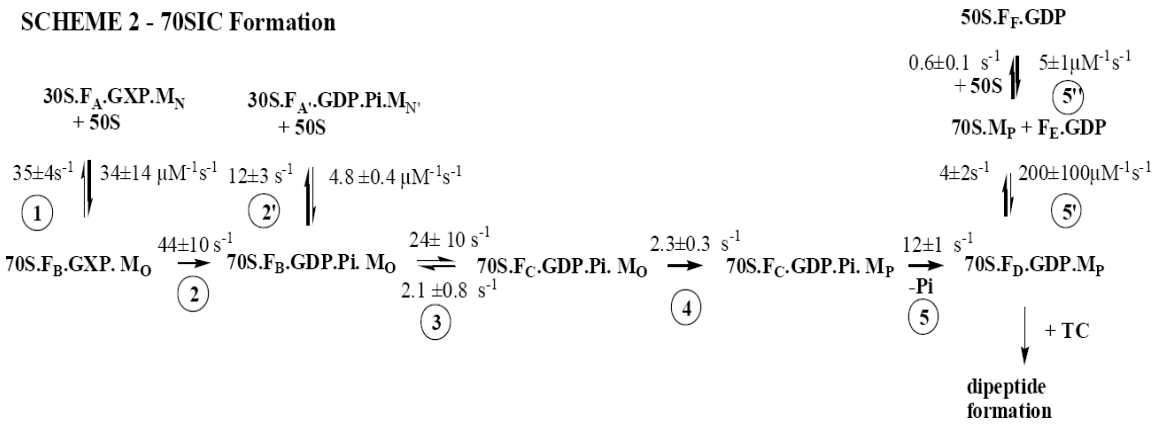

Figure 5.3. A quantitative kinetic scheme for 70 S translation initiation complex formation (Grigoriadou et al., 2007**).** GXP is either GTP or GDPCP; F is IF2; M is fMet-tRNA^{fMet}; 30S is 30S containing IF1, IF3, and mRNA; and TC is ternary complex (Phe-tRNA^{Phe}.EF-Tu.GTP).The subscripts A-F and N-P refer to different conformations of IF2C and fMettRNA^{fMet}(prf20), respectively, that have different fluorescent intensities.

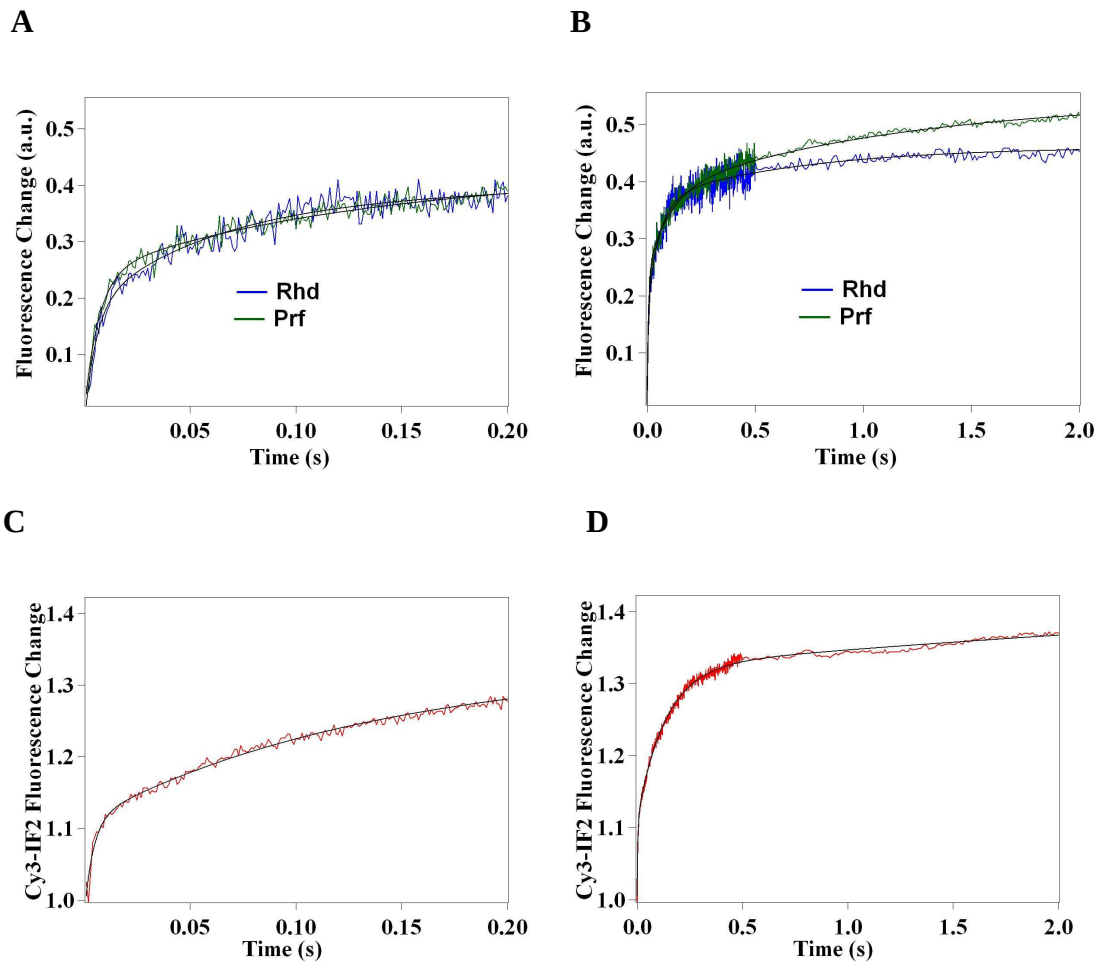

Figure 5.4. The fluorescence change of fMet-tRNA^{fMet}(prf20), fMet-tRNA^{fMet}(rhd20), or Cy3-S660C-IF2 during 70SIC formation. 30S initiation complex containing fMet-tRNA^{fMet}(prf20), fMet-tRNA^{fMet}(rhd20), or IF2^{Cy3} was rapidly mixed with 50S subunit. (A) and (B): The fluorescence changes of fMet-tRNA^{fMet}(prf20) and fMet-tRNA^{fMet}(rhd20). Blue trace: fMet-tRNA^{fMet}(rhd20), excited at 480nm and monitored via a 520nm bandpass filter; green trace: fMet-tRNA^{fMet}(prf20), excited at 462nm and monitored through a 480nm bandpass filter. IF1, IF2, IF3, 0.45 μM; fMet-tRNA^{fMet}(rhd20) or fMet-tRNA^{fMet}(prf20) 0.18 μM; mRNA, 0.9 μM; 30S, 0.3 μM; 50S,

0.5 µM; GTP, 100 µM. (C) and (D): Cy3-IF2 fluorescence change during 70SIC formation, excited at 540nm and monitored by a 570nm bandpass filter. The concentrations are as above except that 0.15 µM Cy3-IF2 and 0.45 µM fMet-tRNA^{fMet}. The curves are fitted by a triple-exponential equation and the apparent rates are shown in Table 5.1.

A **B**

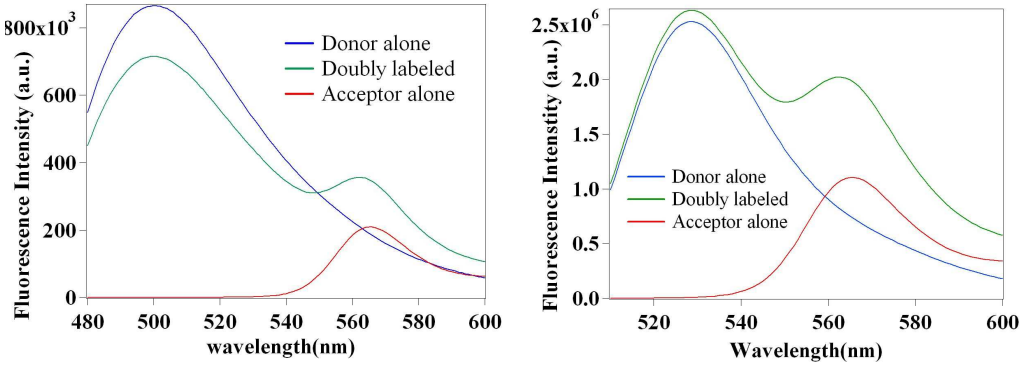

Figure 5.5. Emission spectra examined under donor alone, doubly labeled and acceptor alone samples during 30SIC formation. (A) The emission spectra from fMet-tRNA^{fMet}(prf20) and Cy3-S660C-IF2. (B) The emission spectrums from fMet-tRNA^{fMet}(rhd20) and Cy3-S660C-IF2. IF1, IF2, Cy3-IF2, IF3, 0.45 µM; fMet-tRNA^{fMet}, fMet-tRNA^{fMet}(prf20), fMet-tRNA^{fMet}(rhd20), 0.18 µM; mRNA, 0.90 µM; 30S, 0.30 µM; 50S, 0.50 µM; GTP, 100 µM.

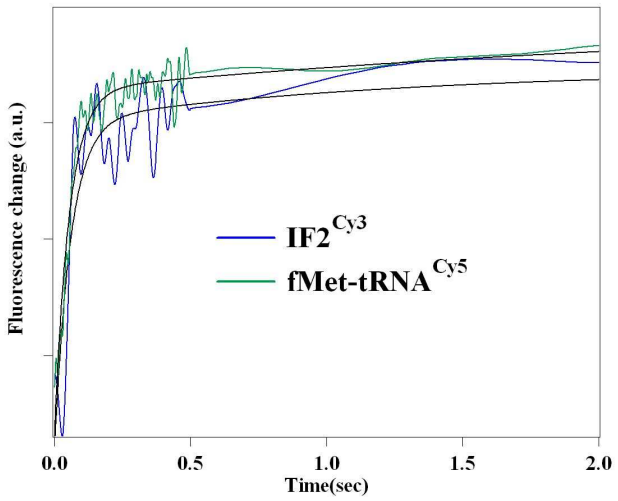

Figure 5.6. Rapid formation of 30SIC. Stopped-flow fluorescence measurements using limiting amounts of either $IF2^{Cy3}$ (prepared as in Qin et al., 2009) or $fMet\text{-}tRNA^{fMet}$ (cy5), were carried out at 20°C with 0.3 µM 30S subunits and 3.0 equivalents of mRNA022, essentially as described (Grigoriadou et al. 2007b). For the $IF2^{Cy3}$ binding experiment, 0.5 equivalent of $IF2^{Cy3}$.GTP was rapidly mixed with a 30S subunit solution containing 1.5 equivalents of IF1, IF3, and $fMet\text{-}tRNA^{fMet}$. For the $fMet\text{-}tRNA^{fMet}$ (cy5)binding experiment, $fMet\text{-}tRNA^{fMet}$ (cy5) (0.6 equivalent) was rapidly mixed with 30S subunit solution containing 1.5 equivalents of IF1, IF2, and IF3. Both 30S-containing solutions were preincubated for 15 min at 37°C prior to rapid mixing. Excitation was at 530 nm or 650 nm and fluorescence was monitored through a bandpass filter (550 ± 10 nm or 680 ±10 nm) for $IF2^{Cy3}$ or $fMet\text{-}tRNA^{fMet}$ (cy5), respectively. Each trace was fit to a single-exponential equation, giving apparent rate constants of 20.7 ± 1.3 sec^{-1} ($IF2^{Cy3}$) and 20.9±0.5 sec^{-1} $fMet\text{-}tRNA^{fMet}$ (cy5).

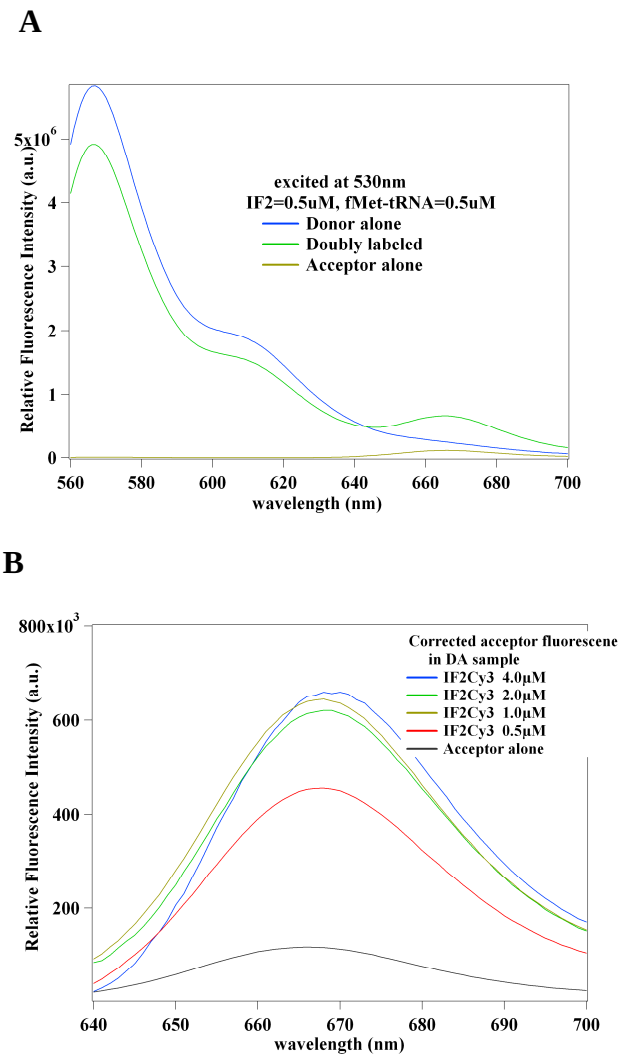

Figure 5.7. The steady-state FRET signal between IF2^{Cy3} and Cy5-fMet-tRNA^{fMet}. The samples were measured at 20 ^{o}C**.** (A) Emission spectra of D, DA and A samples when excited at 530nm. IF2, IF2^{Cy3}, 0.50 μM; fMet-tRNA^{fMet} (cy5), fMet-tRNA^{fMet}, 0.50 μM. (B) The corrected emission spectra of DA. The concentration of IF2^{Cy3} is increasing from 0.5 μM up to 4.0 μM.

A

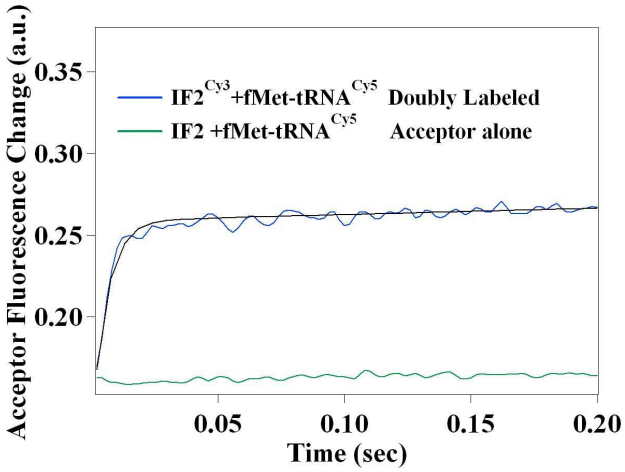

B

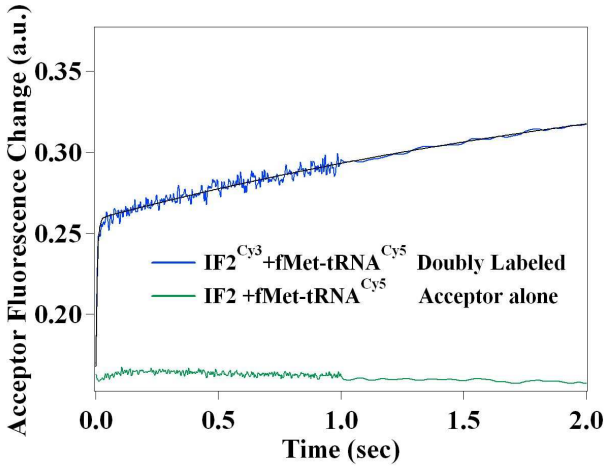

Figure 5.8. Fast kinetic study of IF2 interaction with fMet-tRNA^{fMet} at a short scale (A) and a long scale (B). IF2 was rapidly mixed with fMet-tRNA^{fMet} by stopped flow instrument. Blue trace: doubly labeled; green trace: acceptor alone. IF2, IF2^{Cy3}, 1.0 µM; fMet-tRNA^{fMet} (cy5), fMet-tRNA^{fMet}, 0.50 µM. The curves are fitted by a double-exponential equation.

A

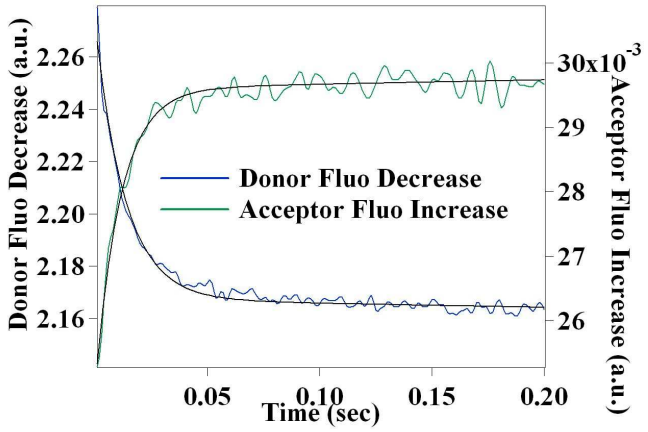

B

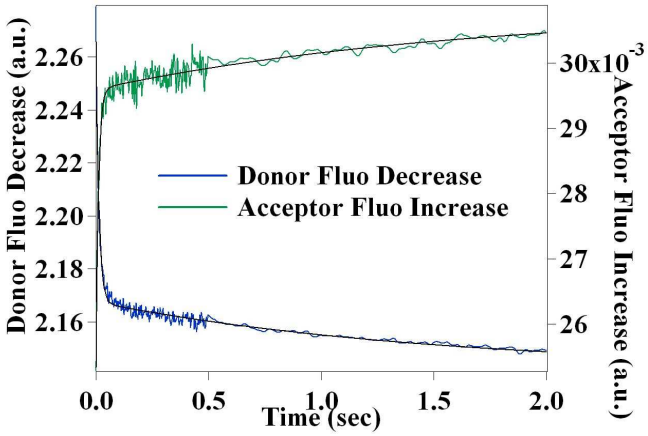

Figure 5.9. Measures of the fluorescence changes in the doubly labeled sample over 0.2 sec (A) or 2.0 sec (B). IF2 was rapidly mixed with fMet-tRNA^{fMet} by Kinteck instrument. Blue trace: donor fluorescence decrease in DA sample, monitored via a 580±10nm bandpass filter; green trace: acceptor fluorescence increase in DA sample, monitored via a 680±10nm bandpass filter. IF2, IF2^{Cy3}, 0.6 µM; fMet-tRNA^{fMet} (cy5), fMet-tRNA^{fMet}, 0.30 µM. The curves are fitted by a double-exponential equation.

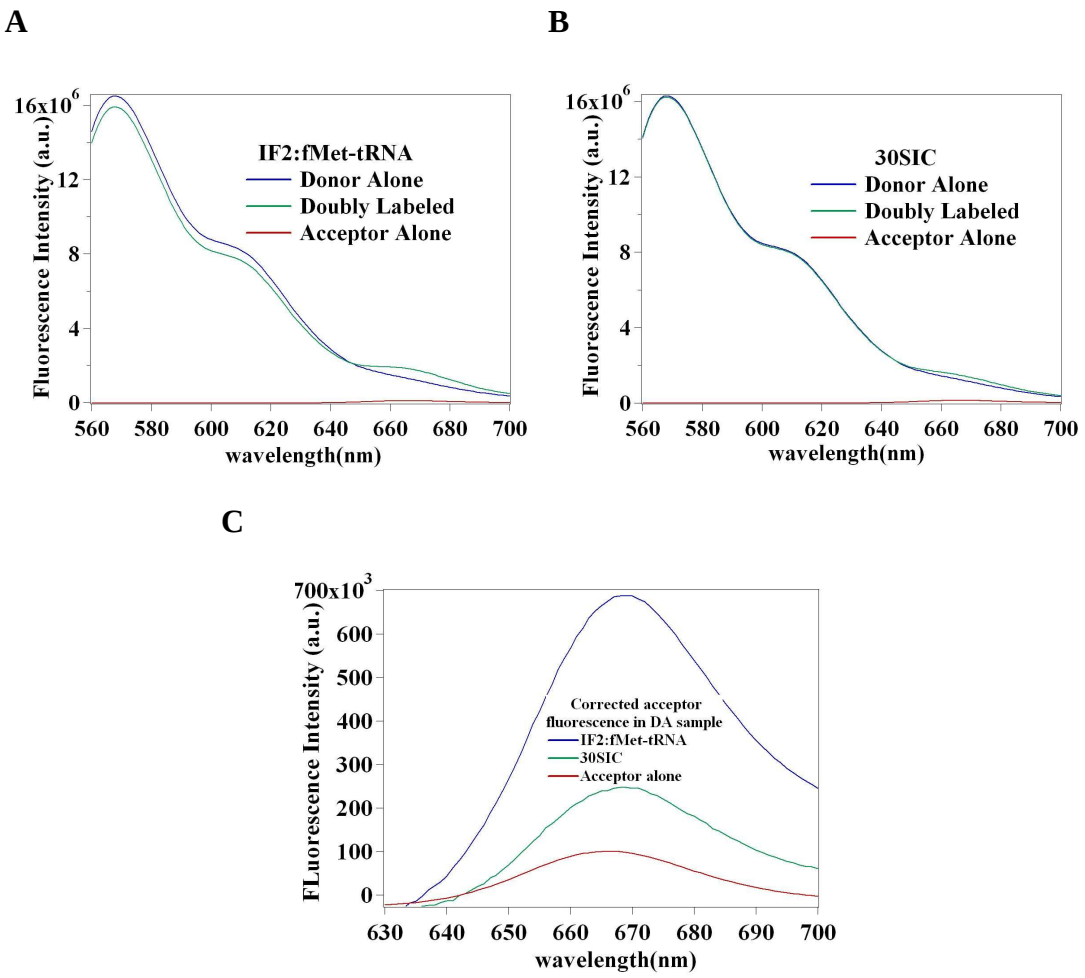

Figure 5.10. Equilibrium study of the transition from a binary complex to a 30SIC. (A) The binary complex of IF2 and fMet-tRNA^{fMet} or (B) the 30S initiation complex was examined under D, DA and A samples. Blue trace: donor alone sample; green trace: doubly labeled sample; red trace: acceptor alone sample. (C): Comparison of corrected acceptor fluorescence emissions from the binary complex, 30SIC and acceptor alone sample. IF1, IF2, IF2^{Cy3}, IF3, 2.25 µM; fMet-tRNA^{fMet} (cy5), fMet-tRNA^{fMet}, 0.50 µM; mRNA, 4.5 µM; 30S, 1.5 µM; 50S, 3.0 µM; GTP, 1000 µM.

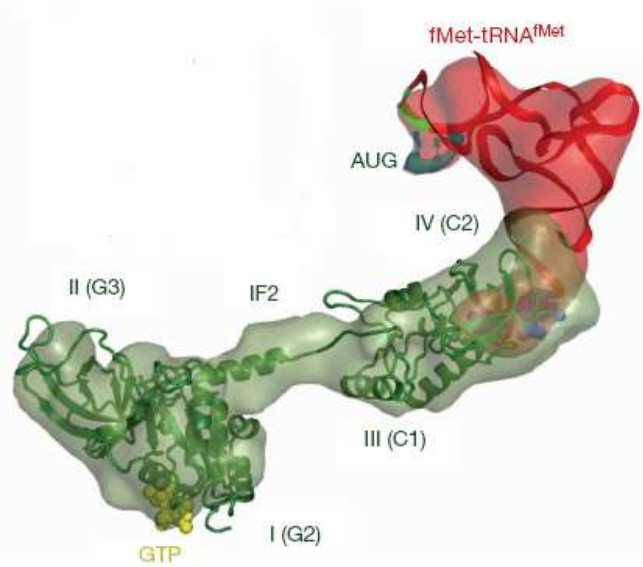

Fiugre 5.11. View of the IF2–fMet-tRNA^{fMet} sub-complex on the 30S initiation complex adapted from Simonetti et al., 2008.

A

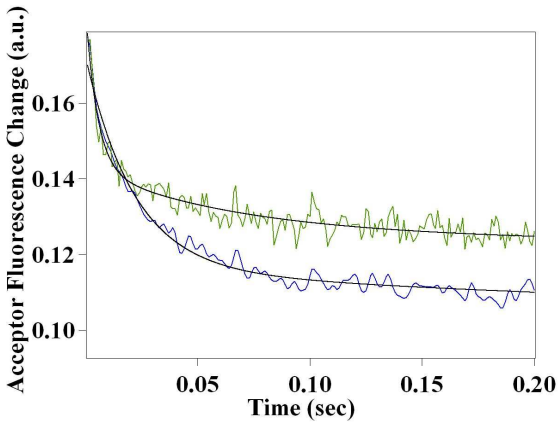

B

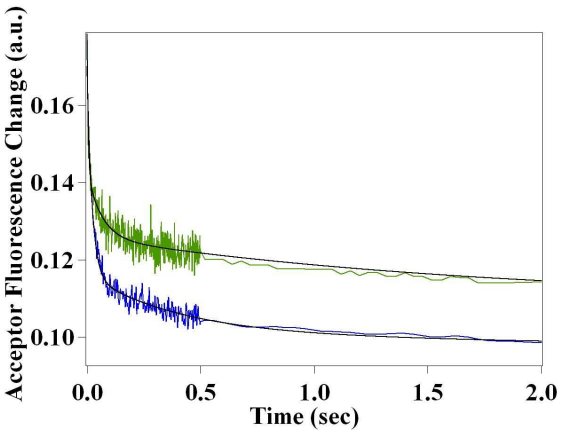

Figure 5.12. The acceptor fluorescence change of DA sample when the binary complex was rapidly mixed with the pre-30SIC. The concentration of each component of pre-30SIC in the blue trace is double that in the green trace. In the green trace, IF1, $IF2^{Cy3}$, IF3, 0.45 µM; $fMet\text{-}tRNA^{fMet}$ (cy5), 0.15 µM; mRNA, 0.90 µM; 30S, 0.30 µM; GTP, 100 µM.

Table 5.1: Apparent rate constants (s^{-1}) for Figure 5.4.

	Rhd-tRNA	Prf-tRNA	Cy3-IF2
kapp1	187 ± 27	148 ± 9	237 ± 15
kapp2	17.4 ± 1.2	9.7 ± 0.5	7.5 ± 0.19
kapp3	1.44 ± 0.11	0.89 ± 0.03	0.16 ± 0.01
Amp1	0.21 ± 0.02	0.25 ± 0.01	0.13 ± 0.01
Amp2	0.19 ± 0.01	0.14 ± 0.01	0.21 ± 0.01
Amp3	0.094 ± 0.004	0.166 ± 0.002	0.164 ± 0.007
Endpoint	0.46 ± 0.01	0.54 ± 0.01	1.49 ± 0.01

Table 5.2: Apparent rate constants (s^{-1}) for Figure 5.8.

kapp1	170±6
kapp2	0.34±0.01
Amp1	0.128±0.001
Amp2	0.118±0.001
Endpoint	0.377±0.0.001

Table 5.3: Apparent rate constants (s^{-1}) for Figure 5.9.

	Donor fluorescence decrease	Acceptor fluorescence increase
kapp1	75.5 ± 0.9	89.5 ± 2.0
kapp2	0.67 ± 0.01	0.61 ± 0.02
Amp1	0.106 ± 0.001	0.005 ± 0.001
Amp2	0.026 ± 0.001	0.0012 ± 0.001
Endpoint	2.14 ± 0.01	0.031 ± 0.001

Table 5.4: Apparent rate constants (s^{-1}) for Figure 5.12.

	Green trace	Blue trace
kapp1	46 ±1	48 ± 2
kapp2	0.90 ± 0.04	1.04 ± 0.04
Amp1	0.040 ± 0.001	0.057 ± 0.001
Amp2	0.019 ± 0.001	0.018 ± 0.001
Endpoint	0.109 ± 0.001	0.095 ± 0.001

CHAPTER 6

IDENTIFICATION OF NOVEL THIOPEPTIDE-ANTIBIOTIC PRECURSOR LEAD COMPOUNDS USING TRANSLATION MACHINERY ASSAYS

6.1 ABSTRACT

Most thiopeptide antibiotics target the translational machinery: Thiostrepton (ThS) and nosiheptide (NoS) target the ribosome and inhibit translation factor function, whereas GE2270A/T binds to the elongation factor EF-Tu and prevents ternary complex formation. We have utilized several *in vitro* translational machinery assays to screen a library of thiopeptide antibiotic precursor compounds and identified four families of precursor compounds that are either themselves inhibitory or are able to relieve the inhibitory effects of ThS, NoS, or GE2270T. Some of these precursors represent novel compounds with respect to their ability to bind to ribosomes. The results provide not only insight into the mechanism of action of thiopeptide compounds, but also demonstrate the potential of such assays for identifying novel lead compounds that might be missed using conventional inhibitory screening protocols.

6.2 INTRODUCTION

The translational machinery represents one of the major targets within the cell for antibiotics (reviewed by Spahn and Prescott, 1996; Wilson, 2004). Many clinical important classes of antibiotics, such as the tetracyclines, phenylpropanoids (chloramphenicol), macrolides (erythromycin), and aminoglycosides (gentamycin) inhibit translation by binding to the ribosome. Despite the potency of many of these drug classes, antibiotic resistance among clinically relevant pathogens is an increasing problem and thus the need for new antibiotics is more urgent than ever before. One class of antibiotics that has received renewed interest in the recent years is the thiopeptide family (reviewed by Bagley et al., 2005; Nicolaou et al., 2009), because of their effectiveness against Gram-positive bacteria, in particular, methicillin-resistant *Staphlococcus aureus* (MRSA), as well as against the malarial parasite *Plasmodium falciparum* (McConkey et al., 1997). Thiopeptide antibiotics are composed of sulphur- and nitrogen-containing heterocycles as well as non-natural amino acids that are linked together to form complex macrocyclic frameworks (Figure 6.1A-D).

Two distinct families of thiopeptide compounds target the translational apparatus, one that targets the ribosome, referred to here as Class I thiopeptides, and the other, referred to as Class II thiopeptides, which targets the elongation factor EF-Tu. The best characterized of the Class I compounds include thiostrepton (ThS) and nosiheptide (NoS) (Figure 6.1 A, B), both of which have been crystallized bound to the large ribosomal subunit (Harms et al., 2008) (see later Figure 6.6A, B and G). These structures reveal that

the Class I thiopeptides bind within a region of the ribosome is part of the GTPase associated center (GAC), so-named because it is involved in translation G-protein factor binding and stimulation of GTPase activity (Wilson and Nierhaus, 2005). Biochemically, Class I thiopeptides have been shown to inhibit 70S initiation complex (70SIC) formation, by interfering with the initiation G-protein IF2 (Brandi et al., 2004) and references therein; (Grigoriadou et al., 2007) as well as elongation, by interfering with both the G-proteins EF-Tu (Gale et al., 1981; Gonzalez et al., 2007; Modelell et al., 1971) necessary for rapid cognate aminoacyl-tRNA binding to the ribosome, and EF-G, which catalyzes translocation of the $tRNA_2$-mRNA complex from the A and P sites to the P and E-sites (Pan et al., 2007; Pestka, 1970; Rodnina et al., 1999; Seo et al., 2006; Weisblum and Demohn, 1970). In contrast, the structurally similar Class II thiopeptides (Figure 6.1D) do not bind to the ribosome, but instead interact directly with EF-Tu (reviewed by Parmeggiani and Nissen, 2006). The crystal structure of the Class II thiopeptide GE2270A bound to EF-Tu reveals that the drug binds within a cleft between domains I and II of EF-Tu and directly overlaps with the binding site of the terminal end of the aminoacyl-tRNA (Parmeggiani et al., 2006; Parmeggiani and Nissen, 2006) (see later Figure 6.7A-C). Binding of the drug has been proposed to prevent the closing of domain I and II, which is necessary for the induced-fit binding of EF-Tu to the tRNA, and thus the drug prevents ternary complex formation (Parmeggiani and Nissen, 2006).

Although ThS is already in veterinary usage, its low water solubility and poor bioavailability has so far precluded its use in human medicine. Recent success has been

reported in the total synthesis of a number of Class I and II thiopeptides (reviewed by Hughes and Moody, 2007; Nicolaou et al., 2009), including amongst others ThS (Nicolaou et al., 2005a; Nicolaou et al., 2005c), and GE2270A (Nicolaou et al., 2008b; Nicolaou et al., 2006). Such synthetic studies pave the way to generating improved thiopeptide derivatives by identifying synthetic fragments (or derivatives thereof) that display biological activity or can act as new lead compounds.

We have utilized a series of translation machinery assays to screen a library of thiopeptide antibiotic precursor compounds. Unlike the parent antibiotics thiostrepton, nosiheptide and GE2270T, only a few of the precursor compounds display any significant inhibitory properties, even at high concentrations. Instead, however, four structurally distinct families of precursor compounds (Figure 6.1E-H) were discovered that relieve the inhibitory effect imparted by the parent compounds. The different precursor families exhibit differential effects with respect to the inhibitory antibiotic that is counteracted, as well as the target whether the ribosome or EF-Tu. Two of the families represent completely new compounds with respect to their ability to bind to ribosomes and thus open the path to the development of novel antimicrobials. The application of such screening strategies will enable the identification of new lead compounds that are not detected using conventional inhibitory screening protocols.

The work presented here is a collaborating effort by our group and Dr. Wilson's group. Specifically the experiments in Figs 6.2, 6.3C, and 6.3D are completed by our group and the rest of the data is accomplished by Dr. Wilson's group.

6.3 MATERIALS AND METHODS

6.3.1 Component preparation

GE2270A, T and C1 and the library of thiopeptide precursor compounds were synthesized as described previously (Nicolaou et al., 2005b; Nicolaou et al., 2008a; Nicolaou et al., 2008b; Nicolaou et al., 2006). Thiostrepton was purchased from Sigma, while nosiheptide was the kind gift from Prof. Floss and micrococcin P1 was supplied by Dr. Torsten Stachlhaus. With an extinction coefficient of 27,000 cm^{-1} M^{-1} at 280 nm in DMSO (Bausch et al., 2005), the concentration of ThS is higher by weight than by absorbance but the difference within a 10-20% range is acceptable. Northcote et al. 1994 reported the UV spectrum (in methanol) of glycothiohexide has extinction coefficients at 296 nm (33,200 cm^{-1} M^{-1}) and 349 nm (23,800 cm^{-1} M^{-1}). Because of the structural similarity between glycothiohexide and nosiheptide, it is reasonable to estimate the concentration of nosiheptide, in the same magnitude with one by weight.

The *tetM* gene (Tn916) cloned into the pET24b vector was the kind gift from Prof. V. Burdett. Tet(M) protein was expressed in BL21 (DE3) pRIL cells in 20 °C with 0.2 mM IPTG. *E. coli* EF-G cloned into pQE70 vector was expressed in XL1 blue cells. Both proteins were purified using Ni-NTA metal-affinity chromatography (Qiagen), followed by gel-filtration chromatography on a HiLoad 26/60 Superdex 75 prep grade column (Amersham-Pharmacia). For the experiments described in Figures 2 and 5, ribosomes, $IF2_{Cy3}$, IF1, IF3, 30S subunits, MDCC-labeled phosphate-binding protein (PBP),

022AUG mRNA, and fMet-tRNA^{fMet}, were prepared as described previously (Qin et al., 2009) as was EF-G (Pan et al., 2007).

6.3.2 IF2^{Cy3} fluorescence change assay

Reactions were carried out in a 384-well assay plate. 50S subunits were preincubated (15 min at 37 °C) with a series of concentrations of the test compounds in DMSO that are transferred from a premade compound plate to the assay plate by a Perkin-Elmer Evolution P3 liquid handler. Reaction was initiated by addition of 30S initiation complex (30SIC) to each well of the plate. Fluorescence (579 nm) was read with a 2103 EnVision Multilabel Plate Reader on excitation at 550 nm. For the reversal experiment, 30SIC was preincubated with ThS (10 min, 37 °C), followed by a second preincubation with test compounds (10 min, 37 °C), and reaction was initiated by 50S addition.

6.3.3 GTPase activity assays

For both assays described below, reactions performed in the absence of ribosomes were used as a background signal to account for the intrinsic GTPase activity of EF-G or Tet(M).

By Malachite Green. GTPase activity was measured using the Malachite Green Phosphate Kit (BioAssay) that quantifies the green complex formed between Malachite Green, molybdate and free orthophosphate. All reactions contained 30 nM *E. coli* 70S

ribosomes, 20 μM GTP and 60 nM protein in the presence or absence of antibiotics as necessary. Reactions were transferred into 96-well microtiter plates and color formation was measured on Tecan - Infinite M1000 microplate reader at 650 nm.

*By MDCC-labeled PBP***.** GTPase activity was measured using the MDCC-labeled PBP complex, which measures free phosphate release as an increase in fluorescence, and utilizes a Pi-MOP system to minimize the background due to phosphate present in the original medium (Brune et al., 1994; Seo et al., 2006). Reactions were carried out in a 384-well assay plate. Ribosomes were preincubated (15 min at 37 °C) with a series of concentrations of the test compounds in DMSO that are transferred from a premade compound plate to the assay plate by a Perkin-Elmer Evolution P3 liquid handler. Reaction was initiated by addition of an ice-cold solution containing EF-G, PBP-MDCC, and GTP to each well of the plate, a process that was completed in under 30 sec. Fluorescence (450 nm) was read within 1 min using a 2103 EnVision Multilabel Plate Reader, on excitation at 405 nm. For the reversal experiment, ribosomes were preincubated with ThS (10 min, 37 °C), followed by a second preincubation with test compounds (10 min, 37 °C), and reaction was initiated by EF-G, PBP-MDCC, and GTP as above.

6.3.4 In vitro transcription-translation assay

All coupled transcription-translation experiments were performed using an *E. coli* lysate-based system in the presence and absence of antibiotics as described previously

(Dinos et al., 2004; Szaflarski et al., 2008). Reactions were transferred into 96-well microtiter plates and the GFP fluorescence was measured with a Typhoon Scanner 9400 (Amersham Bioscience) using a Typhoon blue laser module (Amersham Bioscience). Images were then quantified using ImageQuantTL (GE Healthcare) and represented graphical using SigmaPlot (Systat Software, Inc.).

6.3.5 Modeling and figure preparation

Chemical structures for the precursor compounds were drawn and converted to 3D coordinates using ChemDraw (Advanced Chemistry Development, Inc. Toronto, Canada). PA2 models utilized the thiostrepton binding position on the *Deinococcus radiodurans* 50S (D50S) subunit (PDB ID 3CF5) (Harms et al., 2008), whereas PD1 and PD2 were based on the D50S-nosiheptide complex (PDB ID 2ZJP) (Harms et al., 2008). PyMol (http://www.pymol.org) was used to model the PB1 and PC compounds, align EFTu ●GE2270A (yellow; PDB ID 2C77; Parmeggiani et al., 2006) and EF-Tu●tRNA (blue; PDB ID 1TTT; Nissen et al., 1995) on basis of domain II, as well as prepare all gray-traced figures.

6.4 RESULTS

Several assays were used to examine thiopeptide precursor compounds for their abilities to bind to the thiostrepton binding site, either by mimicking ThS inhibition of specific ribosomal functions, or by protecting the ribosome against the inhibitory effects of ThS via a competition effect. These assays, which are discussed in turn below,

measure (i) IF2 conformational change during the conversion of 30S initiation complex (30SIC) to 70S initiation complex (70SIC), (ii) ribosome-dependent stimulation of the GTPase activity of EFG and (iii) the cell-free synthesis of green fluorescent protein (GFP) using an *Escherichia coli in vitro* coupled transcription-translation (TT) assay.

6.4.1 The thiopeptide precursor PA1 inhibits 70SIC formation.

The initiation factor IF2 is essential for 70SIC formation from 30SIC and 50S subunits (Antoun et al., 2003; Grigoriadou et al., 2007). Elsewhere we have shown that the fluorescence of a Cy3 derivative of IF2 ($IF2_{Cy3}$) increases on 70SIC formation resulting from the binding of a 50S subunit to a 30SIC containing $IF2_{Cy3}$ (Qin et al., 2009). This increase is inhibited by both ThS and NoS (Figure 6.2A), largely as a result of the effect of these antibiotics in inhibiting both the rate and extent of 70SIC formation (Grigoriadou et al., 2007) and data not shown. Measuring the extent of fluorescence change is thus a convenient way of monitoring thiopeptide precursor effects on 70SIC formation. A library of thiopeptide precursor compounds, as well three forms of the EF-Tu inhibitor GE2270 (A, T, and C1) were screened for this activity, along with ThS and NoS as positive controls. Only one precursor, denoted PA1 (Figure 6.2B), showed any measurable activity in inhibiting the fluorescence change, with an apparent K_i, 25 μM, some 60 – 400-fold higher than for ThS or NoS, respectively. Although PA1 does not bind with very high affinity, it apparently does so with considerable structural specificity, since the inhibitory effect was not seen for compounds PA2-PA3 which have only minor

structural differences from PA1 (Figure 6.1E). The thiopeptide precursors were also screened for their abilities to reverse ThS inhibition of the $IF2_{Cy3}$ fluorescence increase on 70SIC formation. In no case was such reversal observed.

6.4.2 Differential effects of precursor compounds on factor-dependent GTPase assays

Vacant 70S ribosomes are known to stimulate the GTPase activity of EF-G via formation of a 70S•EF-G•GTP complex. Such stimulation is strongly inhibited by ThS (Pestka, 1970; Weisblum and Demohn, 1970). We used two multiple turnover GTPase assays to screen thiopeptide precursors for inhibitory activity.

The first assay measured EF-G GTPase activity, via formation of a Malachite Green complex, for hundreds of turnovers. Under conditions for which ThS (1 μM) almost completely abolished such activity, we identified three distinct classes of precursor compounds (PA-PC; Figure 6.1E-G) that exhibited modest inhibitory effects when added at 50 μM (Figure 6.3A). However, we note that none of these compounds added at 10 μM showed appreciable inhibition (data not shown). As expected, the negative control, GE2270T, had no effect at a concentration of 50 μM (Figure 6.3A). In order to determine whether the modest inhibitory effects seen in Figure 6.3A were specific for EF-G, we next checked whether these compounds could also inhibit the ribosome-dependent stimulation of the Tet(M) GTPase. Tet(M) is a GTPase that binds to the ribosome analogously to EF-G, and confers resistance to the antibiotic tetracycline by weakening

its binding to the ribosome (reviewed by Connell et al., 2003). Similar to the results for EF-G, representatives of the PA and PC families exhibited modest inhibitory effects on Tet(M) GTPase at high concentration (100 μM) (Figure 6.3B). However, in contrast to EF-G, little or no inhibition was observed for the PB family, suggesting that it is specific for EF-G.

The second assay measured EF-G GTPase activity from the fluorescence increase of released Pi binding to the fluorescent phosphate binding protein MDCC-PBP (He et al., 1997; Seo et al., 2006). This assay, which can in principle be used for single turnover measurement, was here employed to measure several turnovers, as determined by the stoichiometric ratio (5:1) of MDCC-PBP to ribosome. As performed, this assay could only detect very potent inhibitors of EF-G GTPase, since fluorescence wasn't measured until 1 min after initiation of reaction, whereas in the absence of inhibition the full fluorescence change is complete within 5 – 10 sec (data not shown). It is thus no surprise, given the results presented in Figure 6.3A, that although ThS inhibited this assay with an apparent K_i of 1.1 μM, neither any of the precursors tested, nor even NoS or MiC, showed measurable inhibition up to a concentration of 100 μM (Figure 6.3C). In contrast, both NoS and MiC added at very low concentration protected against inhibition by 1.2 μM ThS, with half-maximal effects seen at 0.04 μM and 0.11 μM, respectively (Figure 6.3D). However, none of the precursor compounds afforded similar protective effects up to 50 – 100 μM of added precursor.

6.4.3 Protective effects of precursor compounds on thiopeptide-mediated translation inhibition

Although as expected, ThS, NoS and GE2270T were potent inhibitors of GFP synthesis using an *in vitro* TT assay (Figure 6.4, lanes 2-4), none of the precursor compounds tested displayed any significant inhibitory activity in this assay (Figure 6.4, white bars), even at high concentrations (50-100 μM). In contrast, addition of 50 μM of representatives precursor compounds from four structural distinct classes PA-PD (Figure 6.1E-G), could reverse the inhibitory effect of 5 μM ThS (Figure 6.4**,** grey bars). The most effective protection was seen with PA2, which restored translation back to levels observed in the absence of antibiotic (Figure 6.4, lane 6), whereas in comparison, PB1, PC1 and PD1 restored translation to 40-60% (Figure 6.4, lanes 13-28). Additionally, we find that the 5S, 6R stereoisomer of PA2 (PA4) exhibited some protective properties (~35% compared to 100% for PA2). The structural specificity of these effects is clear from the failure of precursors that are chemically related to exhibit similar protective effects against ThS inhibition. These include PA3, (Figure 6.4, lanes 6 and 8), which differs from PA2 by lacking only a double bond within the central piperidine ring (Figure 6.1E), and PD2 (Figure 6.4, lanes 26 and 28) which, with respect to PD1, has an altered side-chain on one of the thiazole rings (Figure 6.1H).

Interestingly, PA2, PB1, PC1 and PD1 displayed marked differences in their abilities to reverse the inhibitory effects of NoS (5 μM) and GE2270T (25 μM), as compared to the inhibitory effects of ThS. Thus, as shown in Figure 6.5, PA2 was an omnipotent protector of translation, restoring translation levels in the presence of all three thiopeptide

inhibitors, with the following order of efficiency: ThS (100 %) > GE2270T (80 %) > NoS (60 %), PD1 rescued translation in the presence of ThS and GE2270T, but not NoS, and PB1 and PC1 efficiently rescued translation only against ThS. As was true for ThS, neither PA3, PB2, PC2, nor PD2 were able to reverse inhibition by NoS or GE2270T (data not shown).

6.4.4. Interaction of thiopeptide precursors with the ribosome

The specific protective effect of the precursor compounds against ThS suggests that these compounds specifically compete with ThS for binding to the ribosome. Structural (Harms et al., 2008; Jonker et al., 2007) and biochemical data (Spahn and Prescott, 1996; Xing and Draper, 1996) for ThS suggests that the high affinity of this drug for the ribosome results from cooperative interaction between nucleotides in H43/44 of the 23S rRNA and the L11-NTD (Figure 6.6A, B). Given the structural similarity between PA2 and ThS, it is possible to model the position of this compound bound to the ribosome (Figure 6.6C, Harms et al., 2008). The substitution of the double-bond in the piperidine ring of PA2 to generate PA3 abolishes the protective effect of the compound (Figure 6.4). The chemical structure of PA3 suggests that the piperidine ring would not be planar as in PA2. This in turn changes the relative position (by 0.5 Å) of the attached thiazole moiety (data not shown), which based on the model would shift it towards Pro27 of L11-NTD and thus encroach on the thiopeptide binding site. Such modest displacements within

drug binding sites have been shown to have dramatic effects on the affinity of compounds, and often lead to antibiotic resistance (Blaha et al., 2008; Tu et al., 2005).

Although it is more difficult to model the PB and PC series of compounds based on the available structures, it is clear that the aromatic rings within these families suggest a potential mode of binding that establishes simultaneous stacking interactions with both H43/44 and L11-NTD (Figure 6.6D, E). Alterations that disrupt these rings, as seen for PC2 (Figure 6.6F), could explain a reduced binding and corresponding loss in protection (Figure 6.4). The PD class of precursors is structurally most similar to the pyridine core of NoS (Figure 6.1). NoS is oriented differently on the ribosome compared to ThS, establishing stacking interactions with Pro22 but not Pro26 (Figure 6.6G; Harms et al., 2008). Based on our modeling, PD1 can make analogous interactions with Pro22 as nosiheptide (Figure 6.6H), whereas the inactive PD2 cannot (Figure 6.6I).

6.4.5 Interaction of thiopeptide precursors with EF-Tu

The thiopeptide GE2270A has been crystallized in complex with EF-Tu, revealing the drug binds within a covered groove in domain II, as well as spanning across the active site cleft of EF-Tu to interact with the domain I, the G domain (Figure 6.7A; Parmeggiani et al., 2006). GE2270A overlaps the binding site of the terminal A76 and aminoacyl moiety of the tRNA (Figure 6.7B) and is proposed prevent the closing of domains I and II necessary for the induced fit binding of aa-tRNA (Figure 6.7C), and thereby preventing ternary complex (EFTu• GTP•tRNA) formation (reviewed by Parmeggiani and Nissen,

2006). The structural similarity between the PA and PD with GE2270A (Figure 6.1) suggests that these compounds would also bind within the groove of domain II of EF-Tu (Figure 6.7D) and overlap with the A76 of the tRNA (Figure 6.7E). However, the truncated nature of these compounds prevents them from establishing additional interactions with domain I, even in the closed tRNA-bound ternary complex state of EF-Tu (Figure 6.7F).

6.5 DISCUSSION

Here we present several translation-related assays utilizing high-throughput 96- or 384-microtiter plate formats that have been used to screen a library of thiopeptide precursor compounds for their abilities to inhibit one or more aspects of translation and/or reverse the inhibition of known thiopeptide antibiotics. These screens identified four distinct families of precursor compounds, termed PA-PD, which could act as potential lead compounds for development of novel antimicrobials.Two of the families identified, PA and PD, contain a six-membered nitrogen heterocycle core (PA, dehydropiperidine; PD, pyridine) analogous to the thiopeptide antibiotics thiostrepton and GE2270A (Figure 6.1). The crystal structures of thiopeptides bound to the ribosome (Harms et al., 2008) and of GE2270A bound to EF-Tu (Parmeggiani et al., 2006) reveal the importance of the heterocycle core of these compounds for interaction with their respective targets, and enables a model to be presented for how PA and PD members are likely to interact with the ribosome and/or EF-Tu (Figure 6.5 and 6.6). Such models are

consistent with the fact that both families have members, such as PA2 and PD2, which can rescue translation in the presence of ThS and GE2270T, probably by direct competition for binding between the precursor compound and the thiopeptide antibiotic. In addition, PA1 and PA2 displayed inhibitory activity against translational GTPases IF2 (Figure 6.2B), and EF-G and Tet(M) (Figure 6.3A,B), respectively. However, compared to the parent thiopeptide compounds, much higher concentrations of the precursor compounds were necessary to exhibit similar effects, most likely indicating the much lower binding affinity of the precursors. The ineffectiveness of precursor compound PA2 as a direct inhbitor was surprising, since this compound has been previously reported to exhibit antimicrobial activity against methicillin-resistance *Staphlococcus aureus* and vancomycin-resistant *Enterococcus faecalis* with a minimal inhibitory concentration (MIC) of 5 μM (Nicolaou et al., 2005b). Our results suggest therefore that the inhibitory effect of PA2 *in vivo* may in fact not be related to translation, but verification of this point will require further investigation.

The other two families identified in our screen, PB and PC, to our knowledge have not been previously reported to target the translational machinery. PB1 is chemically similar to the thiazolidine precursor compound used to generate the pyridine core of amythiamicins (Nicolaou et al., 2008a), which target EF-Tu analogously to GE2270A (Parmeggiani et al., 2006; Parmeggiani and Nissen, 2006), whereas the PC series of compounds contain a protected β-hydroxy-α-aminoacid, which is a precursor in the synthesis of GE2270A/T/C1. Curiously, the PB and PC families display much higher

specificity for the ribosome than for EF-Tu, as evidenced by the ability of PB1 and PC1 to restore translation more efficiently in the presence of ThS, as compared with GE2270A (Figure 6.5). Although PB1 and PC1 are structurally distinct (Figure 6.1), we believe the common aromatic/cyclic nature of both these compounds is important for ribosome binding. Accommodation of EF-G on the ribosome involves the insertion of domain V of EF-G into the crevice between H43/44 and L11-NTD. Inhibition by Class I thiopeptides has been proposed to stem in part from their physically linking L11-NTD to H43/44, thereby locking the cleft shut (Harms et al., 2008). We suggest that PB1 and PC1 can also span the L11-rRNA crevice (Figure 6.6D, E) and perform this locking function, analogous to ThS/PA1 (Figure 6.6B, C) and NoS/PD1 (Figure 6.6G, H). Similarly to PA/D, the high concentrations of PB/C required to inhibit the ribosome-dependent GTPase activity of EF-G \ indicative of their low binding affinities for the ribosome. Such low affinity may allow translation factors, such as IF2 or EF-G, to displace the precursor from the drug binding site during accommodation on the ribosome, or for EF-Tu binding to tRNA during ternary complex formation, thus explaining the absence of any direct inhibitory effect of any of the precursors on GFP synthesis. The differential effects of the precursors on the GTPase assays compared to the TT assay is probably related to the ribosome concentrations in the GTPase assays being ~10x - 100x less (30 - 300 nM) compared to the TT assay (~2 μM) and to the putative higher affinity of EF-G for translating rather than empty ribosomes (Sergiev et al., 2005).

The majority of clinically used antibiotics targeting the ribosome bind either to the decoding region on the small subunit or within either the peptidyltransferase center or the adjacent peptide exit tunnel of the large subunit, where they interact almost exclusively with ribosomal RNA (Spahn and Prescott, 1996; Wilson, 2004). The Class I thiopeptide compounds, however, are distinct in that they target a different region of the ribosome, namely the GTPase-associated region or translation-factor binding site, where they interact with both rRNA and ribosomal protein L11. As a consequence, no cross-resistance has been found between thiopeptide antibiotics and other clinically important drugs. Therefore, the identification of compounds such as PA-PD provides a good base as lead compounds for the development of novel antimicrobial agents that target this region of the ribosome. Furthermore, the ability of some precursor compounds, such as PA1 and PD1, to bind both EF-Tu and the ribosome suggests the feasibility of developing antimicrobials that are dual inhibitors of ribosomes and ternary complex formation.

6.6 SIGNIFICANCE

We present a series of translation machinery assays that can be used to screen for novel lead compounds that not only inhibit specific steps of translation, but also relieve the inhibitory effects of other inhibitory compounds. Using these assays to screen a library of thiopeptide precursor compounds, we have identified four distinct families of compounds that inhibit either IF2, EF-G and/or Tet(M), as well as confer protective effects against thiopeptide translation inhibitors of both the ribosome and EF-Tu. Our

findings not only elucidate the mechanism of action of thiopeptide compounds, but also illustrate the potential of such highthroughput assays to identify novel lead compounds that might be missed using conventional inhibitory screening protocols. Whereas the IF2 and EF-G GTPase assays are specifically useful for screening antibiotics interfering with translation G-factor proteins, the TT assay is generally applicable for screening all classes of translation inhibitors, including those targeting the peptidyltransferase and decoding centers of the ribosome, and other novel ribosomal sites, in addition to those interfering with translation G-factor proteins.

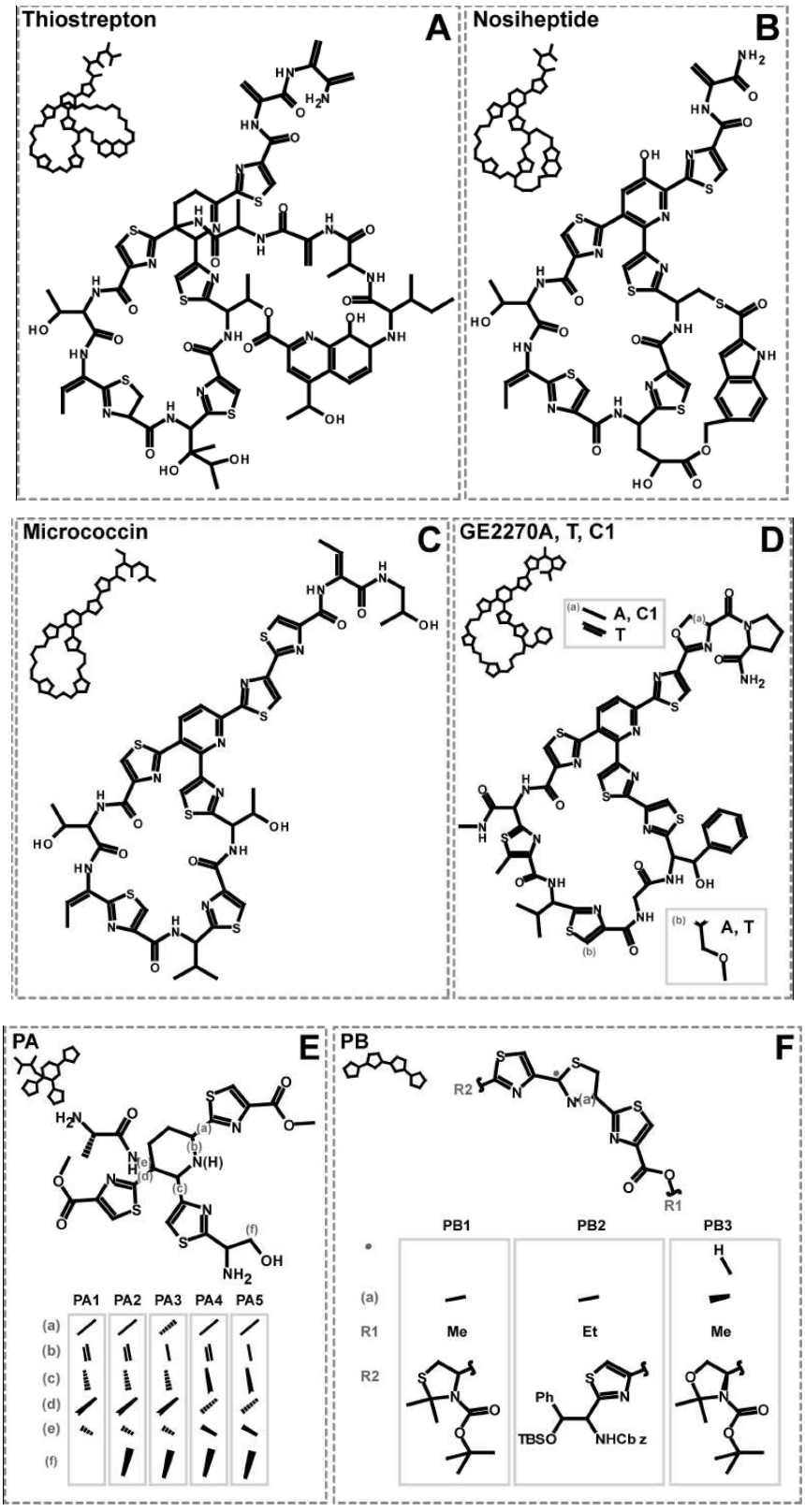
Thiostrepton
A
Nosiheptide
B
Micrococcin
C
GE2270A, T, C1
D
A, C1
T
A, T
PA
E
PA1 PA2 PA3 PA4 PA5
(a)
(b)
(c)
(d)
(e)
(f)
PB
F
R2
R1
PB1 PB2 PB3
(a)
R1
R2
Me
Et
Me
Ph
TBSO
NHCbz

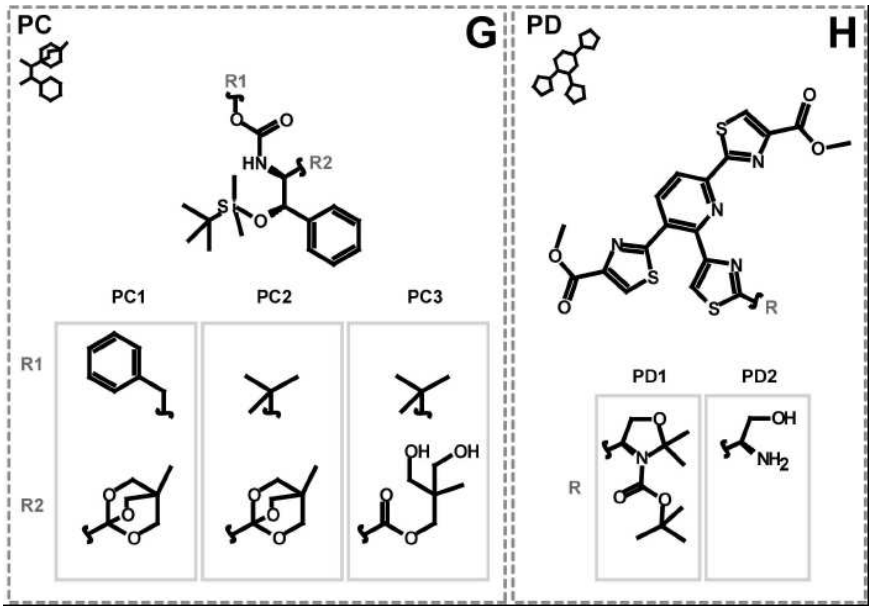

Figure 6.1. Chemical structures of thiopeptide antibiotics and precursor families PA–PD

Chemical structures of the thiopeptide antibiotics (A) thiostrepton (ThS), (B) nosiheptide (NoS), (C) micrococcin (MiC), and (D) GE2270A/T/C1, and precursor families (E) PA1-5, (F) PB1-3, (G) PC1-3, and (H) PD1-2.

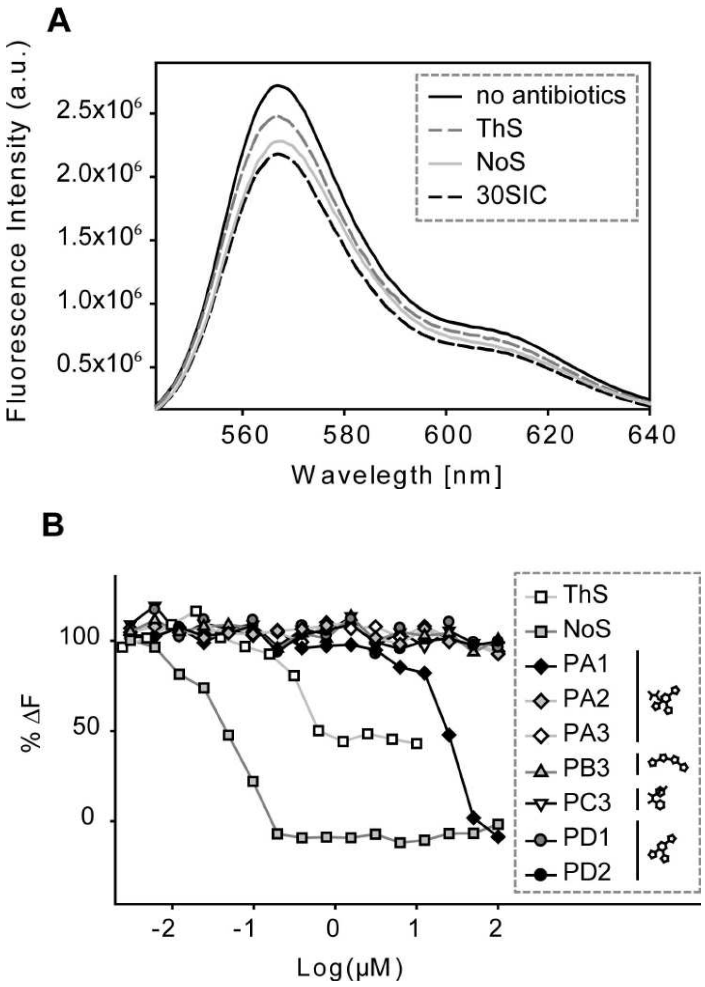

Figure 6.2. The IF2 fluorescence change assay.

(A) Emission spectra of IF2Cy3-containing 30S initiation complex mixed with 50S subunits in the presence of ThS or NoS. 50S was pre-incubated with antibiotics for 5 min at 37 ^{o}C and then rapidly mixed with 30S initiation complex at 20 oC, followed by 5 min incubation before measurements. Black solid trace: no antibiotics; gray dashed trace: thiostrepton; gray solid trace: nosiheptide; black dashed trace: 30S initiation complex alone. The final concentrations are IF1, IF3, fMet-tRNAfMet, 0.45 μM; IF2Cy3, 0.15 μM; mRNA, 0.90 μM; 30S, 0.30 μM; 50S 0.30 μM; GTP, 100 μM and ThS, MiC, NoS, 1.5

μM. (B) Dose response curves for the inhibition of fluorescence change on mixing IF2Cy3-containing 30S initiation complex with 50S subunits in the presence of thiopeptide compounds. The Y-axis indicates the % ΔF in the presence of added compound relative to the ΔF in the absence of added compound relative to the fluorescence of 70SIC by itself. Final concentrations are IF2Cy3, 0.15 μM; IF1, IF3, fMet-tRNAfMet, 0.45 μM; 022AUGmRNA, 0.9 μM; 30S, 0.30 μM; 50S, 0.30 μM; GTP, 100 μM.

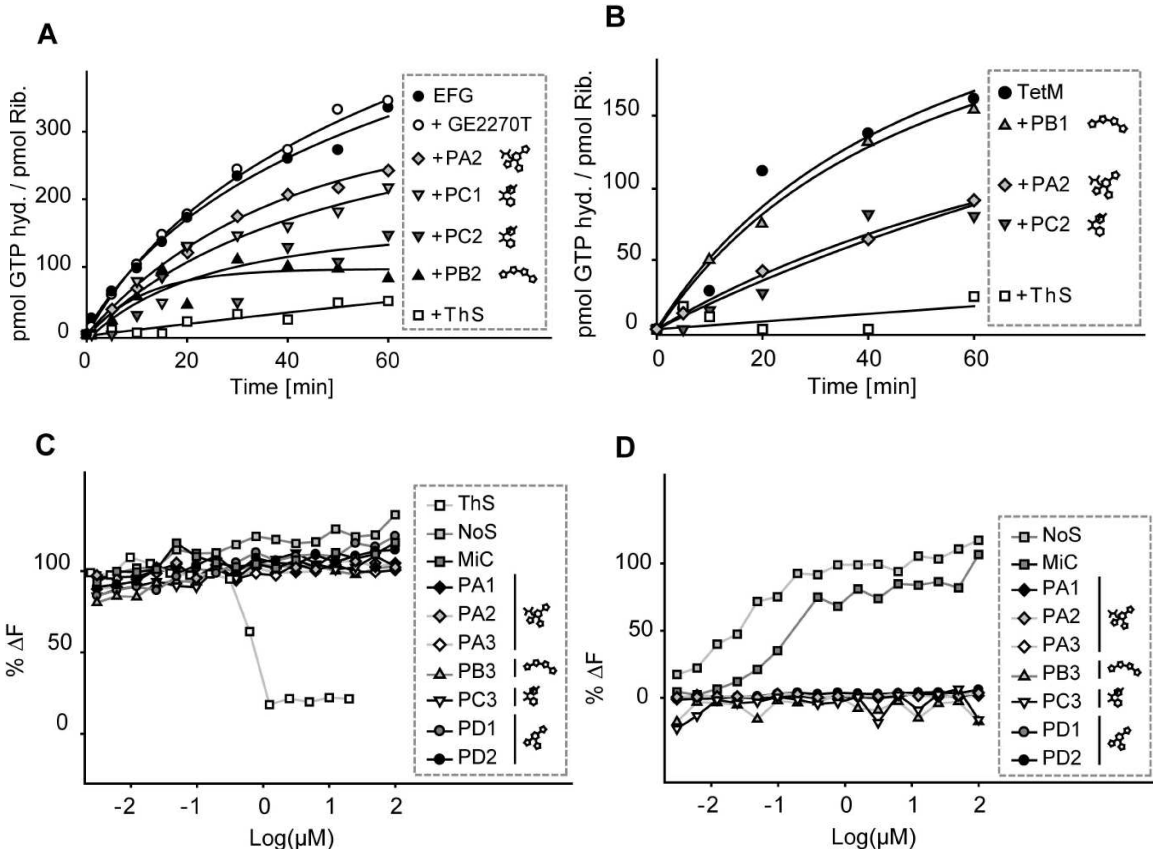

Figure 6.3. Effect of thiopeptides and precursor compounds on GTPase activity of EF-G and Tet(M)

(A) Inhibition of uncoupled ribosome-dependent EF-G GTPase by thiopeptides ThS (1 μM), GE2270T (25 μM) and precursors PA2, PB2, PC1 and PC2 (50 μM). Closed circles indicate GTPase activity of EF-G in the absence of antibiotic. (B) Inhibition of uncoupled ribosome-dependent TetM GTPase by ThS (1 μM) and precursors PA2, PB1 and PC2 (100 μM). Closed circles indicate GTPase activity of TetM in the absence of antibiotic. (C) The dose response curves of Pi release in the presence of ThS, NoS, MiC or precursor compounds. The Y axis indicates the % ΔF due to Pi release in the presence of added compound relative to the ΔF in the absence of added compound relative to the

fluorescence from EF-G interaction with the ribosome in the absence of any compound. The final concentrations are 70S, 0.3 μM; EF-G, 0.75 μM; MDCC-PBP, 1.5 μM; GTP,100 μM;7-methylguanine, 200 μM; nucleotide phosphorylase, 0.3 unit/ml. (D) Dose response curves for reversal of ThS inhibition of Pi release by NoS, MiC, or precursor compounds. The final concentrations for each component are 70S, 0.3 μM; EF-G, 0.75 μM; ThS, 1.2 μM; MDCC-PBP, 1.5 μM; GTP, 100 μM; 7-methylguanine, 200 μM;nucleotide phosphorylase, 0.3 unit/ml.

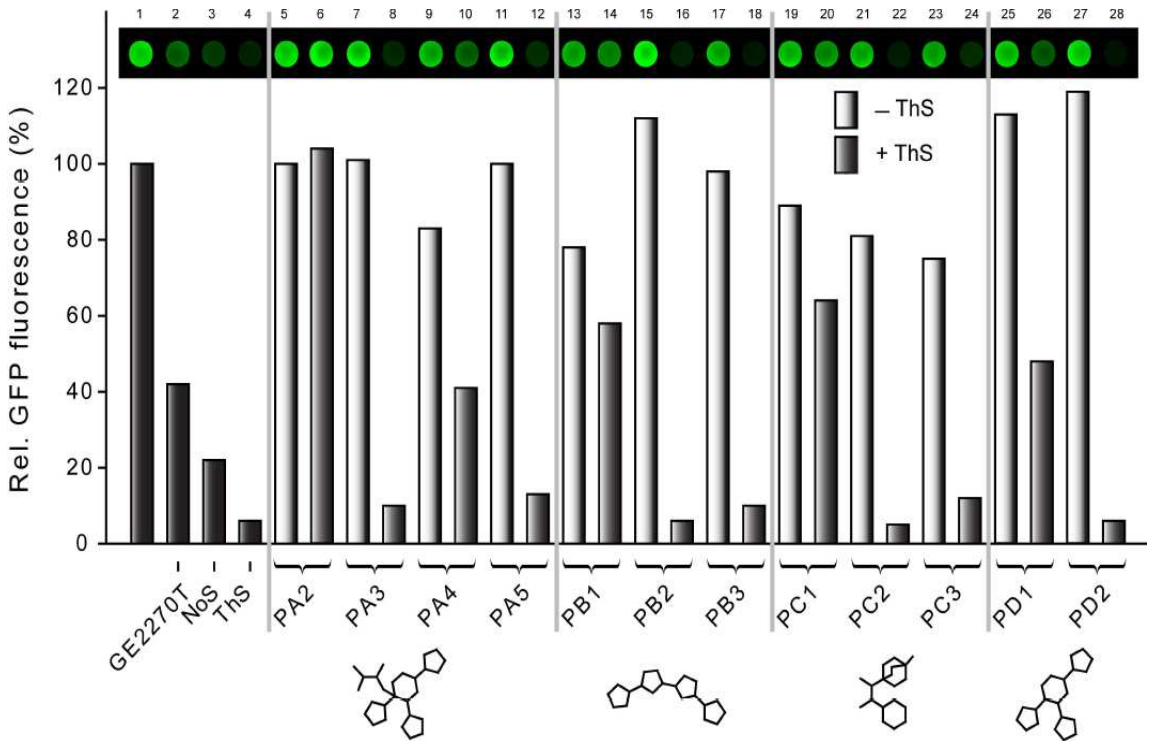

Figure 6.4. Precursor compounds protect translation from thiostrepton inhibition

In vitro transcription-translation of GFP in the absence or presence of ThS 25 μM GE2270T, 5 μM NoS and 5 μM ThS (black bars), or in the presence (50 μM) of precursor families PA2-5, PB1-3, PC1-3 and PD1-2 (-ThS, white bars) or with additional presence of 5 μM thiostrepton (+ThS, grey bars). GFP fluorescence from microtiter plate wells shown above each lane were quantified and represented as bars, with the fluorescence detected in the absence of antibiotic assigned to 100 %.

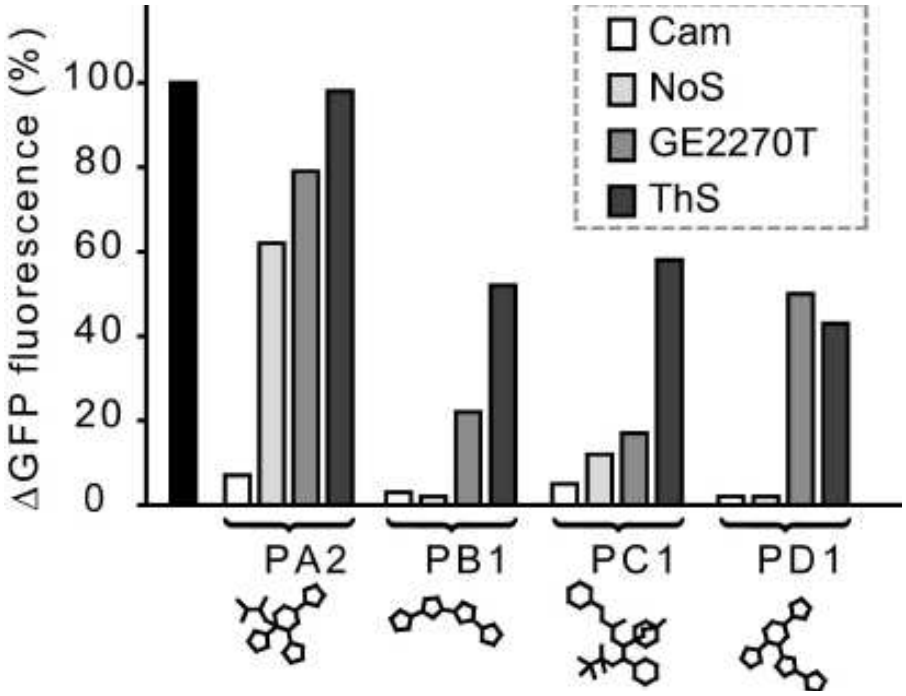

Figure 6.5. Differential protective effects of precursors against thiopeptide inhibition. Protection profiles of representative precursors from all described groups against chloramphenicol (Cam, 10 μM), nosiheptide (NoS, 5 μM), GE2270T (25 μM) and thiostrepton (ThS, 5 μM). GFP fluorescence in the absence of antibiotic assigned to 100 %, whereas the precursor results are presented as the % protection, given as the difference between the inhibition of translation by the active compound (Cam, NoS, GE2270T or ThS) in the presence and absence of the precursor compound (50 μM).

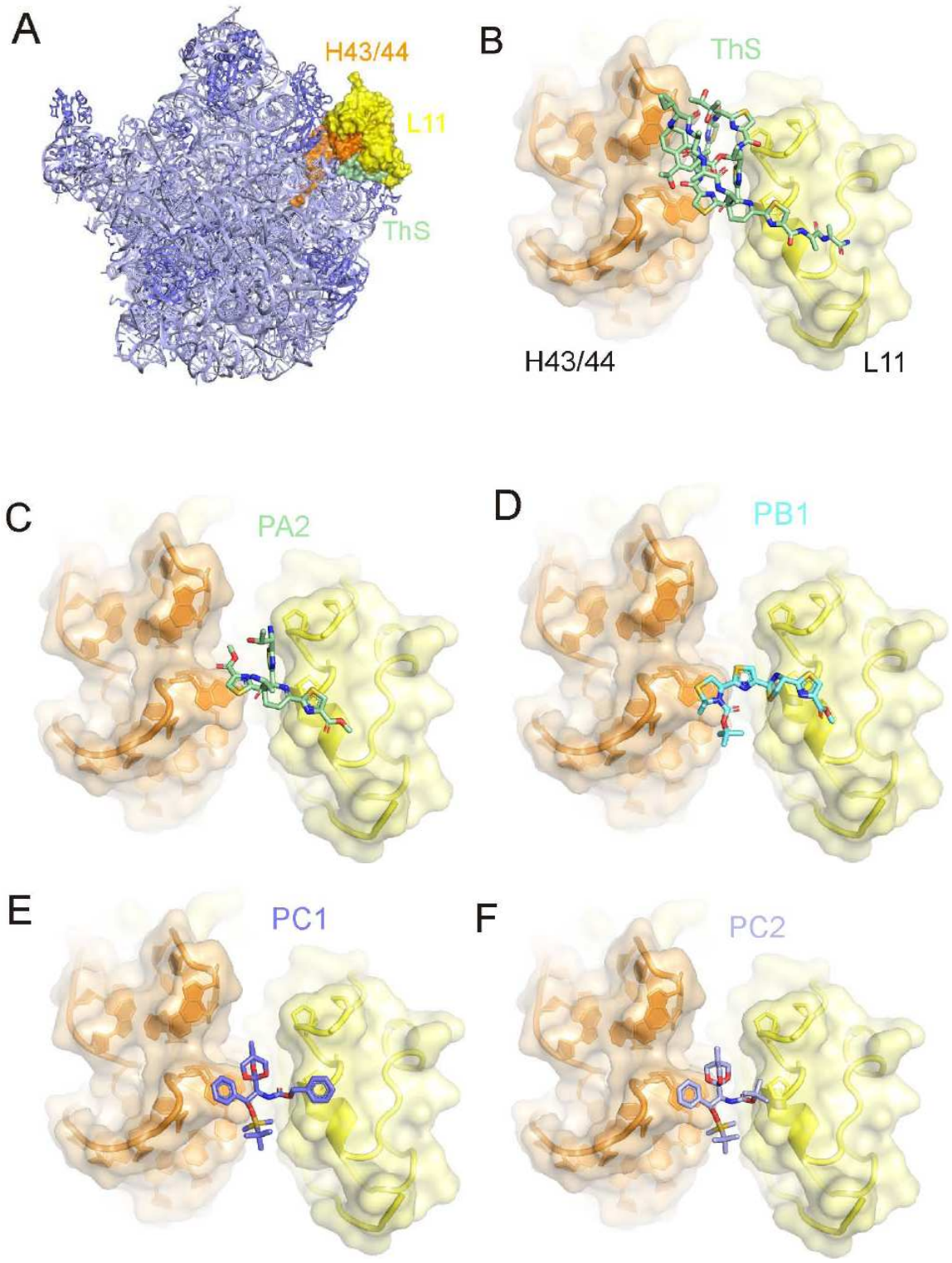
A
H43/44
L11
ThS
B
ThS
H43/44
L11
C
PA2
D
PB1
E
PC1
F
PC2

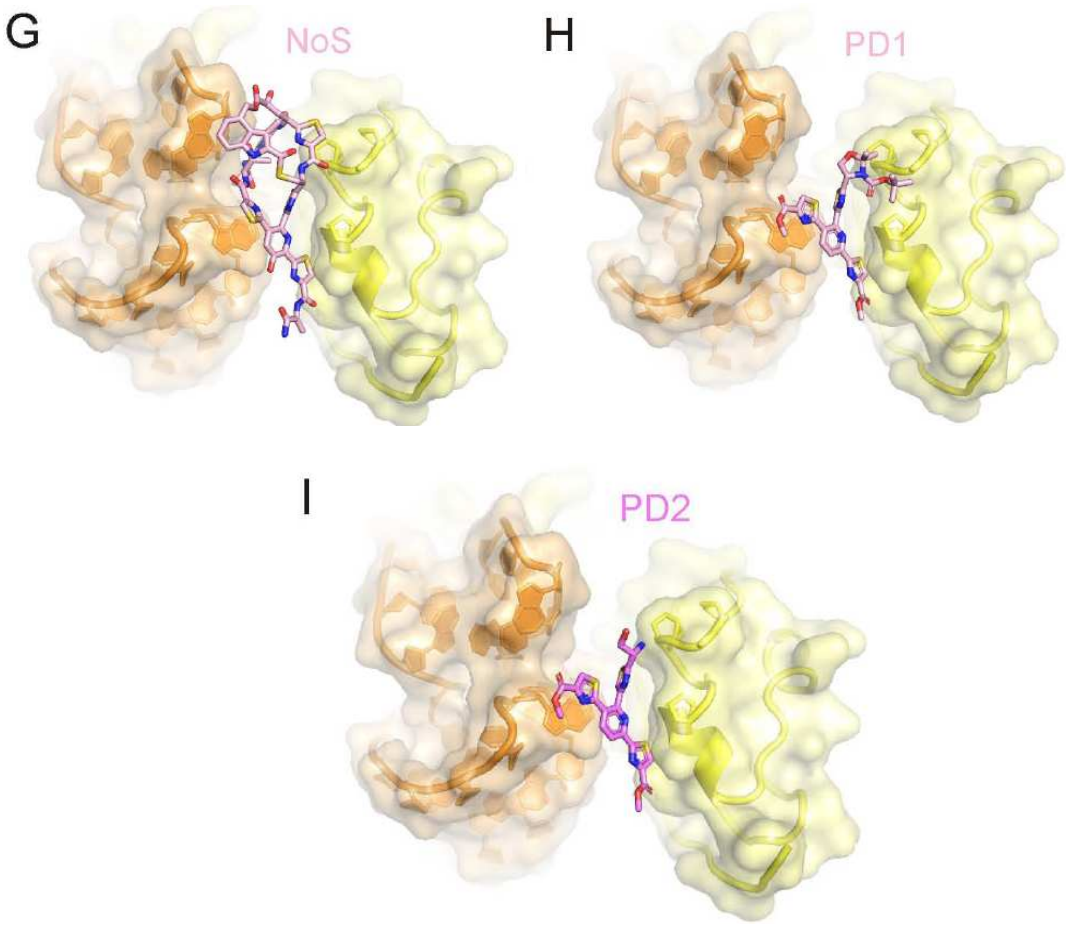

Figure 6.6. Binding site of precursor compounds on the ribosome

(A) Overview of thiopeptide binding site on the large ribosomal subunit. Interface view with helix 43 and 44 (H43/44, orange), L11 (yellow) and thiostrepton (green) highlighted with surface representation (from PDB ID 3CF5) (Harms et al., 2008). (B) The thiazole rings of ThS (green) interact with the RNA bases at the tips of H43/44 as well as the Prolines in the Nterminal domain of L11 (yellow). (C) Model for precursor PA2 bound to the ribosome, based on the position of ThS. PA1, but not PA3 (see text), bind similarly. (D-F) Possible modes of binding for precursors PB1 and PC1 based on ring stacking interactions with RNA and protein components of the ribosome, whereas PC2 lacks one

phenyl ring compared to PC1. (G) Nosiheptide (pink) interacts with the RNA bases at the tips of H43/44 as well as the N20 terminal domain of L11 (yellow), but in a distinct manner compared to ThS (using PDB ID 2ZJP; Harms et al., 2008). (H-I) Model for precursor PD1 and PD2 bound to the ribosome, based on the position of nosiheptide. PD2 lacks one ring moiety, suggesting binding would be destabilized.

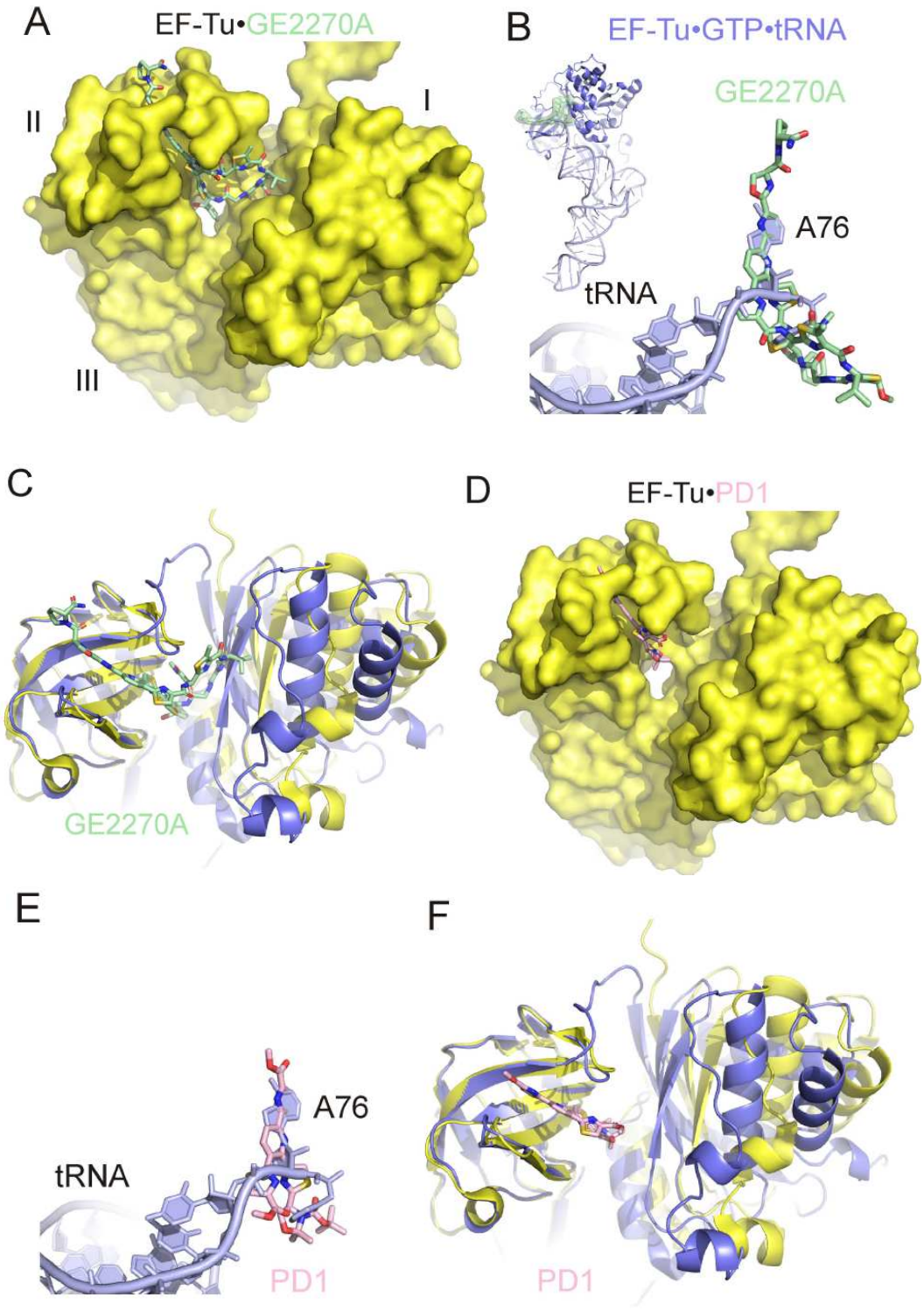
A
EF-Tu•GE2270A
II
I
III
B
EF-Tu•GTP•tRNA
GE2270A
A76
tRNA
C
GE2270A
D
EF-Tu•PD1
E
A76
tRNA
PD1
F
PD1

Figure 6.7. Binding site of precursor compounds on EF-Tu

(A) Structure of the thiopeptide GE2270A (green) bound to EF-Tu (yellow), with domains I, II and III indicated (PDB ID 2C77) (Parmeggiani et al., 2006). (B) GE2270A overlaps the binding position on EF-Tu of the terminal A76 and aminoacyl moiety of tRNA. Inset shows overview of EF-Tu●tRNA ternary complex (PDB ID 1TTT) (Nissen et al., 1995) with superimposition of GE2270A. (C) Superimposition of EF-Tu●GE2270A (yellow) and EFTu ●tRNA (blue), aligned on basis of domain II. Note that GE2270A (green) clashes with domain I of EF-Tu from the ternary complex (blue). (D) Model for precursor PD1 bound to EF-Tu based on EF-Tu●GE2270A complex (PDB ID 2C77) (Parmeggiani et al., 2006). (E) PD1 (pink) overlaps the binding position on EF-Tu of the terminal A76 and aminoacyl moiety of tRNA (blue). (F) as (C) but with PD1 instead of GE2270A. Note that PD1 does not clash with domain I of EF-Tu from the ternary complex (blue)

REFRENCE

Agrawal, R.K., Penczek, P., Grassucci, R.A., and Frank, J. (1998). Visualization of elongation factor G on the Escherichia coli 70S ribosome: the mechanism of translocation.Visualization of elongation factor G on the Escherichia coli 70S ribosome: the mechanism of translocation. Proc Natl Acad Sci USA *95*, 6134-6138.

Agrawal, R.K., Heagle, A.B., Penczek, P., Grassucci, R.A., and Frank, J. (1999). EF-G-dependent GTP hydrolysis induces translocation accompanied by large conformational changes in the 70S ribosome. Nat Struct Biol *6*, 643-647.

Agrawal, R.K., Penczek, P., Grassucci, R.A., Burkhardt, N., Nierhaus, K.H., and Frank, J. (1999b). Effect of buffer conditions on the position of tRNA on the 70 S ribosome as visualized by cryoelectron microscopy. J Biol Chem *274*, 8723-8729.

Agrawal, R.K., Linde, J., Sengupta, J., Nierhaus, K.H., Frank, J. (2001). Localization of L11 protein on the ribosome and elucidation of its involvement in EF-G-dependent translocation. J Mol Biol *311*, 777-787.

al-Karadaghi, S., Aevarsson, A., Garber, M., Zheltonosova, J., and Liljas, A. (1996). The structure of elongation factor G in complex with GDP: conformational flexibility and nucleotide exchange. Structure *4(5)*, 555-565.

Allen, G.S., Zavialov, A., Gursky, R., Ehrenberg, M., and Frank, J. (2005). The cryo-EM structure of a translation initiation complex from Escherichia coli. Cell *121*, 703-

712.

Allen, G.S., and Frank, J. (2007). Structural insights on the translation initiation complex: ghosts of a universal initiation complex. Molecular Microbiology *63*, 941-950.

Antoun, A., Pavlov, M.Y., Tenson, T., and Ehrenberg, M. (2004). Ribosome formation from subunits studied by stopped-flow and Rayleigh light scattering. Biol Proced Online *6*, 35-54.

Antoun, A., Pavlov, M.Y., Lovmar, M., and Ehrenberg, M. (2006). How initiation factors tune the rate of initiation of protein synthesis in bacteria. EMBO J *25(11)*, 2539-2550.

Arai, K., Kawakita, M., and Kaziro, Y. (1972). Studies on polypeptide elongation factors from Escherichia coli. II. Purification of factors Tu-guanosine diphosphate, Ts, and Tu-Ts, and crystallization of Tu-guanosine diphosphate and Tu-Ts. J Biol Chem *247*, 7029-7037.

Bagley, M.C., Dale, J.W., Merritt, E.A., and Xiong, X. (2005). Thiopeptide antibiotics. Chem Rev *105(2)*, 685-714.

Baker, N.A., Sept, D., Joseph, S., Holst, M.J., and McCammon, J.A. (2001). Electrostatics of nanosystems: application to microtubules and the ribosome. Proc Natl Acad Sci USA *98*, 10037-10041.

Berk, V., and Cate, J.H. (2007). Insights into protein biosynthesis from structures of bacterial ribosomes. Curr Opin Struct Biol *17*, 302-309.

Blaha, G., Gurel, G., Schroeder, S. J., Moore, P. B., and Steitz, T. A. (2008). Mutations outside the anisomycin-binding site can make ribosomes drug-resistant. J Mol Biol *379*, 505-519.

Blanchard, S.C., Kim, H.D., Gonzalez, R.L. Jr., Puglisi, J.D., and Chu, S. (2004). tRNA dynamics on the ribosome during translation. Proc Natl Acad Sci USA *101*, 12893-12898.

Boelens, R., and Gualerzi, C.O. (2002). Structure and function of bacterial initiation factors. Curr Protein Pept Sci *3*, 107-119.

Bradford, M.M. (1976). A rapid and sensitive method for the quantitation of microgram quantities of protein utilizing the principle of protein-dye binding. Analytical Biochemistry *72*, 248-254.

Brandi, L., Marzi, S., Fabbretti, A., Fleischer, C., Hill, W.E., Gualerzi, C.O., and Stephen, L.J. (2004). The translation initiation functions of IF2: targets for thiostrepton inhibition. J Mol Biol *335*, 881-894.

Brombach, M., Gualerzi, C.O., Nakamura, Y., and Pon, C.L. (1986). Molecular cloning and sequence of the Bacillus stearothermophilus translational initiation factor IF2 gene. Mol Gen Genet *205*, 97-102.

Brune, M., Hunter, J. L., Corrie, J. E., and Webb, M. R. (1994). Direct, real-time measurement of rapid inorganic phosphate release using a novel fluorescent probe and its application to actomyosin subfragment 1 ATPase. Biochemistry *33*, 8262-8271.

Caldas, T., Laalami, S., and Richarme, G. (2000). Chaperone properties of bacterial elongation factor EF-G and initiation factor IF2. J Biol Chem *275*, 855-860.

Calogero, R.A., Pon, C.L., Canonaco, M.A., and Gualerzi, C.O. (1988). Selection of the mRNA translation initiation region by Escherichia coli ribosomes. Proc Natl Acad Sci USA *85(17)*, 6427-6431.

Cameron, D.M., Thompson, J., March, P.E., and Dahlberg, A.E. (2002). Initiation factor IF2, thiostrepton and micrococcin prevent the binding of elongation factor G to the Escherichia coli ribosome. J Mol Biol *319(1)*, 27-35.

Canonaco, M.A., Gualerzi, C.O., and Pon, C.L. (1989). Alternative occupancy of a dual ribosomal binding site by mRNA affected by translation initiation factors. Eur J Biochem *182(3)*, 501-506.

Caserta, E., Tom步c, J., Spurio, R., Teana, A.L., Pon, C.L., and Gualerzi, C.O. (2006). Translation initiation factor IF2 interacts with the 30 S ribosomal subunit via two separate binding sites. J Mol Biol *362*, 787-799.

Celano, B., Pawlik, R.T., and Gualerzi, C.O. (1988). Interaction of Escherichia coli translation-initiation factor IF-1 with ribosomes. Eur J Biochem *178(2)*, 351-355.

Cenatiempo, Y., Deville, F., Dondon, J., Grunberg-Manago, M., Sacerdot, C., Hershey, J.W., Hansen, H.F., Petersen, H.U., Clark, B.F., and Kjeldgaard, M. (1987). The protein synthesis initiation factor 2 G-domain. Study of a functionally active C-terminal 65-kilodalton fragment of IF2 from Escherichia coli. Biochemistry *26(16)*, 5070-5076.

Cerutti, P.a.M., N. (1967). Selective reduction of yeast transfer ribonucleic acid with sodium borohydride. J Mol Biol *26(1)*, 55-66.

Cohlberg, J.A., and Nomura, M. (1976). Reconstitution of Bacillus stearothermophilus 50 S ribosomal subunits from purified molecular components. J Biol Chem *251*, 209-221.

Connell, S.R., Tracz, D. M., Nierhaus, K. H., and Taylor, D. E. (2003). Ribosomal protection proteins and their mechanism of tetracycline resistance. Antimicrob Agents Chemother *47*, 3675-3681.

Connell, S.R., Takemoto, C., Wilson, D.N., Wang, H., Murayama, K., Terada, T., Shirouzu, M., Rost, M., Schuler, M., Giesebrecht, J., et al. (2007). Structural basis for interaction of the ribosome with the switch regions of GTP-bound elongation factors. Mol Cell *25*, 751-764.

Cornish, P.V., Ermolenko, D.N., Noller, H.F., and Ha, T. (2008). Spontaneous intersubunit rotation in single ribosomes. Mol Cell *30*, 578-588.

Cundliffe, E., Dixon, P., Stark, M., Stoffler, G., Ehrlich, R., Stoffler-Meilicke, M., and Cannon, M. (1979). Ribosomes in thiostrepton-resistant mutants of Bacillus megaterium lacking a single 50 S subunit protein. J Mol Biol *132(2)*, 235-252.

Diaconu, M., Kothe, U., Schluzen, F., Fischer, N., Harms, J.M., Tonevitsky, A.G., Stark, H., Rodnina, M.V., and Wahl, M.C. (2005). Structural basis for the function of the ribosomal L7/12 stalk in factor binding and GTPase activation. Cell *121*, 991-1004.

Dinos, G., Kalpaxis, D.L., Wilson, D.N., and Nierhaus, K.H. (2005). Deacylated tRNA is released from the E site upon A site occupation but before GTP is hydrolyzed by EF-Tu. Nucleic Acids Res *33*, 5291-5296.

Dinos, G., Wilson, D. N., Teraoka, Y., Szaflarski, W., Fucini, P., Kalpaxis, D., and Nierhaus, and H., K. (2004). Dissecting the ribosomal inhibition mechanisms of edeine and pactamycin: the universally conserved residues G693 and C795 regulate P-site tRNA binding. Mol Cell *13*, 113-124.

dos Remedios, C.G., and Moens, P.D. (1995). Fluorescence resonance energy transfer spectroscopy is a reliable "ruler" for measuring structural changes in proteins. Dispelling the problem of the unknown orientation factor. J Struct Biol *115*, 175-185.

Dottavio-Martin, D., Suttle, D.P., and Ravel, J.M. (1979). The effects of initiation factors IF-1 and IF-3 on the dissociation of Escherichia coli 70 S ribosomes. FEBS Lett *97(1)*, 105-110.

Fortier, P.L., Schmitter, J.M., Garcia, C., and Dardel, F. (1994). The N-terminal half of initiation factor IF3 is folded as a stable independent domain. Biochimie *76(5)*, 376-383.

Frank, J., and Agrawal, R.K. (2000). A ratchet-like inter-subunit reorganization of the ribosome during translocation. Nature *406*, 318-322.

Frank, J., Gao, H., Sengupta, J., Gao, N., and Taylor, D.J. (2007). The process of mRNA-tRNA translocation. Proc Natl Acad Sci USA *104*, 19671-19678.

Gale, E.F., Cundliffe, E., Reynolds, P. E., Richmond, M. H., and Waring, M. J. (1981). Antibiotic inhibitors of ribosome function. In The molecular basis of antibiotic action. Bristol, UK, John Wiley and sons, 278-379.

Gao, H., Zhou, Z., Rawat, U., Huang, C., Bouakaz, L., Wang, C., Cheng, Z., Liu, Y., Zavialov, A., et al. (2007). RF3 induces ribosomal conformational changes responsible for dissociation of class I release factors. Cell *129*, 929-941.

Gonzalez, R.L.J., Chu, S., Puglisi, J.D. (2007). Thiostrepton inhibition of tRNA delivery to the ribosome. RNA *13(12)*, 2091-2097.

Gottlieb, M.a.D., B.D. (1975). The irreversible step in formation of initiation complexes of Escherichia coli. Biochemistry *14(5)*, 1047-1051.

Gotz, F., Fleischer, C., Pon, C.L., and Gualerzi, C.O. (1989). Subunit association defects in Escherichia coli ribosome mutants lacking proteins S20 and L11. Eur J Biochem *183*, 19-24.

Griaznova, O.a.T., R.R. (2000). Deletion of C-terminal residues of Escherichia coli ribosomal protein L10 causes the loss of binding of one L7/L12 dimer: ribosomes with one L7/L12 dimer are active. Biochemistry *39(14)*, 4075-4081.

Grigoriadou, C., Marzi, S., Kirillov, S., Gualerzi.C.O., and Cooperman, B.S. (2007a). A quantitative kinetic scheme for 70 S translation initiation complex formation. J Mol Biol *373*, 562-572.

Grigoriadou, C., Marzi, S., Pan, DL., Gualerzi,C.O., and Cooperman, B.S. (2007b). The translational fdelity function of IF3 during transition from the 30 S iInitiation

complex to the 70 S iInitiation complex. J Mol Biol *373*, 551-561.

Grunberg-Manago, M., Dessen, P., Pantaloni, D., Godefroy-Colburn, T., and Wolfe, A.D., Dondon, J. (1975). Light-scattering studies showing the effect of initiation factors on the reversible dissociation of Escherichia coli ribosomes. J Mol Biol *94(3)*, 461-478.

Gualerzi, C.O., Spurio, R., La Teana, A., Calogero, R., Celano, B., and Pon, C.L. (1989). Site-directed mutagenesis of Escherichia coli translation initiation factor IF1. Identification of the amino acid involved in its ribosomal binding and recycling. Protein Eng *3(2)*, 133-138.

Gualerzi, C.O., Severini, M., Spurio, R., La Teana, A., and Pon, C.L. (1991). Molecular dissection of translation initiation factor IF2. Evidence for two structural and functional domains. J Biol Chem *266(25)*, 16356-16362.

Gualerzi, C.O., Brandi, L., Caserta, E., Garofalo, C., Lammi, M., La Teana, A., Petrelli, D., Spurio, R., Tomsic, J., and Pon, C.L. (2001). Role of the initiation factors in the early events of mRNA translation in bacteria. Cold Spring Harbor Symp Quant Biol *66*, 363-376.

Gualerzi, C.O.a.P., C.L. (1990). Initiation of mRNA translation in prokaryotes. Biochemistry *29*, 5881-5889.

Guenneugues, M., Caserta, E., Brandi, L., Spurio, R., Meunier, S., Pon, C.L., Boelens, R., and Gualerzi, C.O. (2000). Mapping the fMet-tRNA(f)(Met) binding site of initiation factor IF2. EMBO J *19(19)*, 5233-5240.

Guillon, J.M., Mechulam, Y., Schmitter, J.M., Blanquet, S., and Fayat, G. (1992). Disruption of the gene for Met-tRNA(fMet) formyltransferase severely impairs growth of Escherichia coli. J Bacteriol *174(13)*, 4294-4301.

Haggerty, T.J.a.L., S.T. (1993). Suppression of recJ mutations of Escherichia coli by mutations in translation initiation factor IF3. J Bacteriol *175(19)*, 6118-6125.

Harms, J.M., Wilson, D.N., Schluenzen, F., Connell, S.R., Stachelhaus, T., Zaborowska, Z., Spahn, C.M., and Fucini, P. (2008). Translational regulation via L11: molecular switches on the ribosome turned on and off by thiostrepton and micrococcin. Mol Cell *30(1)*, 26-38.

Hartz, D., McPheeters, D.S., and Gold, L. (1989). Selection of the initiator tRNA by Escherichia coli initiation factors. Genes Dev *3(12A)*, 1899-1912.

Hartz, D., Binkley, J., Hollingsworth, T., and Gold, L. (1990). Domains of initiator tRNA and initiation codon crucial for initiator tRNA selection by Escherichia coli IF3. Genes Dev *4(10)*, 1790-1800.

He, Z.H., Chillingworth, R. K., Brune, M., Corrie, J. E., Trentham, D. R., Webb, M. R., and Ferenczi, M. A. (1997). ATPase kinetics on activation of rabbit and frog permeabilized isometric muscle fibres: a real time phosphate assay. J Physiol *501*, 125-148.

Heimark, R.L., Hersehy, J.W., and Traut, R.R. (1976). Cross-linking of initiation factor IF2 to proteins L7/L12 in 70 S ribosomes of Escherichia coli. J Biol Chem *251(24)*, 779-784.

Helgstrand, M., Mandava, C.S., Mulder, F.A.A, Liljas, A., Sanyal,S., and Akke,M. (2007). The ribosomal stalk binds to translation factors IF2, EF-Tu, EF-G and RF3 via a conserved Region of the L12 C-terminal domain. J Mol Biol *365*, 468-479.

Hughes, R.A., and Moody, C. J. (2007). From amino acids to heteroaromatics--thiopeptide antibiotics, nature's heterocyclic peptides. Angew Chem Int Ed Engl *46*, 7930-7954.

Jones, T.A., Zou, J.Y., Cowan, S.W., Kjeldgaard, M. (1991). Improved methods for building protein models in electron density maps and the location of errors in these models. Acta Crystallogr A *47*, 110-119.

Jonker, H.R., Ilin, S., Grimm, S. K., Wohnert, J., and Schwalbe, H. (2007). L11 domain rearrangement upon binding to RNA and thiostrepton studied by NMR spectroscopy. Nucleic Acids Res *35*, 441-454.

Kaempfer, R. (1972). Initiation factor IF-3: a specific inhibitor of ribosomal subunit association. J Mol Biol *71(3)*, 583-598.

Karimi, R., Pavlov, M.Y., Heurgue Hamard, V., Buckingham,R.H., and Ehrenberg,M. (1998). Initiation factors IF1 and IF2 synergistically remove peptidyl-tRNAs with short polypeptides from the P-site of translating Escherichia coli ribosomes. J Mol Biol *281*, 241-252.

Klaholz, B.P., Myasnikov, A.G., and Van Heel, M. (2004). Visualization of release factor 3 on the ribosome during termination of protein synthesis. Nature *427*, 862-865.

Korostelev, A., Trakhanov, S., Laurberg, M., and Noller, H.F. (2006). Crystal structure of a 70S ribosometRNA complex reveals functional interactions and rearrangements. Cell *126*, 1065-1077.

Kothe, U., Wieden, H.J., Mohr,D., and Rodnina,M.V. (2004). Interaction of helix D of elongation factor Tu with helices 4 and 5 of protein L7/12 on the ribosome. J Mol Biol *336*, 1011-1021.

Krafft, C., Diehl, A., Laettig, S., Behlke, J., Heinemann, U., Pon, C.L., Gualerzi, C.O., and Welfle, H. (2000). Interaction of fMet-tRNA(fMet) with the C-terminal domain of translational initiation factor IF2 from Bacillus stearothermophilus. FEBS Lett *471(2-3)*, 128-132.

Kycia, J.H., Biou, V., Shu, F., Gerchman, S.E., Graziano, V., and Ramakrishnan, V. (1995). Prokaryotic translation initiation factor IF3 is an elongated protein consisting of two crystallizable domains. Biochemistry *34(18)*, 6183-6187.

La Teana, A., Pon, C.L., and Gualerzi, C.O. (1993). Translation of mRNAs with degenerate initiation triplet AUU displays high initiation factor 2 dependence and is subject to initiation factor 3 repression. ProcNatl AcadSci USA *90*, 4161-4165.

La Teana, A., Gualerzi, C.O., and Brimacombe, R. (1995). From stand-by to decoding site. Adjustment of the mRNA on the 30S ribosomal subunit under the influence of the initiation factors. RNA *1(8)*, 772-782.

La Teana, A., Pon, C.L., and Gualerzi, C.O. (1996). Late events in translation initiation. Adjustment of fMet-tRNA in the ribosomal P-site. J Mol Biol *256*, 667-675.

La Teana, A., Gualerzi, C.O., and Dahlberg, A.E. (2001). Initiation factor IF 2 binds to the alpha-sarcin loop and helix 89 of Escherichia coli 23S ribosomal RNA. RNA *7(8)*, 1173-1179.

Lakowicz, J.R., Gryczynski, I. I., and Gryczynski, Z. (1999). High Throughput Screening with Multiphoton Excitation. J Biomol Screen *4(6)*, 355-362.

Lambert, J.M., Boileau, G., Howe, J. G., and Traut, R. R. (1983). Levels of ribosomal protein S1 and elongation factor G in the growth cycle of Escherichia coli. J Bacteriol *154*, 1323-1328.

Lammi, M., Pon, C.L., and Gualerzi, C.O. (1987). The NH2-terminal cleavage of Escherichia coli translational initiation factor IF3. A mechanism to control the intracellular level of the factor? FEBS Lett *215(1)*, 115-121.

Laursen, B.S., Kjaergaard, A.C., Mortensen, K.K., Hoffman, D.W., and Sperling-Petersen, H.U. (2004). The N-terminal domain (IF2N) of bacterial translation initiation factor IF2 is connected to the conserved C-terminal domains by a flexible linker. Protein Sci *13(1)*, 230-239.

Laursen, B.S., Sorensen, H.P., Mortensen, K.K., and Sperling-Petersen, H.U. (2005). Initiation of protein synthesis in bacteria. Microbiol Mol Biol Rev 69, 101-123.

Li, W., Sengupta, J., Rath, B.K., and Frank, J. (2006). Functional conformations of the L11-ribosomal RNA complex revealed by correlative analysis of cryo-EM and molecular dynamics simulations. RNA *12*, 240-1253.

Li, W., and Frank, J. (2007). Transfer RNA in the hybrid P/E state: correlating molecular

dynamics simulations with cryo-EM data. Proc Natl Acad Sci U S A 104, 16540-16545.

Lockwood, A.H., Sarkar, P., and Maitra, U. (1972). Release of polypeptide chain initiation factor IF-2 during initiation complex formation. Proc Natl Acad Sci USA *69*, 3602-3605.

Lockwood, A.H., and Maitra, U. (1974). Relation between the ribosomal sites involved in initiation and elongation of polypeptide chains. Evidence for two guanosine triphosphatase sites. J Biol Chem *249*, 346-352.

Luchin, S., Putzer, H., Hershey, J.W., Cenatiempo, Y., Grunberg-Manago, M., and Laalami, S. (1999). In vitro study of two dominant inhibitory GTPase mutants of Escherichia coli translation initiation factor IF2. Direct evidence that GTP hydrolysis is necessary for factor recycling. J Biol Chem *274*, 6074-6079.

Marzi, S., Knight, W., Brandi, L., Caserta, E., Soboleva, N., Hill, W.E., Gualerzi, C.O., and Lodmell, J.S. (2003). Ribosomal localization of translation initiation factor IF2. RNA *9*, 958-969.

McConkey, G.A., Rogers, M.J., and McCutchan, T.F. (1997). Inhibition of Plasmodium falciparum protein synthesis. Targeting the plastid-like organelle with thiostrepton. J Biol Chem *272(4)*, 2046-2049.

McCutcheon, J.P., Agrawal, R.K., Philips, S.M., Grassucci, R.A., Gerchman, S.E., Clemons, W.M. Jr, Ramakrishnan, V., and Frank, J. (1999). Location of translational initiation factor IF3 on the small ribosomal subunit. Proc Natl Acad

Sci USA *96(8)*, 4301-4306.

Mesters, J.R., Potapov, A.P., de Graaf, J.M., and Kraal, B. (1994). Synergism between the GTPase activities of EF-Tu.GTP and EF-G.GTP on empty ribosomes. Elongation factors as stimulators of the ribosomal oscillation between two conformations. J Mol Biol *242*, 644-654.

Meunier, S., Spurio, R., Czisch, M., Wechselberger, R., Guenneugues, M., Gualerzi, C.O., and Boelens, R. (2000). Structure of the fMet-tRNA(fMet)-binding domain of B. stearothermophilus initiation factor IF2. EMBO J *19(8)*, 1918-1926.

Milon, P., Konevega, A.L., Gualerzi, C.O., and Rodnina, M.V. (2008). Kinetic checkpoint at a late step in translation initiation. Mol Cell 30(6), 712-720.

Mitra, K., and Frank, J. (2006). Ribosome dynamics: insights from atomic structure modeling into cryo-electron microscopy maps. Annu Rev Biophys Biomol *35*, 299-317.

Moazed, D., Robertson, J.M., and Noller, H.F. (1988). Interaction of elongation factors EF-G and EF-Tu with a conserved loop in 23S RNA. Nature *334(6180)*, 362-364.

Moazed, D., Samaha, R.R., Gualerzi, C., and Noller, H.F. (1995). Specific protection of 16 S rRNA by translational initiation factors. J Mol Biol *248(2)*, 207-210.

Modelell, J., Cabrer, B., Parmeggiani, A., and Vazquez, D. (1971). Inhibition by siomycin and thiostrepton of both aminoacyl-tRNA and factor G binding to ribosomes. Proc Natl Acad Sci USA *68*, 1796-1800.

Moreau, M., de Cock, E., Fortier, P.L., Garcia, C., Albaret, C., Blanquet, S., Lallemand,

J.Y., and Dardel, F. (1997). Heteronuclear NMR studies of E. coli translation initiation factor IF3. Evidence that the inter-domain region is disordered in solution. J Mol Biol *266(1)*, 15-22.

Mujumdar, R.B., Ernst, L.A., Mujumdar, S. R., Lewis, C. J., and Waggoner, A.S. (1992). Cyanine Dye Labeling Reagents: Sulfoindocyanine Succinimidyl Esters. Bioconjugate Chemistry *4*, 105-111.

Myasnikov, A.G., Marzi, S., Simonetti, A., Giuliodori, A.M., Gualerzi, C.O., Yusupova, G., Yusupov, M., and Klaholz, B.P. (2005). Conformational transition of initiation factor 2 from the GTP- to GDP-bound state visualzied on the ribosome. Nature Structural and Molecular Biology *12*, 1145-1149.

Naaktgeboren, N., Schrier, P., Moller, W., and Voorma, H.O. (1976). The involvement of protein L11 in the joining of the 30-S initiation complex to the 50-S subunit. Eur J Biochem *62*, 117-123.

Nechifor, R., Murataliev, M., and Wilson, K.S. (2007). Functional interactions between the G' subdomain of bacterial translation factor EF-G and ribosomal protein L7/L12. J Biol Chem *282*, 36998-37005.

Nicolaou, K., Safina, M., Zak, M., Lee, S., Nevalainen, M., Bella, M., Estrada, A., Funke, C., Zecri, F., and Bulat, S. (2005a). Total synthesis of thiostrepton. Retrosynthetic analysis and construction of key building blocks. J Am Chem Soc *127*, 1159-1175.

Nicolaou, K., Zak, M., Rahimipour, S., Estrada, A., Lee, S., O'Brate, A., Giannakakou,

P., and Ghadiri, M. (2005b). Discovery of a biologically active thiostrepton fragment. J Am Chem Soc *127*, 15042-15044.

Nicolaou, K., Zak, M., Safina, M., Estrada, A., Lee, S., and Nevalainen, M. (2005c). Total synthesis of thiostrepton. Assembly of key building blocks and completion of the synthesis. J Am Chem Soc *127*, 11176-11183.

Nicolaou, K.C., Zou, B., Dethe, D. H., Li, D. B., and Chen, D. Y. (2006). Total synthesis of antibiotics GE2270A and GE2270T. Angew Chem Int Ed Engl *45*, 7786-7792.

Nicolaou, K.C., Dethe, D. H., and Chen, D. Y. (2008a). Total syntheses of amythiamicins A, B and C. Chem Commun (Camb), 2632-2634.

Nicolaou, K.C., Dethe, D. H., Leung, G. Y., Zou, B., and Chen, D. Y. (2008b). Total synthesis of thiopeptide antibiotics GE2270A, GE2270T, and GE2270C1. Chem Asian J *3*, 413-429.

Nicolaou, K.C., Chen, J.S., Edmonds, D.J., and Estrada, A.A. (2009). Recent advances in the chemistry and biology of naturally occurring antibiotics. Angew Chem Int Ed Engl *48(4)*, 660-719.

Nishizuka, Y., and Lipmann, F. (1966). The interrelationship between guanosine triphosphatase and amino acid polymerization. Arch Biochem Biophys *116(1)*, 344-351.

Nissen, P., Kjeldgaard, M., Thirup, S., Polekhina, G., Reshetnikova, L., Clark, B. F., and Nyborg, J. (1995). Crystal structure of the ternary complex of Phe-tRNAPhe, EF-Tu, and a GTP analog. Science *270*, 1464-1472.

Olsson, C.L., Graffe, M., Springer, M., and Hershey, J.W. (1996). Physiological effects of translation initiation factor IF3 and ribosomal protein L20 limitation in Escherichia coli. Mol Gen Genet *250(6)*, 705-714.

Pan, D., Kirillov, S., Zhang, C.M., Hou, Y.M., and Cooperman, B.S. (2006). Rapid ribosomal translocation depends on the conserved 18-55 base pair in P-site transfer RNA. Nature Structural and Molecular Biology *13*, 354-359.

Pan, D., Kirillov, S.V., Cooperman, B.S. (2007). Kinetically competent intermediates in the translocation step of protein synthesis. Mol Cell *25*, 519-529.

Pan, D., Qin, H., and Cooperman, B.S. (2009). Synthesis and functional activity of tRNAs labeled with fluorescent hydrazides in the D-loop. RNA *15(2)*, 346-354.

Pape, T., Wintermeyer,W., and Rodnina,M.V. (1998). Complete kinetic mechanism of elongation factor Tu-dependent binding of aminoacyl-tRNA to the A site of the E.coli ribosome. EMBO Journal *17*, 7490-7497.

Parmeggiani, A., and Swart, G.W. (1985). Mechanism of action of kirromycin-like antibiotics. Annu Rev Microbiol *39*, 557-577.

Parmeggiani, A., Krab, I. M., Okamura, S., Nielsen, R. C., Nyborg, J., and Nissen, P. (2006). Structural basis of the action of pulvomycin and GE2270 A on elongation factor Tu. Biochemistry *45*, 6846-6857.

Parmeggiani, A.a.N., P. (2006). Elongation factor Tu-targeted antibiotics: four different structures, two mechanisms of action. FEBS Lett *580(19)*, 4576-4581.

Pediconi, D., Spurio, R., LaTeana, A., Jemiolo, D., Gualerzi, C.O., and Pon, C.L. (1995).

Translational regulation of infC operon in Bacillus stearothermophilus. Biochem Cell Biol *73(11-12)*, 1071-1078.

Peske, F., Rodnina, M.V., and Wintermeyer, W. (2005). Sequence of steps in ribosome recycling as defined by kinetic analysis. Mol Cell *18*, 403-412.

Pestka, S. (1970). Thiostrepton: a ribosomal inhibitor of translocation. Biochem Biophys Res Commun *40*, 667-674.

Petrelli, D., Garofalo, C., Lammi, M., Spurio, R., Pon, C.L., Gualerzi, C.O., and La Teana, A., (2003). Mapping the active sites of bacterial translation initiation factor IF3. J Mol Biol *331(3)*, 541-556.

Pioletti, M., Schlunzen, F., Harms, J., Zarivach, R., Gluhmann, M., Avila, H., Bashan, A., Bartels, H., Auerbach, T., Jacobi, C., Hartsch, T., Yonath, A., and Franceschi, F. (2001). Crystal structures of complexes of the small ribosomal subunit with tetracycline, edeine and IF3. EMBO J *20(8)*, 1829-1839.

Pon, C.L., Paci, M., Pawlik, R.T., and Gualerzi, C.O. (1985). Structure-function relationship in Escherichia coli initiation factors. Biochemical and biophysical characterization of the interaction between IF-2 and guanosine nucleotides. J Biol Chem *260*, 8918-8924.

Pon, C.L.a.G., C. (1974). Effect of initiation factor 3 binding on the 30S ribosomal subunits of Escherichia coli. Proc Natl Acad Sci USA *71(12)*, 4950-4954.

Pon, C.L.a.G., C.O. (1984). Mechanism of protein biosynthesis in prokaryotic cells. Effect of initiation factor IF1 on the initial rate of 30 S initiation complex

formation. FEBS Lett *175(2)*, 203-207.

Porse, B.T., Cundliffe, E., Garrett, R.A. (1999). The antibiotic micrococcin acts on protein L11 at the ribosomal GTPase centre. J Mol Biol *287(1)*, 33-45.

Qin, H., Grigoriadou, C., and Cooperman, B.S. (2009). IF2 interaction with the ribosomal GTPase-associated center during 70S initiation complex formation. Biochemistry *48(22)*, 4699-4706.

Ramakrishnan, V.A. (2002). Ribosome structure and the mechanism of translation. Cell *108*, 557-572.

Rheinberger, H.J., and Nierhaus, K.H. (1987). The ribosomal E site at low Mg2+: coordinate inactivation of ribosomal functions at Mg2+ concentrations below 10 mM and its prevention by polyamines. J Biomol Struct Dyn *5*, 435-446.

Richman, N., and Bodley, J.W. (1972). Ribosomes cannot interact simultaneously with elongation factors EF Tu and EF G. Proc Natl Acad Sci USA *69*, 686-689.

Rodnina, M.V., Semenkov, Y.P., and Wintermeyer, W. (1994). Purification of fMet-tRNA(fMet) by fast protein liquid chromatography. Anal Biochem *219*, 380-381.

Rodnina, M.V., Savelsbergh, A., Katunin, V.I., and Wintermeyer, W. (1997). Hydrolysis of GTP by elongation factor G drives tRNA movement on the ribosome. Nature *385(6611)*, 37-41.

Rodnina, M.V., Savelsbergh, A., Matassova, N.B., Katunin, V.I., Semenkov, Y.P., and Wintermeyer, W. (1999). Thiostrepton inhibits the turnover but not the GTPase of elongation factor G on the ribosome. Proc Natl Acad Sci USA *96(17)*, 9586-9590.

Roll-Mecak, A., Cao, C., Dever, T.E., and Burley, S.K. (2000). X-Ray structures of the universal translation initiation factor IF2/eIF5B: conformational changes on GDP and GTP binding. Cell *103(5)*, 781-792.

Sacerdot, C., Dessen, P., Hershey, J.W., Plumbridge, J.A., and Grunberg-Manago, M. (1984). Sequence of the initiation factor IF2 gene: unusual protein features and homologies with elongation factors. Proc Natl Acad Sci USA *81(24)*, 7787-7791.

Sacerdot, C., Vachon, G., Laalami, S., Morel-Deville, F., Cenatiempo, Y., and Grunberg-Manago, M. (1992). Both forms of translational initiation factor IF2 (alpha and beta) are required for maximal growth of Escherichia coli. Evidence for two translational initiation codons for IF2 beta. J Mol Biol *225(1)*, 67-80.

Sands, J.F., Cummings, H.S., Sacerdot, C., Dondon, L., Grunberg-Manago, M., and Hershey, J.W. (1987). Cloning and mapping of infA, the gene for protein synthesis initiation factor IF1. Nucleic Acids Res *15(13)*, 5157-5168.

Sarkar, P., Stringer, E.A., and Maitra, U. (1974). Thiostrepton inhibition of initiation factor 1 activity in polypeptide chain initiation in Escherichia coli. Proc Natl Acad Sci USA *71(12)*, 4986-4990.

Savelsbergh, A., Katunin, V.I., Mohr, D., Peske, F., Rodnina, M.V., and Wintermeyer, W. (2003). An elongation factor G-induced ribosome rearrangement precedes tRNA-mRNA translocation. Mol Cell *11*, 1517-1523.

Schuwirth, B.S., Borovinskaya, M.A., Hau, C.W., Zhang, W., Vila-Sanjurjo, A., Holton, J.M., and Cate, J.H. (2005). Structures of the bacterial ribosome at 3.5 A

resolution. Science *310*, 827-834.

Selmer, M., Dunham, C.M, Murphy, F.V. 4th., Weixlbaumer, A., Petry, S., Kelley, A.C., Weir, J.R., Ramakrishnan, V. (2006). Structure of the 70S ribosome complexed with mRNA and tRNA. Science *313*, 1935-1942.

Seo, H., Kiel, M., Pan, DL., Raj, S., Kaji,A., and Cooperman, B.S. (2004). Kinetics and thermodynamics of RRF, EF-G, and Thiostrepton interaction on the Escherichia coli ribosome. Biochemistry *43*, 12728-12740.

Seo, H., Abedin, S., Kamp, D., Wilson, D.N., Nierhaus, K.H., and Cooperman, B.S. (2006). EF-G-Dependent GTPase on the ribosome. conformational change and fusidic Aacid inhibition. Biochemistry *45*, 2504-2514.

Sergiev, P.V., Bogdanov, A.A., and Dontsova, O.A. (2005). How can elongation factors EF-G and EF-Tu discriminate the functional state of the ribosome using the same binding site? FEBS Lett *579*, 5439-5442.

Severini, M., Spurio, R., La Teana, A., Pon, C.L., and Gualerzi, C.O. (1991). Ribosome-independent GTPase activity of translation initiation factor IF2 and of its G-domain. J Biol Chem *266(34)*, 22800-22802.

Simonetti, A., Marzi, S., Myasnicov, A.G., Fabbretti, A., Yusupov, A., Gualerzi, C.O., and Klaholz, B. (2008). Structure of the 30S translation initiation complex. Nature *455(7211)*:416-20.

Spahn, C.M.a.P., C.D. (1996). Throwing a spanner in the works: antibiotics and the translation apparatus. J Mol Med *74(8)*, 423-439.

Spurio, R., Brandi, L., Caserta, E., Pon, C.L., Gualerzi, C.O., Misselwitz, R., Krafft, C., Welfle, K., and Welfle, H. (2000). The C-terminal subdomain (IF2 C-2) contains the entire fMet-tRNA binding site of initiation factor IF2. J Biol Chem *275(4)*, 2447-2454.

Stark, H., Rodnina, M.V., Wieden, H.J., van Heel, M., and Wintermeyer, W. (2000). Large-scale movement of elongation factor G and extensive conformational change of the ribosome during translocation. Cell *100*, 301-309.

Stark, H., Rodnina, M.V., Wieden, H.J., Zemlin, F., Wintermeyer, W., and van Heel, M. (2002). Ribosome interactions of aminoacyl-tRNA and elongation factor Tu in the codon-recognition complex. Nat Struct Biol *9*, 849-854.

Sussman, J.K., Simons, E.L., and Simons, R.W. (1996). Escherichia coli translation initiation factor 3 discriminates the initiation codon in vivo. Mol Microbiol *21(2)*, 347-360.

Szaflarski, W., Vesper, O., Teraoka, Y., Plitta, B., Wilson, D. N., and Nierhaus, K. H. (2008). New features of the ribosome and ribosomal inhibitors: non-enzymatic recycling, misreading and back-translocation. J Mol Biol *380*, 193-205.

Tedin, K., Moll, I., Grill, S., Resch, A., Graschopf, A., Gualerzi, C.O., and Blasi, U. (1999). Translation initiation factor 3 antagonizes authentic start codon selection on leaderless mRNAs. Mol Microbiol *31(1)*, 67-77.

Tomsic, J., Vitali, L.A., Daviter, T., Savelsbergh, A., Spurio, R., Striebeck, P., Wintermeyer, W., Rodnina, M.V., and Gualerzi, C.O. (2000). Late events of

translation initiation in bacteria: a kinetic analysis. EMBO J *19*, 2127-2136.

Tu, D., Blaha, G., Moore, P., and Steitz, T. (2005). Structures of MLSBK antibiotics bound to mutated large ribosomal subunits provide a structural explanation for resistance. Cell *121*, 257-270.

Valle, M., Sengupta, J., Swami, N.K., Grassucci, R.A., Burkhardt, N., Nierhaus, K.H., Agrawal, R.K., and Frank, J. (2002). Cryo-EM reveals an active role for aminoacyl-tRNA in the accommodation process. EMBO J *21*, 3557-3567.

Valle, M., Zavialov, A., Li, W., Stagg, S. M., Sengupta, J., Nielsen, R.C., Nissen, P., Harvey, S.C., Ehrenberg, M., and Frank, J. (2003a). Incorporation of aminoacyl-tRNA into the ribosome as seen by cryo-electron microscopy. Nature Structural Biology *10*, 899-907.

Valle, M., Zavialov, A., Sengupta, J., Rawat, U., Ehrenberg, M., and Frank, J. (2003b). Locking and unlocking of ribosomal motions. Cell *114*, 123-134.

van der Hofstad, G.A., Buitenhek, A., van den Elsen, P.J., Voorma, H.O., and Bosch, L. (1978). Binding of labeled initiation factor IF-1 to ribosomal particles and the relationship to the mode of IF-1 action in ribosome dissociation. Eur J Biochem *89(1)*, 221-228.

van Heel, M., Harauz, G., Orlova, E.V., Schmidt, R., and Schatz, M. (1996). A new generation of the IMAGIC image processing system. J Struct Biol *116*, 17-24.

Wahler, B.E.a.W., A. (1958). Determination of orthophosphate in the presence of phosphate compounds with an affinity for acids and molybdate. Biochem Z

329(6), 508-520.

Wakao, H., Romby, P., Westhof, E., Laalami, S., Grunberg-Manago, M., Ebel, J.P., Ehresmann, C., and Ehresmann, B. (1989). The solution structure of the Escherichia coli initiator tRNA and its interactions with initiation factor 2 and the ribosomal 30 S subunit. J Biol Chem *264(34)*, 20363-20371.

Wang, Y., Qin, H., Kudaravalli, R.D., Kirillov, S.V., Dempsey, G.T., Pan, D., Cooperman, B.S., and Goldman, Y.E. (2007). Single-molecule structural dynamics of EF-G--ribosome interaction during translocation. Biochemistry *46*, 10767-10775.

Weisblum, B., and Demohn, V. (1970). Inhibition by thiostrepton of the formation of a ribosome-bound guanine nucleotide complex. FEBS Lett *11*, 149-152.

Wilson, D.N., Schluenzen, F., Harms, J.M., Yoshida, T., Ohkubo, T., Albrecht, R., Buerger, J., Kobayashi, Y., and Fucini, P. (2004). X-ray crystallography study on ribosome recycling: the mechanism of binding and action of RRF on the 50S ribosomal subunit. EMBO J *24(2)*, 251-260.

Wilson, D.N.a.N., K.H. (2005). Ribosomal proteins in the spotlight. Crit Rev Biochem Mol Biol *40(5)*, 243-267.

Wintermeyer, W., Peske, F., Beringer, M., Gromadski, K.B., Savelsbergh, A., and Rodnina, M.V. (2004). Mechanisms of elongation on the ribosome: dynamics of a macromolecular machine. Biochem Soc Trans *32*, 733-737.

Wolf, H., Chinali, G., Parmeggiani, A. (1977). Mechanism of the inhibition of protein

synthesis by kirromycin. Role of elongation factor Tu and ribosomes. Eur J Biochem *75*, 67-75.

Wu, X.Q.a.R., U.L. (1997). Effect of the amino acid attached to Escherichia coli initiator tRNA on its affinity for the initiation factor IF2 and on the IF2 dependence of its binding to the ribosome. J Biol Chem *272*, 1891-1895.

Xing, Y.Y., and Draper, D. E. (1996). Cooperative interactions of RNA and thiostrepton antibiotic with two domains of ribosomal protein L11. Biochemistry *35*, 1581-1588.

Yasuda, R., Masaike, T., Adachi, K., Noji, H., Itoh, H., and Kinosita, K. Jr. (2003). The ATP-waiting conformation of rotating F1-ATPase revealed by single-pair fluorescence resonance energy transfer. Proc Natl Acad Sci USA *100*, 9314-9318.

Yusupov, M.M., Yusupova, G.Z., Baucom, A., Lieberman, K., Earnest, T.N., Cate, J.H., and Noller, H.F. (2001). Crystal structure of the ribosome at 5.5 A resolution. Science *292*, 883-896.

Yusupova, G., Reinbolt, J., Wakao, H., Laalami, S., Grunberg-Manago, M., Romby, P., Ehresmann, B., and Ehresmann, C. (1996). Topography of the Escherichia coli initiation factor 2/fMet-tRNA(f)(Met) complex as studied by cross-linking. Biochemistry *35(9)*, 2978-2984.

Yusupova, G., Jenner, L., Rees, B., Moras, D., Yusupov, M. (2006). Structural basis for messenger RNA movement on the ribosome. Nature *444*, 391-394.

Zavialov, A.V., Buckingham, R.H., and Ehrenberg, M. (2001). A posttermination

ribosomal complex is the guanine nucleotide exchange factor for peptide release factor RF3. Cell *107*, 115-124.

Zavialov, A.V., Hauryliuk, V.V., and Ehrenberg, M. (2005). Splitting of the posttermination ribosome into subunits by the concerted action of RRF and EF-G. Mol Cell *18(6)*, 675-686.